

**Looking into living cell systems: Planar waveguide NMR detector
hyphenated with a microfluidic device for the *in vitro* metabolomics of
tumor spheroids**

**Einblick in lebende Zellsysteme: Kopplung eines planaren Wellenleiter-
NMR-Detektors mit einem Mikrofluidikchip für *in vitro* Metabolismus-
Studien an Tumor-Sphäroiden**

In fulfillment of the requirements for the Degree
Dr. rer. nat.
to the faculty „Bio- und Chemieingenieurwesen“
of the „Technische Universität“ Dortmund
Approved Dissertation

Submitted by
M.Sc. Ayten Kalfe
From
Kahramanmaras/Afsin/Turkey

1st Referee: Prof. Dr. Jörg Tiller
2nd Referee: PD Dr. Joachim Franzke

Filing Date: 28.09.2015
Date of oral examination: 11.05.2016

Dortmund 2016
Leibniz-Institut für Analytische Wissenschaften – *ISAS* – e.V.,

Declaration

The research of this thesis was done at the Leibniz-Institut für Analytische Wissenschaften -ISAS-e.V., Department of Interface Processes in Dortmund, Germany. The work presented herein is my own work, unless it is referenced to the contrary in the text.

Dortmund, August 2015

Content

Abstract	1
Zusammenfassung	2
1 Introduction.....	4
2 NMR.....	9
2.1 Introduction	9
2.2 NMR theoretical part	10
2.2.1 Spins.....	10
2.2.2 Chemical shift	17
2.2.3 The ¹ H-NMR spectra	19
2.2.4 Coupling.....	19
3 Microslot NMR detector	22
3.1 Introduction	22
3.2 Background of NMR microcoils	23
3.2.1 Planar waveguide microslot NMR detector – How it works	24
3.3 Materials and Methods.....	27
3.3.1 Photolithography (Microslot NMR detector)	27
3.3.2 Microfabrication via Laser ablation (femtosecond laser)	29
3.3.3 Fabrication of the waveguide microslot NMR probe	30
3.3.4 Quality factor	31
3.3.5 Shimming	32
3.3.6 Nutation curve	34
3.4 Results and Discussion	35
3.4.1 NMR detector fabrication and the setup of a resonance circuit	35
3.4.2 Design and Photolithography of the microstrip detector	35

Content

3.4.3	Laser ablation	38
3.4.4	Assembly of the probehead	40
3.4.5	Simulation of the B_1 field distribution	41
4	Microfluidics and LOC	42
4.1	Microsystems enabling cell-based assays.....	43
4.1.1	Microfabrication and Micropatterning techniques.....	45
4.1.2	Photolithography (fabrication of the silicon wafer for the PDMS chip)...	46
4.1.3	Soft lithography (fabrication of the PDMS chip)	48
4.1.4	PDMS Chip assembly and plasma generator.....	49
4.2	Materials and Methods.....	50
4.2.1	PDMS chip.....	50
4.2.2	Microfluidic glass device.....	50
4.3	Results and Discussion	51
4.3.1	Plasma Generator.....	51
4.3.2	PDMS Chip	53
4.3.3	Microfluidic glass device.....	58
5	Cells	61
5.1	Introduction	61
5.1.1	Cell	61
5.1.2	Metabolism.....	64
5.1.3	Cell culture and <i>in vivo</i> vs <i>in vitro</i>	68
5.1.4	Cancer / Tumor	70
5.1.5	2D and 3D <i>in vitro</i> cell models vs animal models.....	73
5.1.6	Spheroids (3D <i>in vitro</i> cell model)	76
5.1.7	Hanging drop Spheroid Platform.....	80

Content

5.1.8	PDMS Spheroid Microarrays by μ CP	83
5.2	Materials and Methods.....	85
5.2.1	Cell culture.....	85
5.2.2	Spheroid formation with InSphero hanging drop	85
5.2.3	Spheroid formation with a PDMS microarray	86
5.3	Results and Discussion	89
5.3.1	InSphero hanging drop spheroids	89
5.3.2	PDMS Microarray Spheroids	95
6	Hyphenation of NMR + LOC + Cells for long-term metabolomics	99
6.1	Introduction	99
6.2	Materials and Methods.....	99
6.3	Results and Discussion	100
6.3.1	Microslot NMR detector integrated with a microfluidic device.	102
6.3.2	Spheroid vs media on chip for 24 hours.....	104
6.3.3	Off-chip vs on-chip experiment.....	106
6.3.4	The role of lactate and alanine.....	110
6.3.5	The role of ethanol and acetate.....	113
6.3.6	The role of other amino acids	115
6.3.7	Measurement uncertainty.....	116
6.3.8	Comparison of two individual on-chip experiments	117
6.3.9	Metabolic profile of the PDMS microarray spheroids.....	119
6.3.10	On chip experiments with several spheroids	121
6.3.11	Metabolic profile of cells grown in 2D monolayer	124
7	Conclusion	127
8	Outlook.....	129

Content

List of Abbreviations	133
References	135

Abstract

The complex cell metabolism and its link to signaling pathways have received huge interest within the last years. But the lack of advanced analytical tools for the investigation of living cell metabolism is still a challenge to be faced. Therefore, we designed and fabricated a novel miniaturized microslot nuclear magnetic resonance (NMR) detector with on-board heater integrated with a microfluidic device as NMR sample holder. With this new set-up we have analyzed 3D *in vitro* cell culture models (spheroids) because they have turned out to be authentic model systems which successfully bridge the gap between 2D cell cultures and live tissue or animal models. For the first time, a tumor spheroid of 500 μm diameter consisting of approximately 9000 cells has been studied non-invasively and online for 24 hours. The dynamic process of production and degradation of 23 intra- and extracellular metabolites were monitored. Remarkably high concentrations of lactate and alanine were observed being an indicator for a shift from oxidative to glycolytic metabolism. In summary, this methodical development has proven to be a successful analytical tool for the elucidation of cellular functions and their corresponding biochemical pathways. Additionally, the planar geometry of the microslot NMR detector allows the hyphenation with versatile lab-on-a chip (LOC) technology. This opens a new window for metabolomics studies on living cells and can be implemented into new application fields in biotechnology and life sciences. The aim is to use the device as diagnostic tool for the investigation of cell responses to external stress factors as in toxicological or pharmaceutical studies in order to replace tests on animal models.

Zusammenfassung

Untersuchungen des komplexen Metabolismus von Zellen sowie der dazugehörigen Signalwege haben in den letzten Jahren zunehmend an Bedeutung gewonnen. Aber der Mangel an ausgereiften analytischen Geräten, die für Metabolismus-Studien an lebenden Zellen nötig sind, stellt immer noch eine Herausforderung dar, die es zu bewältigen gilt. Aus diesem Grund wurde im Rahmen dieser Arbeit ein neuartiger Mikrostreifenleiter-Detektor für die kernmagnetische Resonanz (NMR) mit einer integrierten Heizvorrichtung entwickelt und mit einem Mikrofluidikchip gekoppelt, der unter anderem als Probenhalter fungiert. Mit dieser neuen Methode wurden 3D *in vitro* Zellkulturmodelle (Sphäroide) analysiert, weil diese hervorragend die Lücke zwischen 2D Zellkulturmodellen und Tiermodellen überbrücken. Erstmals wurde ein Tumorsphäroid, mit 500 µm Durchmesser und ca. 9000 Zellen, nichtinvasiv für 24 Stunden analysiert. Der dynamische Prozess der Produktion und des Abbaus von 23 intra- und extrazellulären Metaboliten konnte verfolgt werden. Bemerkenswert hohe Konzentrationen an Laktat und Alanin wurden beobachtet, was auf eine Verschiebung vom oxidativen zum glykolytischen Metabolismus hinweist. Zusammenfassend lässt sich sagen, dass sich diese methodische Entwicklung als erfolgreiches analytisches Verfahren erwiesen hat, das zur Aufklärung von Zellfunktionen und ihrer zugrunde liegenden biochemischen Reaktionswege dient. Des Weiteren erlaubt die planare Geometrie des Mikrostreifenleiter NMR Detektors die Kopplung mit der vielseitigen Lab-on-a-chip (LOC) Technologie. Mit dieser Entwicklung eröffnen sich neue Perspektiven für Metabolismus-Studien an lebenden Zellen, die neue Anwendungsgebiete in der Biotechnologie und den Lebenswissenschaften eröffnen. Ziel ist es, das Gerät als diagnostisches Werkzeug zur Untersuchung von Zellantworten auf äußere Stressfaktoren in toxikologischen oder pharmazeutischen Studien zu verwenden, um somit später Tierexperimente zu ersetzen.

1 Introduction

Along with the other fields of omics research metabolomics has accelerated the elucidation of fundamental cellular functions and their corresponding biochemical pathways. The concentrations and dynamics of the metabolites not only give direct evidence of the cells' physiological condition like normal or pathogenic. The metabolome shows also the fastest and most sensitive response to the changes in the microenvironment which can be used to study the cellular response to pharmaceuticals or other stress factors.¹⁻³ Nevertheless, the role of metabolites is complex and dynamic and they are involved in many essential life processes. Particularly in regard to pathogenic conditions the relation between altered metabolism and cancer has been shown in many studies over the last decades.⁴⁻⁶ Thus, not only the important role of the metabolites in cellular functions but also the link between metabolism and cancer accentuates the significance of the metabolomics studies. Resulting from this, new measurement techniques must be invented or improved to enable *in vitro* studies on appropriate model systems within suitable microenvironment conditions.^{7,8}

Recently multicellular 3D *in vitro* models (spheroids) have been proven as a suitable *in vivo* like model system. In contrast to classical 2D monolayer based models, spheroids are mimicking the 3D cellular milieu like cell-cell and cell-matrix interactions and the pathophysiological gradients inside tumors. The cells located on the surface of the spheroid mirror the actively cycling tumor cells close to blood vessels, while the cells in the inner core are exposed to hypoxic conditions comparable with avascular tumor areas.⁹⁻¹¹ The 3D microenvironment is also mimicking the barriers of drugs which are a key reason of drug resistance in real tumors. These properties make 3D models a fundamental analytical tool for biochemical studies in omics research, high throughput screenings and preclinical studies. When compared with 3D *in vitro* models animal models seem to be more authentic and effective analysis objects. However, animal models are a controversial issue not only regarding the ethical concerns but also whether the animal models can mimic human diseases or not.¹² More than 80% of the

1 Introduction

potential therapeutics which were tested on animal models fail or even have a toxic effect when tested on humans.¹³ Furthermore, animal models are expensive and highly complex systems which cannot be controlled as good as e.g. 3D *in vitro* models which are accessible for low level safety laboratories. Therefore, 3D *in vitro* models have turned out to be authentic model systems which successfully bridge the gap between 2D cell culture and live tissue or animal models.¹⁴ Therefore, spheroids are appropriate tumor models which show a great potential for the analysis of tumor metabolism and are a suitable tool for high-throughput toxicological screenings and for the investigation of potential drug candidates.⁹⁻¹¹

Although a spheroid consists of several thousand cells and represents already a (in this case unavoidable) population average it is of great interest to investigate single spheroids to uncover subpopulations - a problem impossible to address with conventional nuclear magnetic resonance (NMR) spectroscopy. Its low sensitivity impedes measurements on an ultra small sample like a single tumor spheroid. One reason is the resulting poor filling factor of the conventional radiofrequency (rf) coil, if a very small sample is measured. An NMR measurement with a conventional detection coil on several spheroids will mirror only the population average. However, in single cell analysis it is well known that cells even in genetically and morphologically identical populations reveal heterogeneities.^{3, 15} The analysis of population distributions will mask subpopulations and will provide only average values.¹⁶ Therefore, there is a big need for miniaturized NMR detection coils.

But currently, to overcome the sensitivity problem of NMR usually mass spectrometry (MS) is used. It is one of the most widely used and ultrasensitive analysis techniques and therefore a suitable tool not only for metabolomics analysis. Nowadays it can detect even metabolites from single yeast cells.¹⁷ However, the biggest disadvantage of MS is its destructive nature as it usually requires cell extracts for analysis. For the study of either single cells or cell populations usually the cells are lysed and the metabolites are extracted, i.e. working with living cells is not possible. The metabolism of the cells is stopped at a specific time point and the extracted metabolites are a

1 Introduction

snapshot at the time of lysis. This hinders the analysis of the temporal dynamics of the metabolites.^{15, 18} Since the metabolome shows the fastest and most sensitive reaction to the environmental changes or to external factors the analysis of this dynamic picture is of big importance and highlights the need for living cell analysis.

Therefore, not only the necessity to keep cells alive but also the preservation of the *in vivo* state of vascularized tumors as well as the handling of ultra-small samples emphasize the requirement for microfluidic devices. For this purpose many techniques are available to control the physiological condition of the cell samples by using lab-on-a-chip (LOC) devices.¹⁹ Since the concept of micro total analysis systems (μ TAS), later indicated as LOC²⁰, was introduced the first time by Manz et al. in the early 1990s, the miniaturization of analytical procedures is of great importance in the expanding life sciences. Miniaturized devices not only minimize the sample volume, but also reduce the analysis time and cost, enable high-throughput analysis, allow portability and on site detection.²¹⁻²⁶ Despite this progress in micro technology, detection is one of the main challenges for the miniaturization because of the ultra-small sample sizes. Many analytical tools like MS and optical methods have been integrated to LOC devices for the detection of samples in the nanoliter range.^{1, 3, 18, 19}

However, MS is an invasive method as mentioned above and optical methods are not always well suited for metabolomics analysis since metabolites have a large structural diversity and large dynamical range which require usually fluorescent labeling.¹⁵ In comparison, conventional NMR has a unique non-destructive nature but it is not suitable for small samples. Therefore, miniaturized NMR analysis techniques employing detectors that match the sample size²⁷⁻²⁹ are of high importance to study mass- and volume-limited samples like single tumor spheroids. But another shortcoming of conventional NMR is the helical coil geometry of the detector which allows only cylindrically shaped sample holders to be used, impeding the integration of the versatile LOC devices.^{28, 30, 31} Both shortcomings can best be addressed with rf microslot probes based on planar electromagnetic waveguide technology recently introduced to NMR.^{28, 32-37} These planar microslot probes allow for hyphenation with

1 Introduction

LOC technology, enabling us to design a microslot probehead to measure the metabolites of a multicellular tumor spheroid. Spheroids consisting of approximately 9000 living cells were placed inside a microfluidic glass device with dynamical media and oxygen supply. An on-board temperature sensor and heater accurately controls the temperature in order to maintain the viability of the cells at near physiological conditions for long-term *in vitro* studies. This method preserves the anatomical and functional integrity of cells and enables a time resolved analysis of the living spheroids' metabolic profile and can give a dynamic picture of the biochemical reaction inside a single spheroid. This opens a new window for metabolomics studies on living cells, tissue like samples and later on 3D organ systems with the objective to implement it as a diagnostic tool for the investigation of cell responses to external stress factors as in toxicological or pharmaceutical studies in order to replace tests on animal models.

After this Introduction chapter theoretical background information about NMR will be given in chapter 2. In the following schematic illustration (Figure 1) the work which has been done in this thesis can be seen at a glance.

In chapter 3 the instrumental development of the microslot NMR detector will be presented. The photolithographic fabrication of the probe and the micromachining of the slot via femtosecond laser ablation will be shown and the properties of the novel detector will be discussed.

In chapter 4 a short introduction into some microfabrication and micropatterning techniques will be given. First, the photolithographic fabrication of the silicon wafer for the PDMS chip will be shown and afterwards the soft lithographic production of the PDMS chip will be demonstrated. Then, a microfluidic glass device will be fabricated and the advantages and disadvantages of a polymer based (PDMS chip) and glass based microfluidic device will be discussed.

In chapter 5 the readers will be introduced into cell biology, metabolism and cancer. The advantages and disadvantages of 2D and 3D *in vitro* cell models and animal models for biochemical experiments will be discussed. Finally, two different methods for the formation of 3D *in vitro* cell models (spheroids) will be demonstrated and discussed.

1 Introduction

One method is the hanging drop spheroid platform and the other method is PDMS spheroid microarray.

In chapter 6 the results of chapter 3-5 which have been proven to be successful (microslot detector, microfluidic glass device and spheroids) will be hyphenated. With this setup the aim of this work is to enable long-term metabolomics analysis on living tumor spheroids.

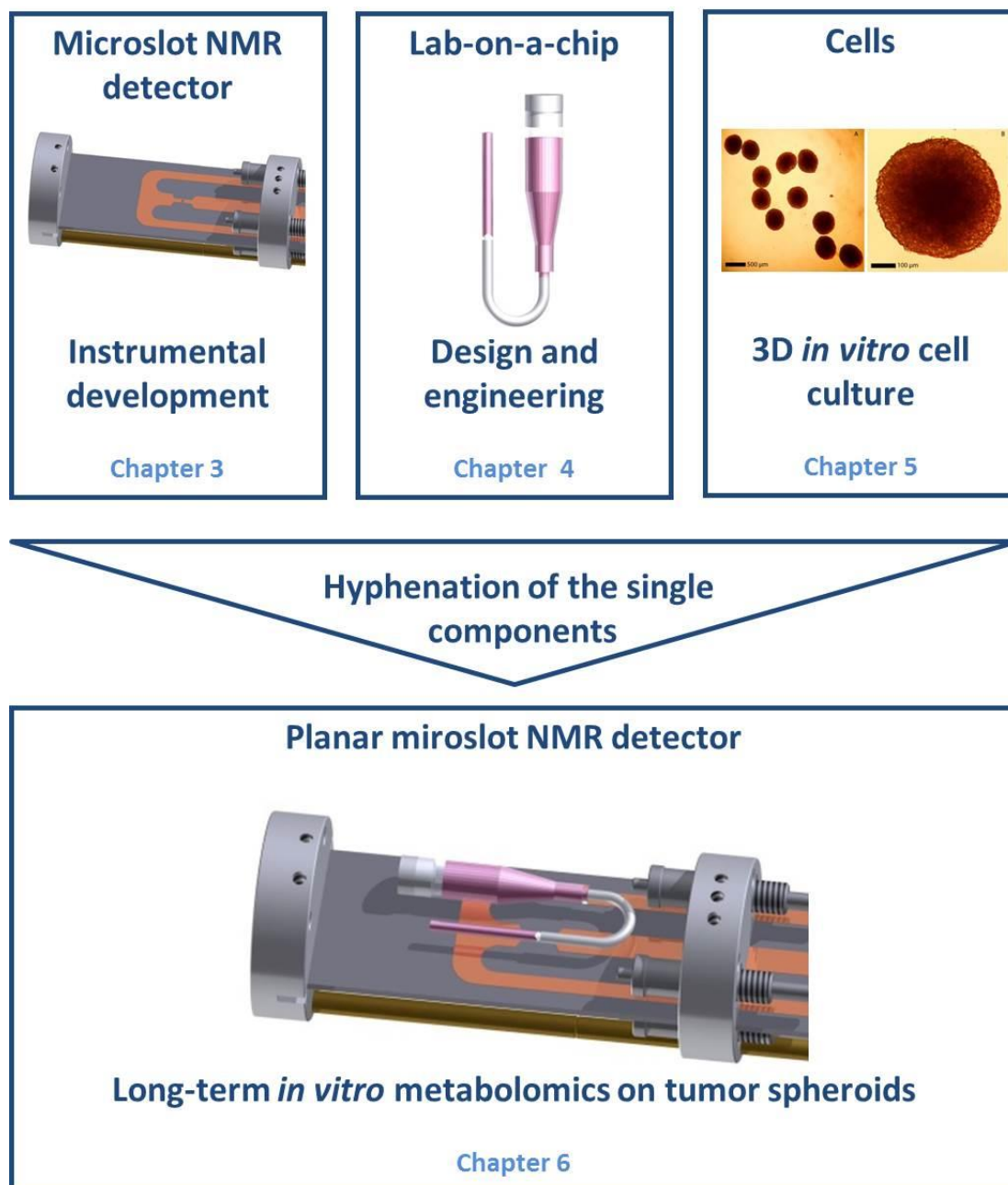


Figure 1: The chapters of this thesis at a glance

2 NMR

2.1 Introduction

Nuclear Magnetic Resonance spectroscopy (NMR) is a uniquely powerful analysis technique due to its high potential for molecular structure identification and its non-destructive nature. With NMR, one can elucidate the structure even of complex macromolecules and it allows also the study of binding kinetics and molecular dynamics.



Figure 2: 600 MHz Bruker AV III NMR spectrometer at the ISAS institute in Dortmund.

In 1902, together with H. Lorentz, P. Zeeman received a Nobel Prize in physics for discovering the Zeeman Effect. It describes the splitting of energy levels of spectral lines proportional to the strength of an external magnetic field. In 1952, F. Bloch and W.M. Purcell got the Nobel Prize for physics for their development of new ways and methods for nuclear magnetic precision measurements and they constructed quasi the first NMR spectrometer. Once again the importance of NMR was highlighted with the Nobel Prizes for chemistry for R.R. Ernst (1991) and K. Wüthrich (2002). In 2003, P. Lauterbur and P. Mansfield shared the Nobel Prize for physiology and medicine for their discoveries concerning magnetic resonance imaging. Therefore, NMR has a huge application field ranging from physics, chemistry, biology, medicine to material sciences. During the last 60 years NMR was established as an advanced analysis

technique finding applications ranging from solution- to solid-state and of course magnetic resonance imaging (MRI) which is used nowadays as a common medical diagnostic tool in hospitals.

2.2 NMR theoretical part

2.2.1 Spins

The analysis technique of NMR is based on the magnetic properties of certain atomic nuclei. The nuclei of some isotopes with uneven proton and/or neutron number (e.g. ^1H , ^{13}C , ^{15}N) have a spin angular momentum p (nuclear spin) which appears via the rotation of the nuclei about its axis as shown in Figure 3.

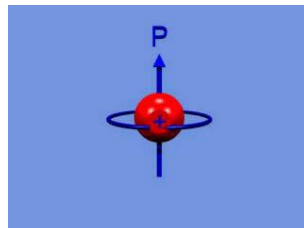


Figure 3: Illustration of an atomic nucleus and its spin angular momentum p .³⁸

It is described as:

$$p = \sqrt{I(I + 1)}\hbar \quad (1)$$

$$\hbar = \frac{h}{2\pi} \quad (2)$$

h is the Planck's Constant and I is the spin quantum number. The latter can have half-integer values for uneven mass numbers and integer values for even mass numbers but uneven proton numbers and in case of even mass and proton number I is zero ($I = 0, 1/2, 1, 3/2, 2, 5/2, \dots, 6$). Nuclei with a spin $\neq 0$ are associated with a magnetic moment $\mu \neq 0$, which is given by

$$\mu = \gamma p \quad (3)$$

with γ being the gyromagnetic ratio, which is characteristic for every nucleus type. And only nuclei with a magnetic moment can orient in a magnetic field. To simplify, these kinds of nuclei behave like small magnets and can be observed via NMR. Without a

static magnetic field (B_0), the nuclear magnetic moments are oriented in random directions as shown in Figure 4. Once an external and static magnetic field (B_0) is applied, the nuclear spins are aligned relative to B_0 .

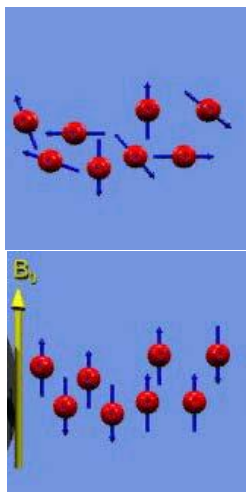


Figure 4: (Top) The spins of the atomic nuclei are oriented randomly. (Bottom) After applying an external magnetic field (B_0), the spins become aligned relative to the external magnetic field B_0 (simplified schematic illustration).³⁸

As the nuclear spin is quantized, the spins can take only discrete alignment states, characterized by the magnetic quantum number m ($m = -I, -I+1, \dots, I-1, I$). The total number of states is given by $2I + 1$. For instance, the nuclei with spin quantum number $I = 1/2$ (like found in ^1H) have magnetic quantum numbers of $m = -1/2$ (spin-down or β) and $+1/2$ (spin-up or α)

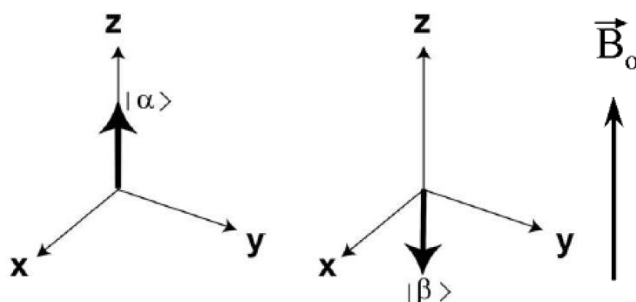


Figure 5: When nuclei with $I = 1/2$ absorb energy, originating from an external electromagnetic radiation source (B_1 -field), the spins are flipped from the lower energy spin state $m = 1/2$ (spin-up or α) to the higher energy spin state $m = -1/2$ (spin-down or β).³⁸

Usually the z-axis is chosen to be parallel to the B_0 field and therefore the z-component of the spin angular momentum vector is given by

$$p_z = m \hbar \quad (4)$$

And consequently the magnetic moment of the z-component is

$$\mu_z = \gamma p_z = \gamma m \hbar \quad (5)$$

The $2I + 1$ alignment states of a spin I (Zeeman splitting) in the field B_0 are shown in Figure 6.

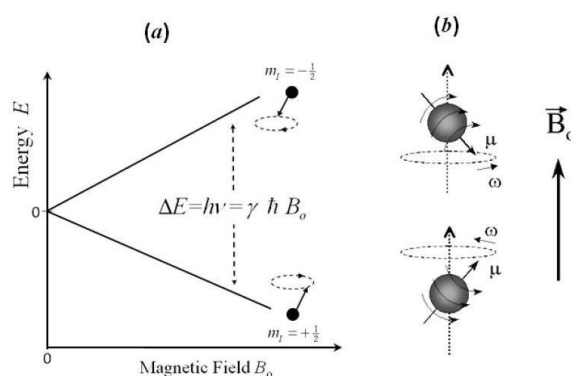


Figure 6: (a) Relative energy of the spin-down ($m = -1/2$) and spin-up ($m = +1/2$) states as a function of the external magnetic field strength. (b) While μ is the magnetic moment, ω_0 is the resonance frequency in radian per second, which is also known as Larmor frequency $\omega_0 = \gamma B_0$.³⁹

The so called nuclear Zeeman levels have the following energy

$$E = -\mu B_0 \quad (6)$$

$$E_m = -\mu_z B_0 = -\gamma p_z B_0 = -\gamma \hbar m B_0 \quad (7)$$

In case of $I = 1/2$ we get two allowed states $m = -1/2$ (spin-down or β), $m = +1/2$ (spin-up or α) and the energy difference between both allowed states of the nuclear spin is given by

$$E_{1/2} = -\mu_z B_0 = -\gamma p_z B_0 = -\gamma \hbar 1/2 B_0 \quad (8)$$

$$E_{-1/2} = -\mu_z B_0 = -\gamma p_z B_0 = \gamma \hbar 1/2 B_0 \quad (9)$$

$$\Delta E = \gamma \hbar B_0 \quad (10)$$

As the moments associated with the spin-up and spin-down states of the nuclear spin have a component in the x-y-plane, the external magnetic field B_0 causes a torque on the magnetic moments. The torque gives rise to a precession of the moments on the surface of a cone, as shown in Figure 7. The rate of precession can be described with the Larmor frequency ν or Larmor resonance frequency ω .

$$\nu_0 = \gamma B_0 / 2 \pi \quad (11)$$

$$\omega_0 = 2 \pi \nu_0 = \gamma B_0 \quad (12)$$

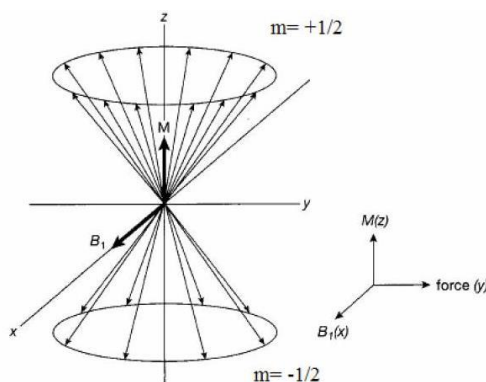


Figure 7: Net magnetization. ³⁹

If an electromagnetic field named B_1 (Figure 7), rotating with the Larmor frequency, is in addition applied in the x-y-plane, the magnetic moments start to precess both around the direction of B_0 and the direction of B_1 . A precession around B_1 gives rise to a change of the energy level, i.e. B_1 exchanges electromagnetic radiation with the spins. Due to this reason the energy difference corresponds to the electromagnetic radiation frequency and the equation (10) can be described as follows:

$$\Delta E = \gamma \hbar B_0 = h \nu \quad (13)$$

With the equations (10 - (13) the magnetic field can be related to the resonance frequency. Figuring out the correct resonance frequency for each atom under investigation is very important in NMR analysis.

2 NMR

The populations N^α and N^β of the energy levels of a nucleus with spin $I = 1/2$ in an external magnetic field B_0 are described by the Boltzmann statistics

$$\frac{N^\alpha}{N^\beta} = \exp\left(\frac{\Delta E}{kT}\right) = \exp\left(\frac{\gamma \hbar B_0}{kT}\right) = \exp\left(\frac{\hbar \nu}{kT}\right) \quad (14)$$

where k is the Boltzmann constant and T the temperature of the spin system, while ΔE is given by equation (10). The lower energy spin-up state α is energetically more favorable to populate, i.e. there are more spins in the energy state α as compared to β . Since all nuclei have a magnetic moment $\mu \neq 0$, the summation of all magnetic moments of the spin system results in a macroscopic bulk magnetization M

$$M = \sum \mu \quad (15)$$

As the spin population in the α state is higher the bulk magnetization is pointing to the z direction (or B_0 direction) which is shown in Figure 7 as a vector M and is usually described as M_z .

Applying a radiofrequency, which is tuned to the Larmor resonance frequency ω_0 (see equation (12)), induces a spin transition between the α and β states. Now more spins are in the spin-down state.

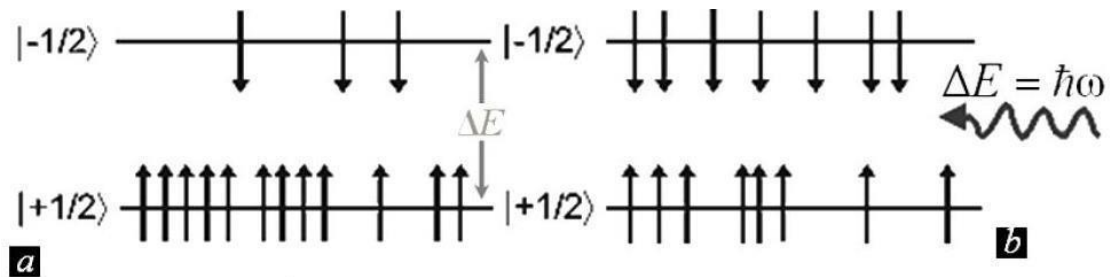


Figure 8: Energy splitting diagram for nuclei with spin $I = 1/2$ in a magnetic field B_0 (a). An r.f. pulse tuned to the Larmor frequency induces a spin transition between the spin-up and spin-down states (b).³⁹

Due to the small energy difference between the two states the wavelengths which are needed for nuclear spin excitation are in the radio frequency range. For instance, the resonance frequency for protons $\nu_0 = f(B_0)$ in a magnetic field of 2.3488 T is 100

MHz, this corresponds to a radio wavelength of $\lambda = 3$ m. The resonance frequency of the spins is proportional to the B_0 field as shown in Table 1.

Table 1: The resonance frequency is proportional to the B_0 field.

B_0 [T] (Tesla)	ν_0 [MHz]
1.4	60
5.9	250
9.4	400
14.1	600
21.2	900

Once the pulse at the resonance frequency is applied and the nuclear spins are excited, the population difference between the two energy levels soon goes to zero (saturation). The excitation process is, however, reversible and after finishing the radio frequency (r.f) pulse a so called relaxation process brings the system back to equilibrium. During the transition of the nuclear spin from higher to lower energy states energy from the spin system is emitted to the lattice and the bulk magnetization orients itself again parallel to the B_0 field (z-axis). The time constant of the recovery of the nuclear magnetization after the perturbation with a r.f. pulse is called the spin-lattice or longitudinal relaxation time T_1 .

As shown in Figure 9, an r.f. pulse (x-axis) tips the bulk magnetization M_z from its longitudinal equilibrium (z-axis) position to the y-axis resulting in a M_y magnetization.

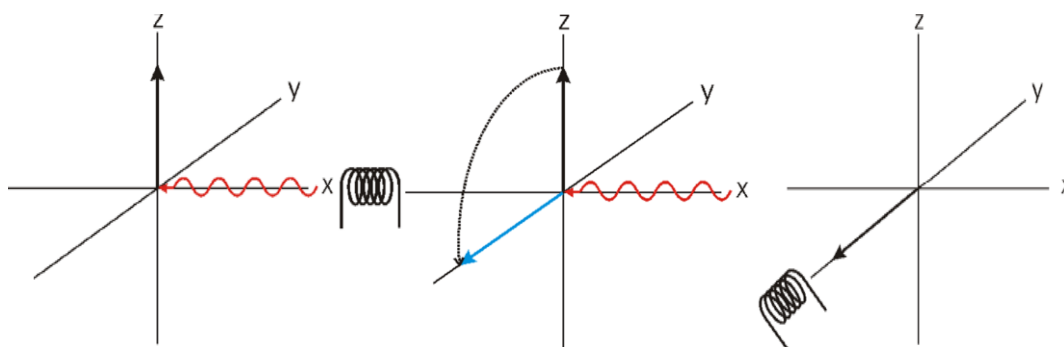


Figure 9: The magnetization under the influence of the radiofrequency coil.³⁸

The precessing transverse magnetization generates an oscillatory voltage in the coil around the y-axis. The oscillatory voltage can be detected with the receiver coil and constitutes the primary NMR signal. As one can see from the schematic drawing (Figure 10) the external magnet confines the magnetic field B_0 and the sample inside a glass tube is placed in the center. As described above the nuclear spins (of the sample) align relative to the B_0 field. The excitation of the spins is conducted by an r.f. coil (transmitter) and the oscillatory voltage created during the precession is registered by a receiver coil (instead of a second coil one can use also a bridge circuit). The amplified signal is transferred to a PC and after an analog to digital transformation the signal can be further processed.

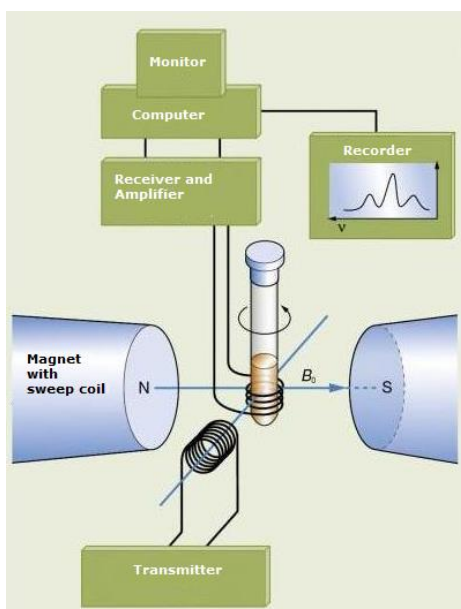


Figure 10: Schematic drawing of an NMR spectrometer (Continuous wave-technique).⁴⁰

The time dependence of the voltage shows a cosine modulation with the Larmor frequency ω_0 of the oscillating nuclei and it decays with the time constant T_2 , the spin-spin relaxation time. During the spin-spin-relaxation process the precessing transverse magnetization fans out in the x-y-plane, which results in an exponential decay of the oscillating voltage. The signal, induced by the precessing transverse magnetization is therefore described as free induction decay (FID). The obtained signal here is a function of time, therefore the time domain has to be converted to the frequency

domain via Fourier transformation (FT). The frequency domain of the signal gives the typical NMR spectra which are obtained in standard NMR measurements.

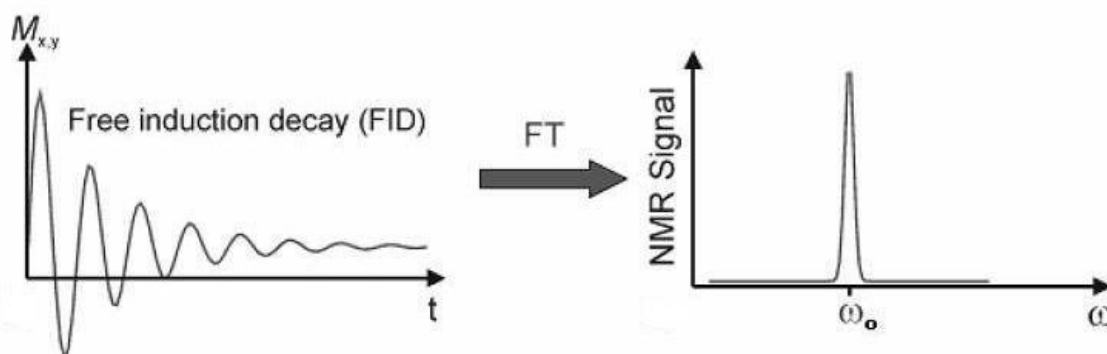


Figure 11: Free induction decay and Fourier transformation.³⁹

2.2.2 Chemical shift

The exact resonance frequency of a certain nucleus type depends on its chemical environment. The external magnetic field B_0 induces an electric current in the electron cloud surrounding the nucleus. This current induces itself a magnetic field. The induced magnetic field counteracts with the magnetic field at the site of the nucleus. Therefore, the effective magnetic field at the site of the nucleus differs from the external magnetic field B_0 resulting in a so called chemical shift δ .

$$B_{eff} = B_0 - \sigma B_0 \quad (16)$$

σB_0 is the induced magnetic field caused by B_0 and σ is the dimensionless shielding constant. Because of the chemical shift the resonance frequency is not the same as the Larmor frequency

$$\omega = \gamma B_0 (1 - \sigma) \quad (17)$$

The stronger a nucleus is shielded the bigger is σ and the smaller is B_{eff} . Therefore, the resonance frequency will be smaller and the signal of the nucleus will appear further right in the NMR spectrum (smaller ppm values, see Figure 12).

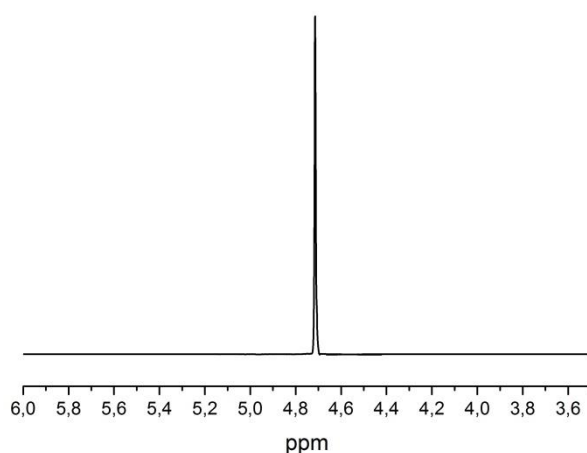


Figure 12: Typical ^1H -NMR spectrum of water

As the resonance frequency of a nucleus depends on the strength of B_0 , spectra taken on NMR machines with different field strengths are not comparable when using a frequency scale. For this reason the resonance frequencies are (1) weighted with the Larmor frequency of the corresponding nucleus at B_0 and (2) measured with respect to a reference compound, which defines a fixed point on the chemical scale (very often the zero point). This procedure defines dimensionless values of δ

$$\delta = \sigma_{ref} - \sigma \quad (18)$$

Where δ is calculated for a nucleus X as follows:

$$\delta(X) = 10^6 \frac{\Delta\omega}{\omega} \text{ with } \delta(\text{TMS}) = 0 \quad (19)$$

For the nucleus ^1H , tetramethylsilane (TMS, $\text{Si}(\text{CH}_3)_4$) is used as a standard and is set to $\delta = 0$. Because $\Delta\omega$ is very small as compared to ω , a factor 10^6 is introduced in equation (19), resulting in δ values given in *parts per million* (ppm, 10^{-6}), which have a convenient size. As an example, the methyl signal of acetic acid appears at 200 MHz which is 420 Hz shifted towards low field compared with the TMS signal. Stated in ppm, this corresponds to $\delta = 2.10$ ppm.

$$\delta_{\text{H}}(\text{CH}_3) = 10^6 \frac{420}{200 \cdot 10^6} = 2.10 \quad (20)$$

2.2.3 The ^1H -NMR spectra

As the example in Figure 13 shows the NMR spectra are giving information about the

- number of the chemically different nuclei of one nucleus type (three types of protons shown in different colors)
- chemical environment via chemical shift and the position of the resonances on the ppm scale (see different ppm values for each signal, e.g. 4.2 ppm etc.)
- number of protons in the vicinity via the structure of the signal and multiplicity (red: four lines, blue: one line etc.)
- relative ratio of protons to each other via integration of the signals (red: two protons, blue: three protons etc.)

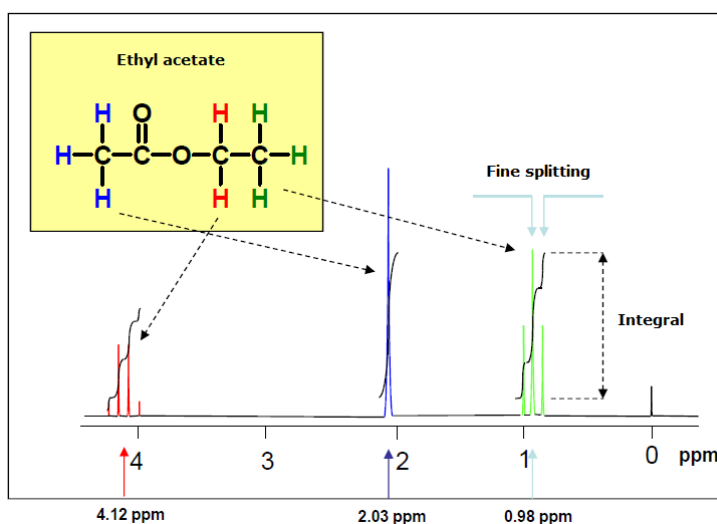


Figure 13: Fine splitting of the NMR signals. ³⁸

2.2.4 Coupling

As shown in the NMR spectrum (Figure 13) some peaks reveal a fine splitting of the signals into multiple subsignals. This splitting is caused by spin-spin coupling which appears via interaction of the magnetic moments of neighbor nuclei. This means that the nuclear magnetization of one nucleus is influenced by the nuclear magnetization of neighbor nuclei and vice versa. The spin-spin-coupling between the same types of nuclei is called homonuclear coupling and the coupling between different nuclei (e.g.

^1H and ^{13}C) is called heteronuclear coupling. For instance, the protons in red are influenced by the green ones and the green ones are influenced by the red ones. Unlike the green and red protons the three protons in blue have no protons in the vicinity and thus no coupling partner and no splitting. We see only one signal for three protons. Due to the reason that equivalent nuclei, i.e. nuclei belonging to the same isotope and having the same chemical shift, do not give rise to a coupling the blue signal in Figure 13 is not split. The splitting patterns that couplings give rise to, can be rationalized as follows: The spins of the neighboring protons of the resonant nucleus can arrange either parallel or antiparallel relative to B_0 . The number of possible arrangements can be determined as following. For instance, the nuclear magnetization of the magnetically equivalent methyl protons is influenced by the spins of neighboring two methylene protons. Possible arrangements are: both spins are parallel or antiparallel or one spin is parallel while the other is antiparallel or vice versa. Four possible arrangements with four energy levels are resulting, while two of them have degenerate energy levels. In this case, the number of signals and their intensities are described as 1:2:1.

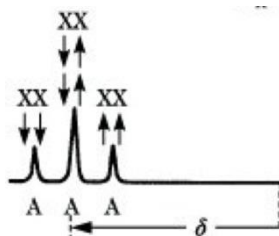


Figure 14: Arrangement of spins, number of signals and their intensities.⁴¹

The multiplicity for a nucleus A in an AX_n System for nuclear spin $I = 1/2$ is given by $n + 1$ lines. The number of neighbors and accordingly the number of signals and their intensities can be taken from the Pascal's triangle (Figure 15).

2 NMR

n , Number of Neighbors	Intensities of the $n + 1$ Lines							
0							1	singlet
1						1	1	doublet
2				1	2	1		triplet
3			1	3	3	1		quartet
4		1	4	6	4	1		quintet
5		1	5	10	10	5	1	sextet
6	1	6	15	20	15	6	1	septet

Figure 15: The Intensity of lines can be taken from the Pascal's triangle.⁴¹

As described in the example above and as it can be seen in the Pascal's triangle two neighbor protons ($n = 2$) are causing a signal to split into three subsignals ($n + 1$) with the intensity of 1:2:1. This type of signal splitting is called triplet. The distance between the sub signals is described by the coupling constant J and is given in Hz .

3 Microslot NMR detector

3.1 Introduction

While the information content of NMR is unsurpassed due to its high potential for structural identification and its non-destructive nature, it is the least sensitive technique within the standard analytical tools making its application to ultra-small samples difficult.^{28-30, 42, 43} Many efforts have been undertaken to enhance the sensitivity of NMR spectroscopy. Approaches like the use of higher magnetic fields⁴⁴ and the implementation of cryogenic probes⁴⁵ have been successfully applied. For instance, higher magnetic fields can be used to maximize ω_0 and accordingly to improve the sensitivity of the NMR spectrometers. One of the world's first high field magnets (23.5 T corresponding to $\omega_0 = 1$ GHz) was installed in 2009 at the Centre Européen de Résonance Magnétique Nucléaire à Très Hauts Champs in Lyon, France. For further sensitivity enhancement cryogenic probes can be used to cool the receiver coil and the preamplifiers to approximately -250°C in order to reduce the thermal noise caused by the coil. These improvements increase the sensitivity by a factor of two to four while the costs for all the improvements increase exponentially.²⁸ Therefore, these solutions involve high costs and could not solve the limitation of NMR particularly for mass- and volume-limited samples. For this purpose NMR probeheads with microcoils were introduced by Webb and coworkers in 1994.²⁷

Microcoils are miniaturized electrical conductor wires with different geometries like helical, saddle or planar. When an electric current is applied an electromagnetic field is generated along the wire. The electromagnetic field in the wire/coil has a magnetic field component B_1 which will be explained in chapter 3.2.1.

All these improvements enabled us to design in this work a microslot probehead which makes it possible to measure the metabolites of the ultra-small living cells sample inside a microfluidic glass device (NMR sample holder) with dynamical media and gas supply and with accurately controlled temperature in order to maintain the viability of the cells at near physiological conditions for long-term *in vitro* studies.

3.2 Background of NMR microcoils

NMR is one of the most powerful, information-rich and non-destructive analysis techniques for a wide range of samples from solid to liquid as mentioned in the NMR chapter 2. But the poor sensitivity is a big disadvantage of NMR. For instance, conventional NMR requires approx. 700 μl of sample whereas natural products and biological samples are found in the low nanoliter range. As one can see from the Figure 10 in chapter 2 the sample to be analyzed is placed inside an NMR glass tube (usually 5 mm inner diameter and filled with $\sim 700 \mu\text{l}$ liquid sample) and surrounded by a detection coil (receiver coil). For mass- and volume-limited samples the detection coil is too big resulting in a bad filling factor (small sample in big detection volume). As described by Hoult and Richards in 1976³¹ the diameter of an NMR coil is inversely proportional to its sensitivity. Therefore, one way to enhance the sensitivity and to enable the analysis of ultra-small samples is to construct a miniaturized radio frequency (rf) coil that will enclose the nanoliter sample to obtain a good filling factor. Currently microcoil probes are being used successfully to enhance the sensitivity of NMR for mass- and volume limited samples.^{27, 31, 46, 47}

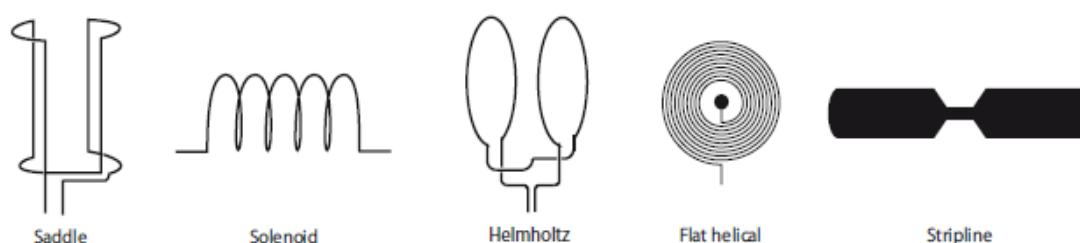


Figure 16: Possible geometries of miniaturized coils for NMR probes.²⁸

Figure 16 shows possible NMR coil geometries which are currently used. The saddle geometry coil generates a highly homogeneous magnetic field and is used in conventional liquid-state NMR. But, it is not suitable for miniaturization due to its complex geometry. The solenoid coil geometry is the easiest to fabricate by helical winding the conductor wire around the sample holder (e.g. capillary). With this method the coil size can be matched to the ultra-small sample size and thus a good filling factor can be achieved. Therefore, the performance of the solenoid coil appears

3 NMR microslot detector

to be better than that of the saddle coil.³¹ But the helical coil geometry impedes the integration of microfluidic chips and hence the use of the versatile LOC technology. Recently, new rf microcoil probes based on planar electromagnetic waveguide technology have been used successfully.^{24, 32-37, 48-51} With this new NMR probe design the hyphenation of the planar microslot probe with a LOC technology became possible.

3.2.1 Planar waveguide microslot NMR detector – How it works

Electromagnetic waveguide technology uses microstrips to route the high frequency signals on printed circuit boards. This new NMR probe (Figure 17) consists of a thin electrical conductor stripline (Figure 17, 101) made from copper which is placed above a non-conductive substrate (Figure 17, 103) consisting of polytetrafluoroethylene (PTFE). The opposite side of the substrate is completely covered with a copper layer, which serves as a ground plane (Figure 17, 105). A small rectangular microslot (Figure 17, 107) is cut out in the center of the stripline. The electric current which is flowing in the copper strip generates a magnetic field. Due to the reduced cross-section at the position of the microslot the current density increases resulting in a strong and confined magnetic field as shown in the schematic drawing (Figure 18) and the simulation (Figure 19). Therefore the microslot is the most sensitive area for detection and the sample (Figure 17, 110) to be analyzed is placed directly above the microslot (Figure 17, 107).⁵²

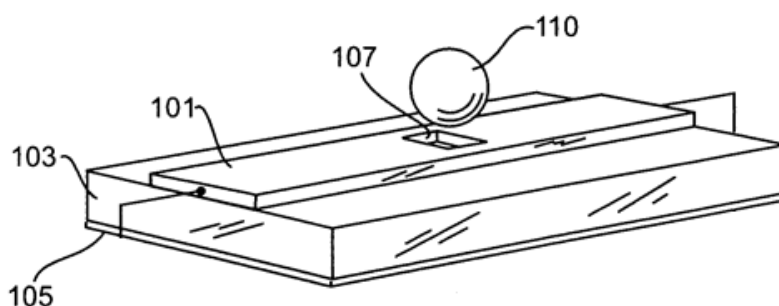


Figure 17: Schematic drawing of the copper/Teflon laminate and the microslot⁵²

3 NMR microslot detector

The NMR signal is just picked up in the $100\ \mu\text{m} \times 200\ \mu\text{m}$ slot area of the microstrip, where the B_1 field is confined. This is exactly the position, where the sample is located. The B_1 field in other areas of the structure is almost zero, as FEM simulations of the B_1 field distribution show (Figure 19).

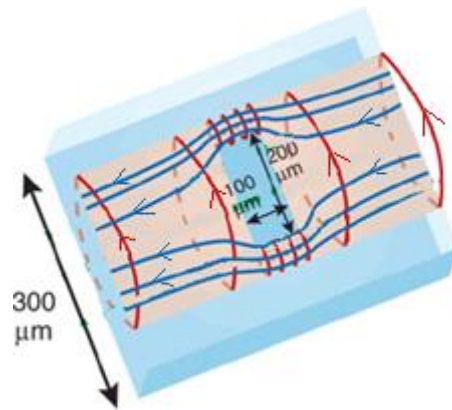


Figure 18: When electric current (blue) is applied a magnetic field is confined around the slot area (red).³⁷

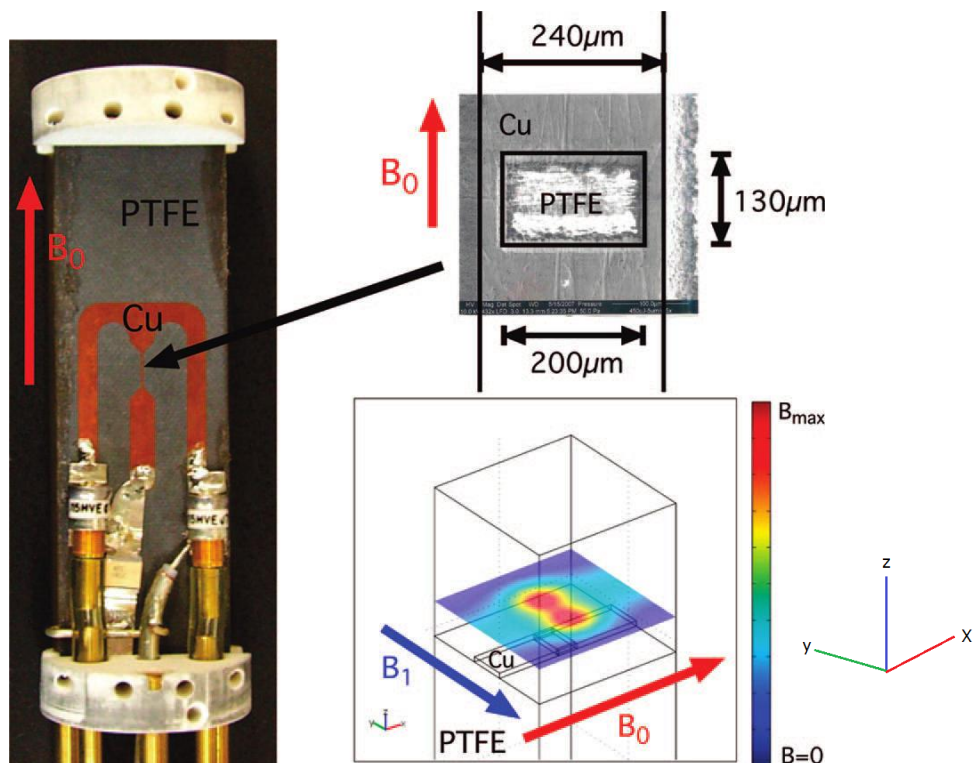


Figure 19: Microslot NMR probe. Magnified slot area and the simulation of the B_1 field distribution³²

3 NMR microslot detector

As mentioned in the Introduction, our aim is to enable long-term metabolomics analysis of living cells. To keep the cells alive under near physiological conditions we need to control the temperature at 37 °C. Therefore, we designed a microslot NMR probe as described by Maguire et al.⁵², improved it and added an on-board integrated heater (Deutsche Patentanmeldung 10 2014 115 702.8)⁵³ on the backside in order to control the temperature during the measurements. The on-board heater does not require any extra pieces and is printed on the copper ground plane which can be seen in chapter 3.4.2 in Figure 25 and in chapter 3.4.3 in Figure 29. The heating current does not produce any magnetic field due to the circular anti-spiral design. The temperature can be controlled from room temperature until 135 °C with low power consumption (0.05 W) and the size and geometry of the heater can be adjusted to the requirements of the experiment. Therefore, the planar, size adjustable and non-magnetic heater is not only highly suitable for NMR measurements but it can be also integrated to many other analytical tools.

3.3 Materials and Methods

3.3.1 Photolithography (Microslot NMR detector)

Photolithography is a common method to print geometric structures onto a substrate which contains a photosensitive chemical layer (photoresist). This method is not only used in semiconductor technology for generating circuit patterns but also widely used in LOC technology for applications in biotechnology and life sciences. The photolithographic generation of circuit patterns will be described here and the process of photolithography and the photolithographic generation of LOC devices will be described more in detail in chapter (4.1.2).

The photolithography technique described in the following part is used for the fabrication of standard printed circuit boards. With this technique a pattern from a mask foil will be transferred onto a substrate which has a thin film of photoresist on its surface. For this purpose a copper clad dielectric from Rogers RF-laminate RT5880 was purchased. This glass reinforced Teflon substrate has one of lowest tangent losses at RF frequencies (≈ 0.0004 at 1 GHz) and leads to an increase in the quality factor of the microslot. The substrate thickness was chosen to be 3 mm to minimize dielectric losses in the material.⁵² Therefore, the laminate consists of a 3 mm PTFE substrate sandwiched between two copper layers (each layer has 35 μm thickness). The copper surface was coated with a 5 μm positive photoresist (Basista - Leiterplatten GmbH, Germany). The geometric structure to be printed on the laminate was generated by Adobe Illustrator CC. The mask foil containing the structure with an optical density (OD) ≈ 3 was purchased (Merlin Belichtungsservice GmbH, Germany). Figure 20 shows the desired pattern, size and geometry of the laminate.

3 NMR microslot detector

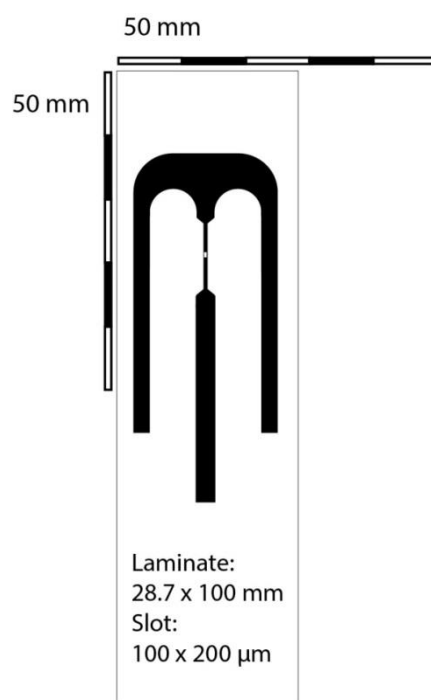


Figure 20: Geometry and size of the microslot probe

The Rogers RF-Laminate was cut into a 9.5 x 3 cm piece and covered from both sides with the mask foil. Afterwards, it was exposed to UV-light under vacuum for four minutes. The black areas of the mask foil have an OD \approx 3 therefore it protects the area underneath from the UV-light while the white areas are transparent and thus permeable for the UV-light. As shown in Figure 21, the photoresist (photosensitive polymer) exposed to UV-light is changing its chemical conformation. In case of a positive photoresist it becomes soluble and can subsequently be removed by rinsing with a 350 mM NaOH solution. After rinsing with distilled water the laminate is placed inside an etching bath with 1.7 M sodium persulfate solution. The solution is stirred for 25 minutes at 50 °C. During this process only the copper areas without photoresist are removed by etching. Afterwards, the laminate was rinsed with water and the remaining photoresist was removed as described above. Finally, the laminate board with the printed patterns was rinsed with water and dried. The results are shown in chapter 3.4 in Figure 29.

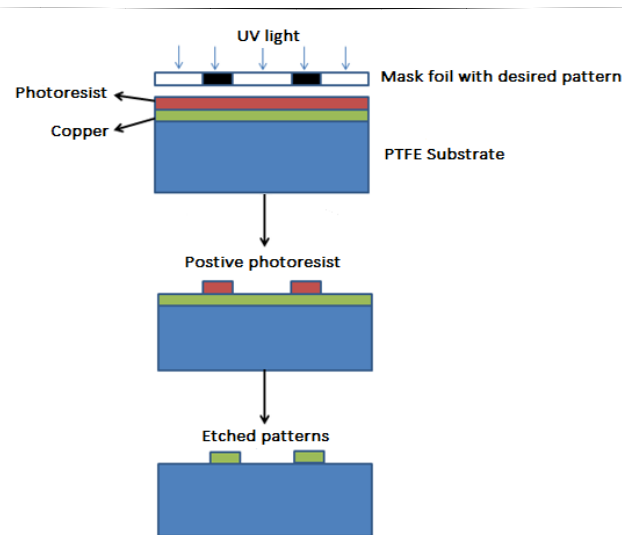


Figure 21: Process of photolithography

3.3.2 Microfabrication via Laser ablation (femtosecond laser)

Photolithography is suitable for printing geometrical structures onto a substrate (like circuit board printing) but it's a limited technique for printing structures in the low μm range with high aspect ratio (describes the ratio between width and height of the vertical structure). To overcome this limitation we have used a femtosecond laser (New Wave Research, USA) for a precise and controllable fabrication of the microslot. After several optimization steps the following parameters for laser ablation were figured out to be the best. The laser spot size was adjusted to $80\ \mu\text{m}$, the energy level of $200\ \mu\text{J}$ was selected and 40 scans were suitable for the ablation of the $35\ \mu\text{m}$ thick copper layer. We used a femtosecond laser for ablation because this method has a high aspect ratio which allows sub-micron accuracy and the short pulses avoid thermal damages and stresses in the copper which degrade the performance of the microslot.^{32, 54}

3.3.3 Fabrication of the waveguide microslot NMR probe

A lumped element circuit model of the waveguide detector is given in Figure 22. The main components of the r.f. resonant circuit are the r.f. coil (microslot) and the tunable capacitors.

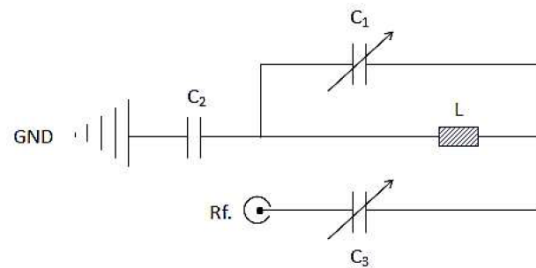


Figure 22: r.f. resonant circuit

C_1 and C_3 are variable capacitors, which are also called trim capacitors. The capacity of C_1 and C_3 can be adjusted mechanically and the resonance frequency can be shifted within a defined range. The C_2 is the fixed-value capacitor and L is the inductivity of the microslot. First, one feed line of the C_2 was connected (by soldering) to the middle copper strip which leads to the microslot. The other feed line of C_2 was connected to the ground (GND) on the backside of the board. The backside must have also a contact with the housing of the probe. The screws for fixing the cap with the housing are serving this purpose. This way, the circuit board is connected with the aluminum housing of the probehead. After the installation of the probehead into the spectrometer, the board is connected to the ground via the housing. Afterwards, the feed line of C_3 was connected to one of the outer copper strips, while the second feed line of C_3 was connected to the semi-rigid RF-cable. The other outer copper strip was connected to one of the feed lines of C_1 , the second feed line of C_1 was connected to C_2 . The trim capacitors have to be accessible for a screwdriver so that their capacity can be changed and adjusted for the following tune and match process. The RF-cable was mounted with the same length, which will be used for assembly of the probe, as the capacity depends on the length of the cable. Then, an N-connector (optionally BNC-connector) was mounted at the other end of the RF-cable and was finally connected to the network analyzer.

3.3.4 Quality factor

With the help of the quality factor Q the sensitivity of a probe can be evaluated. Q is a dimensionless value which describes the effect of damping on an oscillator. In order to figure out the Q value, the microslot probe is connected to the network analyzer (Agilent Technologies, USA). The standing wave ratio (SWR) mode was selected for the analyzer. The marker was set on the desired resonance frequency. By adjusting C_1 and C_3 the marker position was placed on the minimum of the resonance curve so that SWR was close to 1 (1.01 optimum).

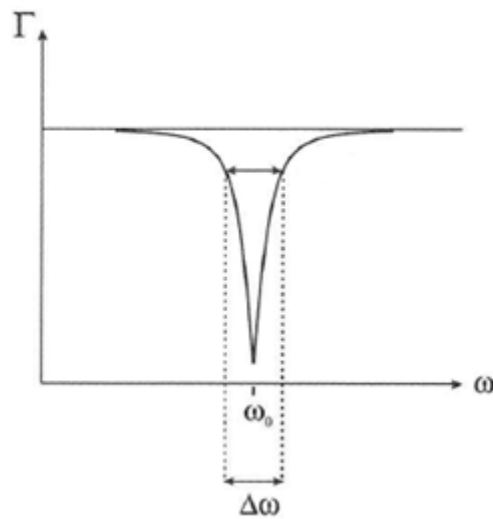


Figure 23: The resonance curve when the Larmor frequency is reached.⁵⁵

In Figure 23 a typical resonance curve can be seen and the Q value can be defined as its resonance frequency divided by its resonance width.

$$Q = \frac{\omega_0}{\Delta\omega} \quad (21)$$

It is visible that a deep resonance curve and a narrow resonance width are leading to a high Q factor. The lower the damping the higher is the Q factor.⁵⁶

3.3.5 Shimming

After the design and fabrication of the microslot probehead a glass capillary with 50 μm wall thickness, 1 mm inner diameter and 3 cm length was filled with water. Both ends of the capillary were closed with Kerr wax. The capillary was placed vertically above the slot and fixed with a Kapton[®] polyimide film tape (3M[™], USA). The cap of the housing is closed with appropriate screws and the probehead is inserted into the spectrometer and connected to the NMR hardware.

After setting the acquisition parameters and starting the measurement, the water signal is distorted, has a large line width and a bad signal to noise ratio (S/N): Insertion of a sample into the magnetic field changes the spatial distribution of the B_0 field, as the diamagnetic susceptibility of the sample differs from that of air. The distribution of the magnetic field strength in the sample volume is reflected in a corresponding distribution of resonance frequencies, as field strength and resonance frequencies are proportional. This results in a distorted NMR signal. Replacing the sample with another having a slightly different fill height, slightly different sample holder/tube etc. will again cause a noticeable change in NMR signal shape.⁵⁷ This problem can be solved by 'shimming', which is a process in which the homogeneity of the field B_0 is corrected. The NMR magnet contains, in addition to the main coil, an array of correction ("shim") coils.⁵⁸ By variation of the magnetic field of the shim coils the homogeneity of the main magnetic field B_0 can be adjusted to the new sample. Since every sample has an influence on the main magnetic field the shimming has to be done after inserting a new sample into the spectrometer. Conventional NMR probeheads can be shimmed automatically with a software on the spectrometer computer. The software uses the signal height of the deuterium signal as an optimization criterion: A second NMR experiment is run in parallel on the deuterium channel (lock channel) of the spectrometer. If the line width of the deuterium signal decreases as a result of "shimming", the signal intensity increases correspondingly. For this purpose the sample to be analyzed has to be deuterated so that the deuterium NMR signal can be used as a lock-signal. However, the homebuilt microslot NMR probehead does not comprise a deuterium channel so that shimming has to be done manually by changing

3 NMR microslot detector

the electric currents of the shim coils in a trial and error procedure. This process is continued until no further signal shape optimization is reached.

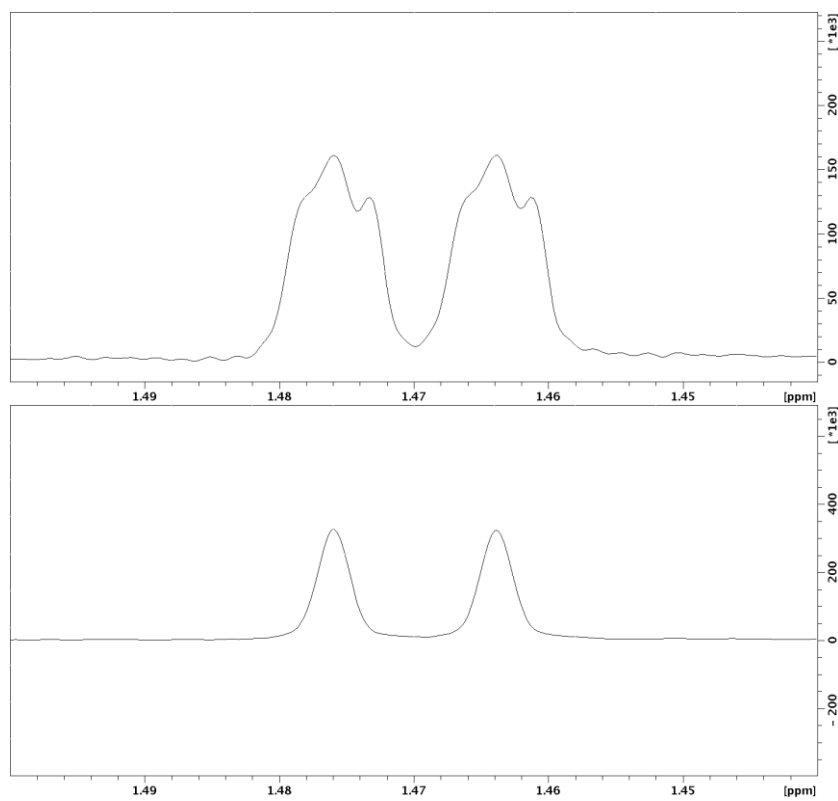


Figure 24: ^1H -NMR spectrum of alanine CH₃ signal (doublet) and the effect of shimming. Signal shape, intensity and line width before (top) are clearly optimized after shimming (bottom).

Since the planar geometry of the microslot probehead is not symmetric like a solenoidal and helical coil, the shimming is more time consuming.

Signal to noise values of 80.000 and line widths of 4 Hz could be achieved.

3.3.6 Nutation curve

Besides the quality factor Q the nutation curve is a characteristic feature and an indicator for the sensitivity of the microslot NMR probe.

After shimming and optimization of the NMR signal shape (linewidth, signal height, S/N-ratio) a nutation curve was recorded. For this purpose, a series of one-pulse experiments were conducted while the pulse length was incremented in steps of 0.5 μs . The nutation curve experiment allows for an analysis of the B_1 -homogeneity of the probe: If two consecutive maxima of the curve, corresponding to the 90 degree and 450 degree pulse, differ by less than 80% in their intensity, the probehead has a B_1 homogeneity comparable to that of a commercial probehead.

3.4 Results and Discussion

3.4.1 NMR detector fabrication and the setup of a resonance circuit

The resonance circuit pattern was designed by the vector graphics software Inkscape V4.0. The resonance conditions, resistivity, joule heating and the heat transfer as well as the circuit quality were simulated with Mini Ring Core Calculator V1.2 and Comsol multiphysics V4.2. The simulated circuit pattern was transferred by photolithography and etching techniques via the prepared photomask on a 3.15 mm reinforced PTFE laminate coated with 35 μm double layer copper (Rogers RT/duroid 5880 high-frequency laminate). The micromachining of the 200 μm x 100 μm microslot detector on a 300 μm copper waveguide was performed by femtosecond laser ablation. A scanning electron microscope (SEM) and a photo microscope were used to control the microslot dimensionality and the shape quality. Nonmagnetic trimmer capacitors (Type NMAJ15HVE, Voltronics Corp., USA) with a range of 1-16 pF were used for tuning the circuit to 600 MHz and matching the circuit impedance to 50 Ohm, the fixed capacitor was a 1 pF ATC chip capacitor (700 C series). A semirigid coaxial cable (EZ 141-TP/M17) was used to transfer and to pick up the r.f. pulses. The resonance condition and the electrical measurements were controlled and measured by using a network analyzer (Agilent AN 1287-1). The resonance circuit of the probe has a Q-factor of about 115.

3.4.2 Design and Photolithography of the microstrip detector

The resonance circuit pattern of the NMR microslot probe was designed by the vector graphics software Inkscape V4.0 and is shown in Figure 25.

3 NMR microslot detector

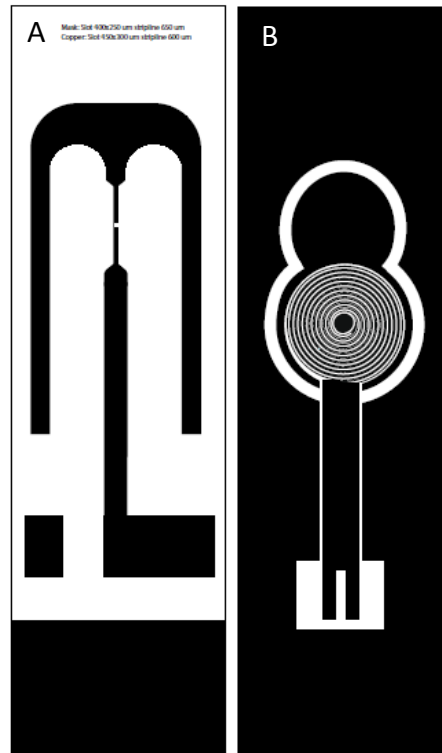


Figure 25: Drawing /design for the mask foil. Front side containing the microslot (A) and back side containing the circular anti-spiral heater (B) of the NMR microslot board. After transferring the pattern on the mask foil onto the copper/Teflon laminate the black areas will consist of copper and the transparent (here white) areas will consist of PTFE.

The designed pattern was transferred onto a mask foil by film exposure (Merlin digital, Germany). This method results in a mask foil with high optical density (OD) of about 3. The OD value has no units and is a suitable way to describe the ability of an optical filter to block the light (e.g. UV light etc.). The higher the OD the better the results of the photolithography will be. Figure 26 shows two examples of mask foils with low (A) OD obtained by printing and high (B) OD obtained by film exposure. As it can be seen clearly the usual printing techniques are not sufficient to create a high OD.

3 NMR microslot detector

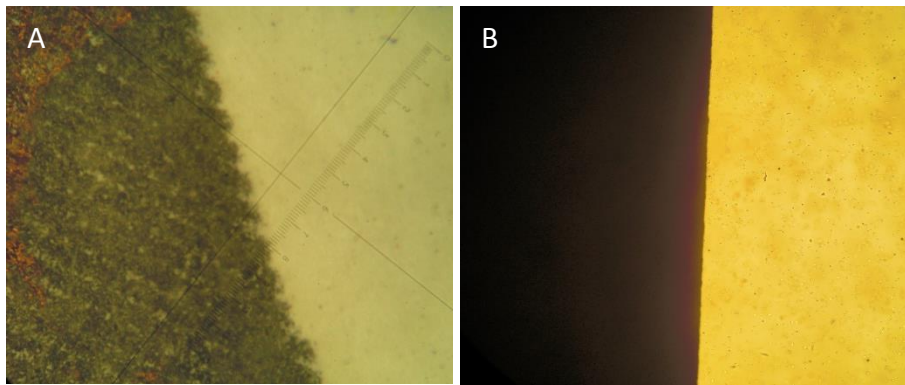


Figure 26: Light microscope image (65x) of the mask foils with low OD (A) generated by printing and high OD (right) generated by film exposure.

Afterwards the mask foils are used to transfer the structures onto the PTFE laminate coated with copper by photolithography and etching (as described in 3.3.1). As it can be seen in Figure 27 the quality of the mask foil has a big effect on the quality of the circuit. The mask foil with lower OD results in a rough copper surface with several bumps and holes (A). This distortions will lead to stress, thermal heating and to small and local magnetic fields around the holes in the copper. While the mask foil with high OD results in a smooth copper surface which in turn will increase the quality of the resonant circuit.

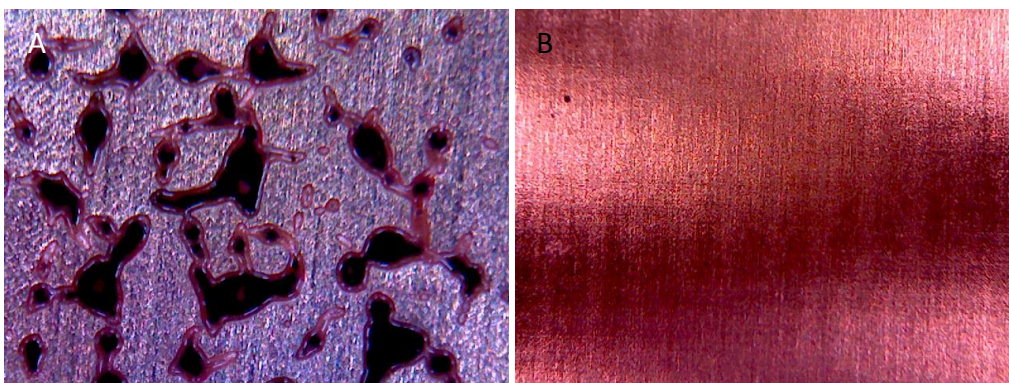


Figure 27: Light microscope image (65x) of the copper surface after photolithography Mask foils with low OD values are causing a rough copper surface with bumps and holes (A).

3.4.3 Laser ablation

The fabrication of sub-microstructures like the microslot on the thick copper layer is limited with standard photolithography techniques or requires high quality mask foils which is accompanied with high costs. Also the etching process after the photo treatment is difficult to control and not always reproducible. As it can be seen from the picture in Figure 28 A and B the shape and the edges of the microslot are not smooth and sharp after the photolithography and etching process. This will lead to thermal heat and stress lowering the performance of the microslot. To overcome the drawbacks of the photolithographic and etching process we used a femtosecond laser. This technique allows the microfabrication of very precise microstructures with high aspect ratio. Via laser ablation, geometric structures down to 1 μm and lower can be printed into a 35 μm thick copper layer with high precision. This technique doesn't require any other additional equipment like mask foil and the structuring process of small areas like the microslot can be done within seconds. By comparing the pictures A-D in Figure 28 the effect of laser ablation can be seen clearly.

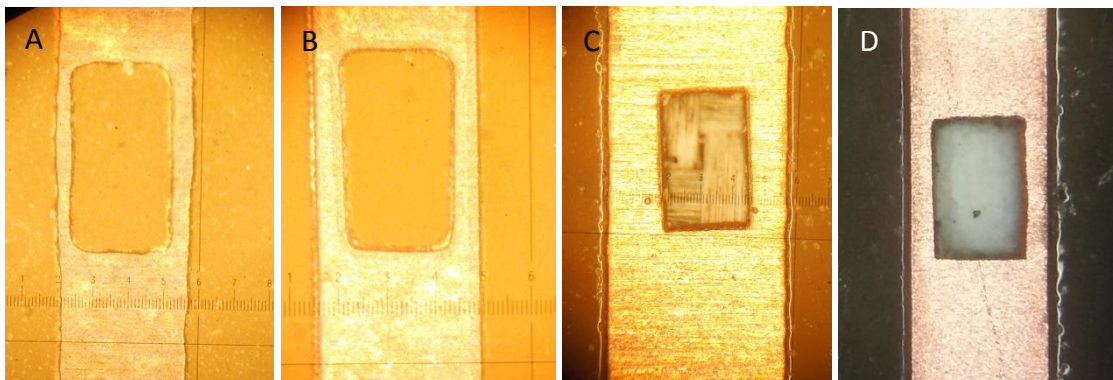


Figure 28: of Light microscope image (50x) of the microslot. After photolithography with low OD mask foil (A), with high OD mask foil, with high OD mask foil and laser ablation (C, D).

The microslot A was obtained with a low OD mask foil and no laser ablation was conducted. Not only the shape of the microslot is distorted but also the copper stripline is wavy and has low quality. The microslot B was obtained with high OD mask foil and also here no laser ablation was conducted. The copper stripline is

3 NMR microslot detector

smooth and sharp showing the positive effect of the high OD mask foil. But the microslot lacks symmetry and requires an additional treatment with laser. Therefore, the same high OD mask foil was used for the microslot C and D and afterwards the slot was shaped via laser ablation. The tilted microslot C is showing that a careful alignment of the laser is here of big importance and has to be taken into account during ablation. Otherwise the slot geometry will be shifted, resulting in a poor performance of the microslot. The microslot D has a good copper stripline quality and after laser ablation the slot geometry is precise and symmetric which will enhance the performance of the NMR microslot detector.

After photolithography, etching and laser ablation the designed pattern in Figure 25 is finally transferred onto the PTFE/copper laminate and can be seen in Figure 29.



Figure 29: Picture of the printed circuit board (NMR microslot detector) after photolithography and laser ablation of the microslot (left) and circular anti-spiral heater (right).

Taken together, the combination of photolithography and laser ablation techniques resulted in a good quality resonance circuit for a reasonable price.

3.4.4 Assembly of the probehead

In the following sections the printed circuit board will be named NMR microslot detector. After photolithography it is ready for further electrical assembling. All necessary details are described in chapters 3.3.3 and 3.4.1. As it can be seen in Figure 30 the NMR microslot detector (D) is mounted on a holder (B, C, E) in order to insert the probehead into the NMR spectrometer (A). The microslot detector has to be placed exactly at the so called sweet spot of the superconducting magnet of the spectrometer. The sweet spot is the most homogeneous area of the superconducting magnet. This spot was determined by manually changing the position of the probehead by lifting it up and down and turning it clockwise or counter clockwise.

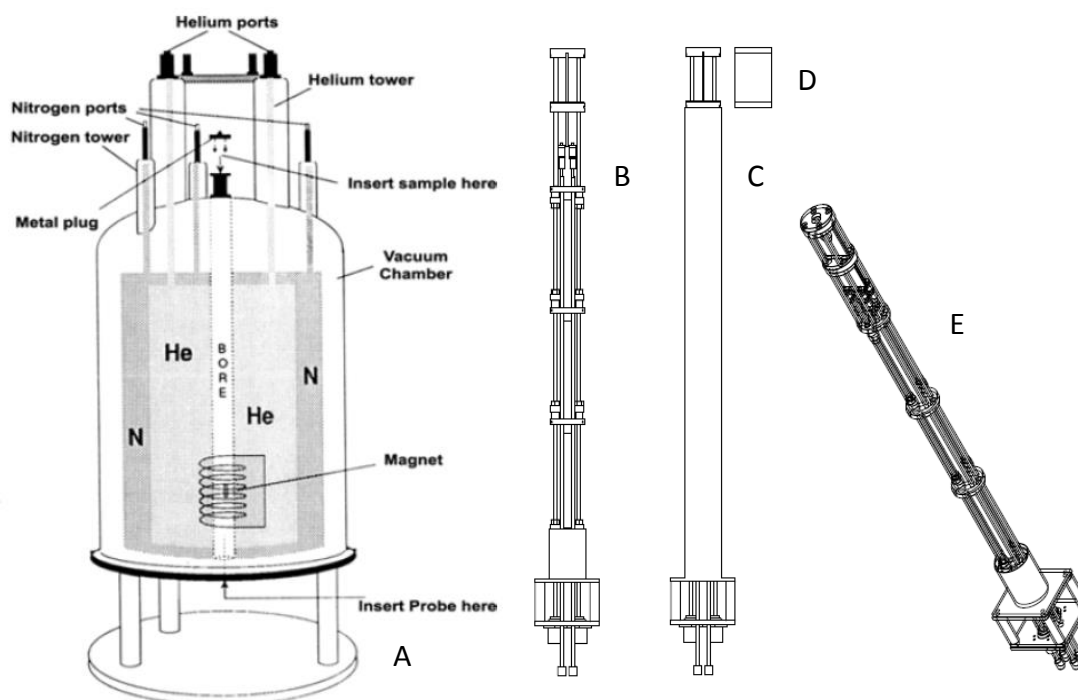


Figure 30: NMR spectrometer magnet inside view (A). NMR probehead without shelf (B) and with shelf (C), NMR microslot detector (D) is shown separated from the probe, 3D view of probehead (E).

3.4.5 Simulation of the B_1 field distribution

The B_1 field distribution of the microslot detector, simulated with COMSOL Multiphysics 4.2, is shown in Figure 31. The B_1 field is confined in the slot area of the microstrip detector. The NMR signal is just picked up in the $100\ \mu\text{m} \times 200\ \mu\text{m}$ slot area of the microstrip, where the B_1 field is confined. This is exactly the position, where the spheroid is located. The B_1 field in other areas is almost zero. Therefore, the microslot is the most sensitive area for detection.

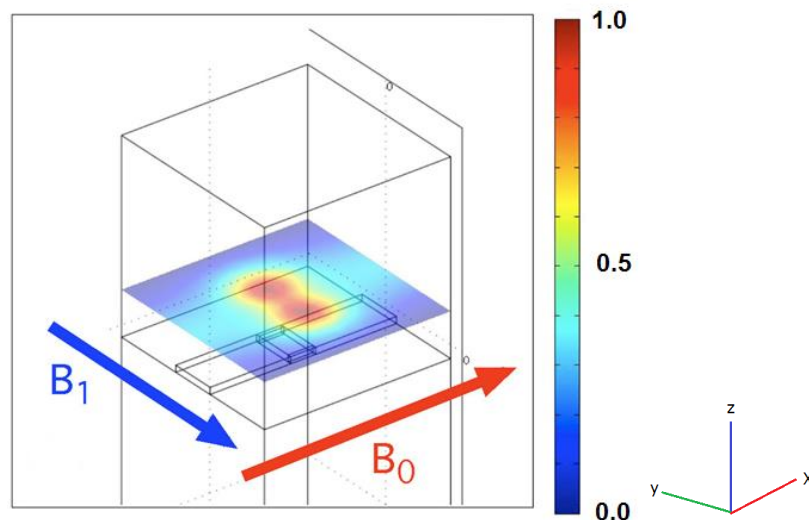


Figure 31: Simulated distribution of the B_1 field strength over the microslot area ($100 \times 200\ \mu\text{m}$). Contour levels are given as a fraction of the nominal B_1 field strength field distribution for the $100 \times 200\ \mu\text{m}$ slot (B_y -field component, B_0 indicates the static magnetic field of the spectrometer magnet and B_1 is the magnetic field generated by the microslot).

4 Microfluidics and LOC

In the section above we discussed the importance of miniaturized detection coils for mass- and volume-limited samples. This improvement led to the idea that miniaturized detection coils require miniaturized sample holders. Therefore, miniaturization opens up the new subject of microfluidics and lab-on-a-chip (LOC).

Microfluidics is the science and technology of systems that deal with ultra-small amounts of fluids (10^{-9} to 10^{-18} liters)⁵⁹ and ultra-small samples (like single cell having diameters between $1\ \mu\text{m}$ to $100\ \mu\text{m}$)⁶⁰. Not only its obvious characteristic -small size- but also the ability to process and manipulate the samples inside microchambers and microchannels with dimensions of tens to hundreds micrometers is of big advantage.⁵⁹ Since the concept of micro total analysis systems (μTAS), later indicated as LOC²⁰, was introduced the first time by Manz et al. in the early 1990s, the miniaturization of conventional laboratory techniques is of great importance in the expanding life sciences.

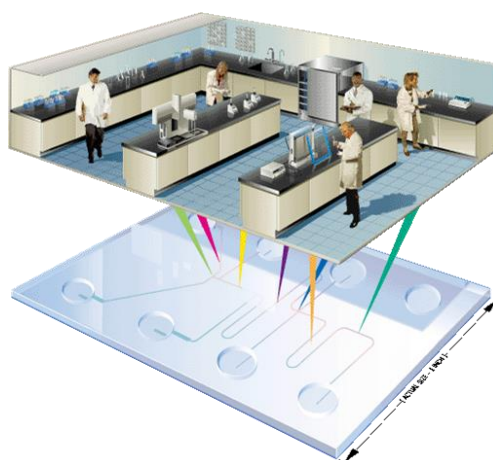


Figure 32: Lab-on-a-chip illustration⁶¹

For instance, in chemical and biological analysis and synthesis as well as in clinical diagnosis or in genomic, proteomic and metabolic studies new systems are developed which aim to replace and improve the conventional laboratory analysis systems. Recent progress in nanotechnology has opened up the development of new and remarkable systems like LOC which should replace and improve conventional

laboratory methods by miniaturization.^{62, 63} The goal of miniaturization is to reduce analysis time and costs with parallel analyses and small sample volumes by providing low limits of detection. Further goals are portability of the system and on-site detection. Thus, the basic idea behind LOC is to perform the functions of large analytical devices in small units and finally to connect these units to a complete analysis system. Therefore, the aim is the miniaturization of an overall analytical process from sample preparation through reaction and separation to detection on a single microchip.^{63, 64} For instance, cell-based assays inside microsystems should cover all steps from cell culture to biochemical analysis as shown in Figure 33.



Figure 33: Microsystems enable the cell-based assays from cell culture to biochemical analysis⁶⁵

In summary, these microsystems should allow the realization of reasonable, fast and cost effective analysis of tiny amounts of samples with enhanced sensitivity and automation of nearly all necessary processes from sample preparation to outcome of analysis results. In consequence, the applications of a LOC device range from clinical diagnostics to biosecurity and to research needs including genomics, proteomics and metabolomics.⁶⁶

4.1 Microsystems enabling cell-based assays

Cells are subjected to multiple internal and external factors which vary in time and space, including hormones, cytokines and growth factors produced by local or distant cells, cell-cell contacts and many other factors (will be explained in detail in chapter 5). Microfluidic devices can keep the cells within these factors in a miniaturized, controllable and reproducible way which is not always possible with standard cell culture. Additionally, these microfluidic systems can be used to link cell culture with

integrated analytical devices like NMR to study the biochemical processes that manage cell behavior which is the overall aim of this work (see chapter 6). While some cell-based microfluidic systems present only the miniaturization of conventional laboratory techniques, others exploit several additional abilities such as to create well-controlled laminar flow which can transport e.g. nutrients in order to ensure the viability of cells.⁶⁵ But microfluidic devices not only keep cells alive, they also enable an easy handling of ultra-small samples and preserve the *in vivo* like state of vascularized tumors. For instance, in an *in vivo* system the homeostatic state of the cell is maintained by constantly removing waste products and delivering nutrients with the help of the blood circulation. For this purpose many microfabricated systems are available to create and control the physiological relevant environment of the cell samples by using LOC framework.¹⁹ With the combination of microfabricated structures and microfluidic networks, LOC frameworks seek to create microsystems which can mimic near physiological conditions like blood vessels, nutrients supply and temperature and gas control. For instance, it was found out that hepatocytes (liver tissue) form a complex 3D environment with blood capillaries and bile canaliculi (see chapter 5.1.5 Figure 55) which allows a perfusion with nutrients, oxygen and soluble factors.⁶⁵ But primary isolated hepatocytes which were kept under standard 2D *in vitro* cell culture conditions have been found out to lose liver specific function. To replicate the liver tissue specific environment a scalable microreactor system was built which promotes the improvement of 3D-perfused micro-tissue units. Gene- and protein expression analysis and biochemical activity metrics revealed that primary rat cells cultured in this system were shown to be closer to native liver tissue when compared to cells cultured by other *in vitro* methods.⁶⁷ Another example of a microfabricated array bioreactor for perfused 3D liver culture⁶⁸ is shown in Figure 34. The silicon substrate consists of perfused liver reactors which have been fabricated on arrays of 300 μm wide channels that comprise the extracellular matrix (ECM) scaffold. The 3D reactor has been filled with pre-aggregated hepatocyte spheroids. With this method the spheroid cultures are viable for approximately 3 weeks and show a stable differentiated phenotype. Proteomics and genomics analysis on these cells revealed similarities with real tissue samples. Also cell-cell contacts, such as tight junctions and

desmosomes are found in 3D liver cultures which are similar to those found in tissue *in vivo*.^{65, 67, 68} Therefore, microfabricated systems create physiologically relevant environment and gave the opportunity to culture cells *in vitro* such as liver cells for long-term. As model systems for *in vitro* analogues of organ tissue it can be applied in toxicological studies by exposing to drugs or environmental factors. This system could also serve as a disease model for the analysis of viral hepatitis infection or even cancer metastasis. These results lead to the idea that microfabricated systems for cells can be implemented in applied and basic biomedical research.^{65, 67}

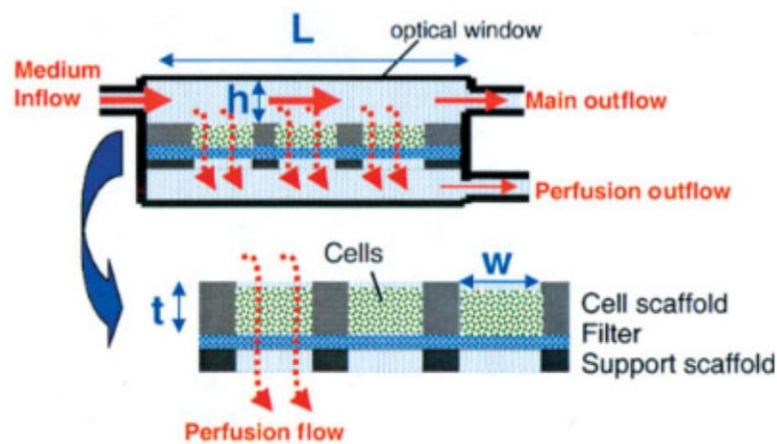


Figure 34: Mimicking *in vivo* like tissue environment in a LOC device⁶⁸

Taken together, microfabricated systems reduce the analysis time and cost, enable high-throughput analysis, allow portability and on site detection.²¹⁻²⁶ Miniaturized devices not only minimize the sample volume, but also create a physiologically relevant *in vivo* like environment. This opens new opportunities for the spatial and temporal control of cell growth and stimuli with the help of microsystems.⁶⁵

4.1.1 Microfabrication and Micropatterning techniques

The adaptation and integration of microsystems technology into cell-based assays emphasizes the need for advanced surfaces that are mimicking the spatial organization of cells in tissues. Microfabrication combined with micropatterning techniques with various surface chemistries enables to reproducibly engineer the surfaces that

replicate the microenvironment of tissues.^{65, 69} For this purpose, many methods were developed to fabricate micro total analysis devices consisting of miniature structures of micrometer sizes and smaller. Techniques like microtransfer molding for generating microstructures of organic polymers and ceramics in three dimensions using a layer-by-layer structuring were used.^{63, 70} Another different microdevice fabrication technique is based on imprinting structures in to polymers like PMMA by using an inverse three-dimensional image of the device micromachined on silicon^{63, 70, 71} or other materials. Another microfabrication technique is based on lithography and uses SU-8 negative photoresist for the fabrication of high-aspect-ratio structures.^{63, 70} Using alternating spin-coating of SU-8 photoresist and exposure steps followed by a single development step to remove the unpolymerized resist Guerin et al. have fabricated monolithic SU-8 channels.^{63, 70, 72} Nowadays, the most popular surface-patterning technique is standard photolithography liftoff techniques, photo reactive chemistry and soft lithography (like microcontact printing (μ CP) which will be used and explained in chapter 5.1.8).

Photolithography was used in chapter 3.3.1 for the fabrication of the NMR microslot probe. In the following chapter photolithography will be used for the fabrication of LOC devices and is explained more in detail.

4.1.2 Photolithography (fabrication of the silicon wafer for the PDMS chip)

The photolithography technique which will be explained more in detail in this section is the process of transferring geometric shapes from a mask to the surface of a substrate wafer.^{63, 73} For this purpose the wafer is coated with a resist and a mask which contains the desired pattern. Figure 35 shows the pattern differences generated from the use of positive and negative resist.

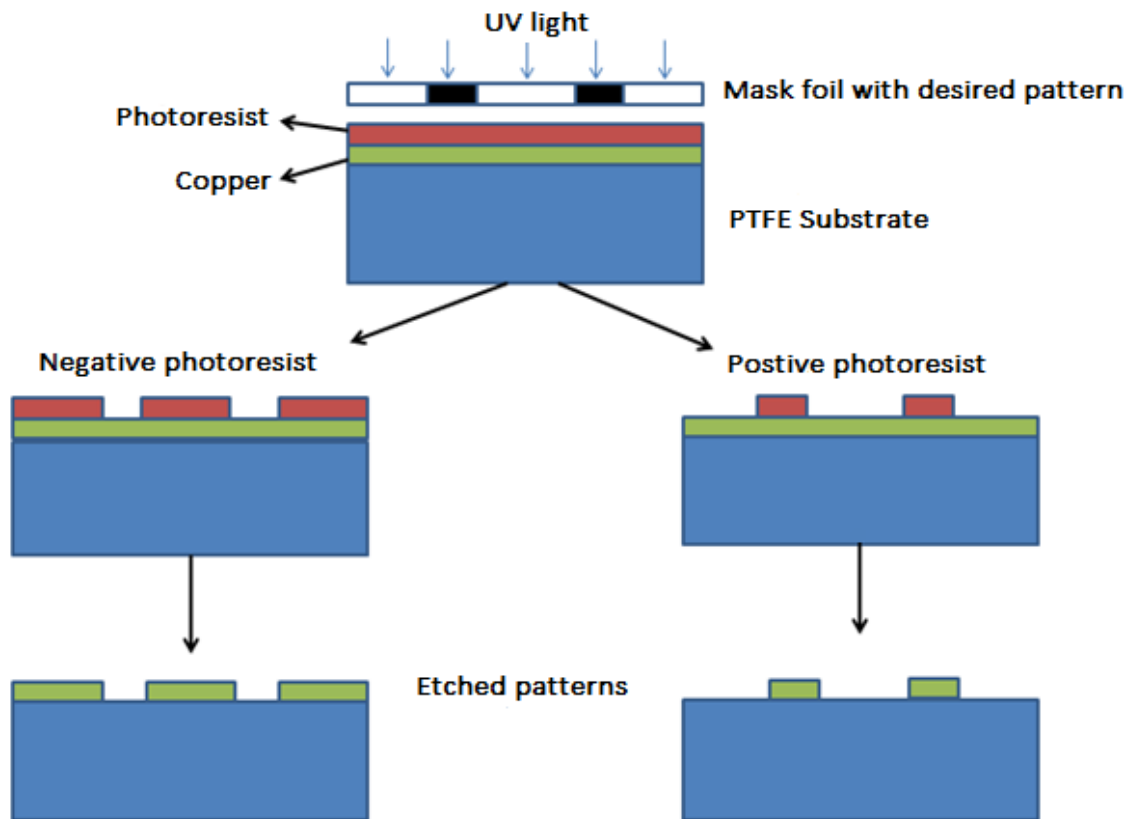


Figure 35: Illustration of the photolithography process with positive and negative resist. The dark field on the mask indicates the area which is impermeable for light. With the positive resist the exact copy of the pattern on the mask is transferred on to the wafer, whereas the inverse pattern is transferred on to the wafer with negative resist ⁷⁴

The positive resist (e.g. AR-U4040) is used wherever the underlying material is to be removed. For instance when the resist is exposed to UV light the chemical structure of the polymer is changed due to photochemically induced chain scissions in the polymer, thus the resist becomes more soluble in the developer. The exposed resist is then washed away by the developer solution leaving windows of the bare underlying material which in turn can be etched away. Finally the exact copy of the desired pattern which was on the mask remains on the surface.

On the contrary, the negative resist (e.g. SU-8) behaves in the exact opposite manner. When the negative resist is exposed to UV light the resist becomes polymerized and thus more difficult to dissolve. Because of this reason the developer solution can

remove only the unexposed resist whereas the exposed resist remains on the surface. This results in the transfer of an inverse pattern which was initially on the mask.

The silicon wafer (chapter 4.3.2, Figure 40) which was used in this work for the production of the PDMS chip was fabricated as described above but the final etching process as shown in Figure 35 was not conducted. For this purpose the silicon wafer was coated with SU-8 photoresist. The UV treated areas of the resist become insoluble while the untreated areas can be removed by a solvent. The silicon wafer with the remaining resist constitutes the desired pattern and is called the master. The PDMS chip can be produced by molding from this resist structure on the master (see 4.1.3 Figure 36). With this method structure sizes down to 120 nm at a pitch of 240 nm can be obtained. Micrometer and millimeter scales can be achieved also e.g. by multilayer processing.⁷⁵

4.1.3 Soft lithography (fabrication of the PDMS chip)

As mentioned in 4.1.1 one of the most common techniques for the fabrication of microfluidic devices is photolithography. Nevertheless, it has some drawbacks like the need for clean rooms for the fabrication of the masters which involves sometimes high costs and limited access to microfabrication labs. Especially when working with silicon or glass as a substrate, a major problem is the bonding of the mating glass substrates in order to enclose the chamber or channel structure (see 4.1.4). Also the surface treatment of glass for the generation of chemical functional groups is problematic since the solvents needed for this treatment are not always biocompatible.⁷⁶

To overcome these drawbacks Whiteside and colleagues⁷⁷ introduced the idea to use a silicon wafer with photoresist structure as a master in order to produce PDMS chips by molding as shown in Figure 36. For this purpose the viscous prepolymer was casted onto the master (see step 2) and allowed to polymerize. Afterwards, the polymer is peeled off and contains the inverted pattern which was on the surface of the master (see step 3). This process is called soft lithography because soft materials like PDMS were used. By using this fast, easy and cheap method one can generate several PDMS

chip replicates without the need for a microfabrication lab. The only time and money consuming part - the silicon master fabrication - needs to be done once at the beginning or can be obtained commercially if no microfabrication lab is available.

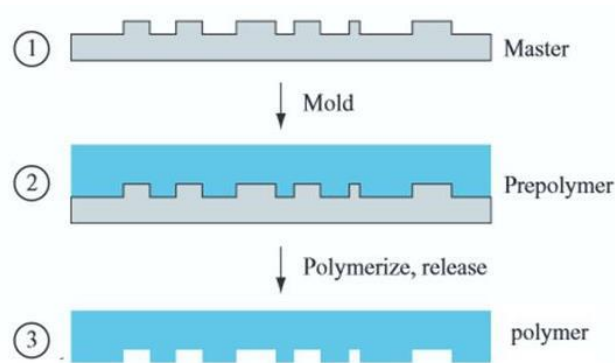


Figure 36: After casting the prepolymer onto the master (which contains usually a resist structure) the molded polymer can be peeled off easily and contains the inverted pattern of the master.

4.1.4 PDMS Chip assembly and plasma generator

Not only the micropatterning but also the bonding of the microchip is of big importance. The molded substrate which is obtained by soft lithography (see 4.1.3) needs to be sealed against an unstructured substrate in order to form microchambers and microchannels e.g. to capture cells and tissues. Compared with glass or silicon the greatest advantage of elastomeric polymers is that they can be easily treated with plasma. Plasma leads to chain scission of the polymer and oxidizes the surface. Finally the plasma activated surface of the mating pieces can be clamped together. The pieces stick to each other and are bonded chemically without the use of additional chemicals and glues (like for glass) and without destroying the structure of the channels.

4.2 Materials and Methods

4.2.1 PDMS chip

The silicon wafer containing the chip structure (master) was fabricated by molding a SU-8 photo resist coated wafer by standard photolithography methods at the MST microfabrication lab at the TU Dortmund. For the PDMS fabrication Sylgard 184 Silicone Elastomer Kit (Dow Corning Corporation, USA) was used. The base reagent was mixed with curing agent at a 10:1 (w/w) ratio. After mixing thoroughly, the prepolymer was degassed for 30 min inside a vacuum chamber. The mixture was then poured onto the master bordered by a frame. The viscous polymer was allowed to cure on 80°C heater for 5-10 min. The protruding channel structures on the master create recessed structures on the PDMS. Afterwards, the inlet and outlet holes were punched by using a sharp stamp with 1 mm diameter.

To enclose the PDMS channels a PDMS cover piece was fabricated. 3 drops of PDMS are poured on a thin glass slide and sandwiched by a second glass slide. After subtle pressure the glass slides were carefully pulled apart so that a thin PDMS film remained on the glass slides. The PDMS film was allowed to cure at 80°C for 10-15 min. To enable plasma bonding the mating surfaces of the PDMS chip were treated with O₂ plasma for 10 min. Finally, the mating surfaces of the PDMS chip and PDMS film were clamped to each other and bonded by subtle pressure.

4.2.2 Microfluidic glass device

The microfluidic device served as an NMR sample holder. The microfluidic glass device consists of a quartz glass capillary (Length = 30 mm, outer diameter = 1.1 mm, inner diameter = 1 mm) with a wall thickness of 50 µm (Figure 2). This capillary is connected with a Teflon tubing (length = 40 mm, outer diameter = 0.95 mm, inner diameter = 0.4 mm) to the second glass unit acting as the reservoir (chapter 4.3.3, Figure 45 A) for the cell culture media. A strong connection between the pieces is ensured via two-component glue based on epoxide resin (UHU GmbH, Germany). Due to the small inner diameter of the tubing and the vertical position of the device the

spheroid (chapter 4.3.3, Figure 45 B) sits on top of the Teflon filter. Therefore, the Teflon tubing acts as a filter to trap the spheroid at one defined position.

To quantify the transport of the components inside the capillary the microfluidic device is filled with water. 50 μ l acetate (100 mM) solution is injected into the reservoir of the device resulting in a total concentration of 16 mM. The capillary of the device is placed above the microslot and the probehead is inserted into the spectrometer. The time dependent transport of the acetate towards the capillary is monitored and shown in chapter 4.3.3 in Figure 45 C.

4.3 Results and Discussion

4.3.1 Plasma Generator

After the soft lithography process the PDMS chip containing the molded microchannel has to be sealed with a second flat PDMS piece. Several techniques were developed for PDMS-PDMS or PDMS-Glass bonding but the easiest and most effective method is the plasma bonding. No additional reagent or glue is required which can plug or destroy the microchannels. For this purpose we assembled a plasma generator as shown in Figure 37 consisting of an electrode inside a chamber which is connected to a vacuum pump and gas supply.

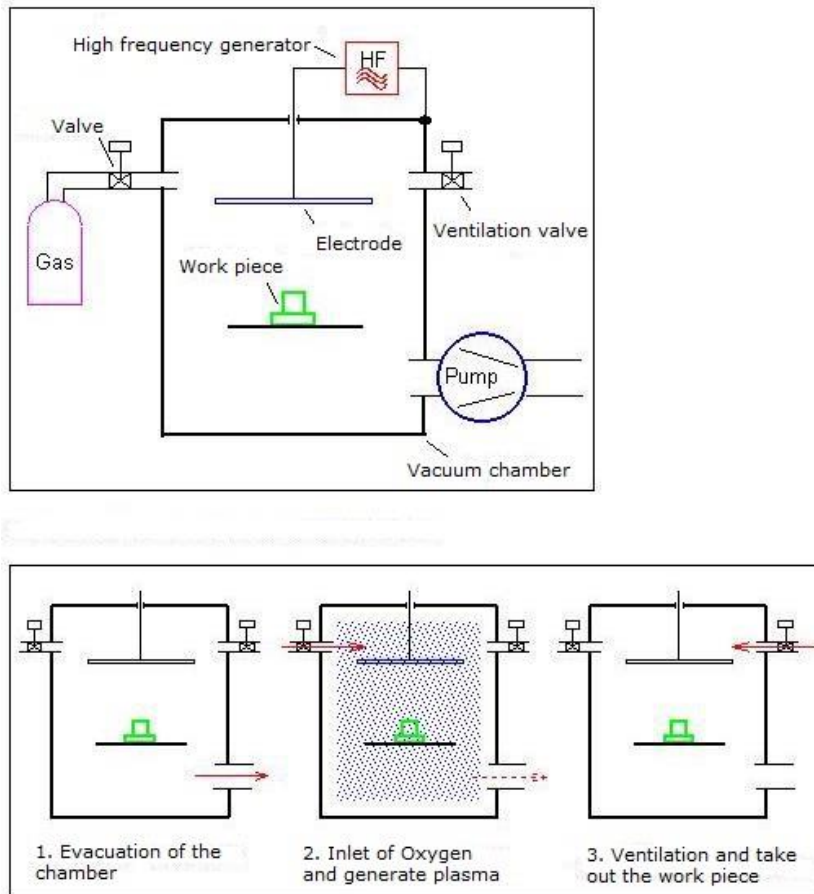


Figure 37: Illustration of the plasma generator.⁷⁸

Once a low pressure of about 3 mbar is reached oxygen is filled inside the chamber and plasma is generated by switching on the high frequency generator. The strong electromagnetic field ionizes the oxygen gas particles. These charged particles collide with surrounding material like PDMS which was placed underneath the electrode. By this method the hydrophobic methyl groups of the polymer are replaced by hydrophilic hydroxyl groups as shown in Figure 38.

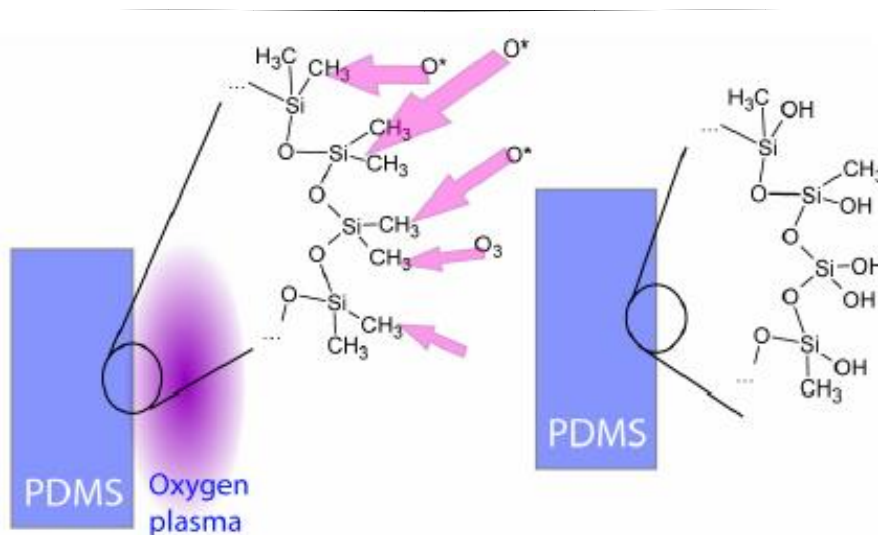


Figure 38: PDMS surface is functionalized by O_2 plasma.⁷⁹

The Si-OH groups on the mating surfaces (PDMS chip and cover piece) are reacting with each other when clamped together. The resulting covalent Si-O-Si bond is strong enough to seal the mating PDMS pieces resulting in leak-tight channels.

4.3.2 PDMS Chip

After molding the PDMS chip by soft lithography the channel structure was enclosed by a second unstructured PDMS substrate in order to enclose the channel/chamber which is shown in Figure 39.

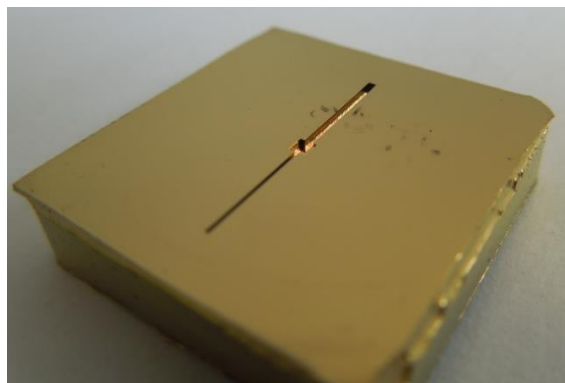


Figure 39: PDMS chip after molding by soft lithography and coated with gold for SEM analysis.

4 Microfluidics and LOC

Since a close contact from sample to the NMR detector is required we have fabricated a thin PDMS film (about 100 μm) on a glass substrate. This PDMS film was sealed against the PDMS chip with the channel structure by using the plasma bonding method.

The Figure 40 shows all results as the SU-8 silicon wafer obtained by photolithography (a) the frame for the soft lithography process (b) and finally the molded and plasma bonded PDMS chip filled with a liquid to show the channel structure (c, d).

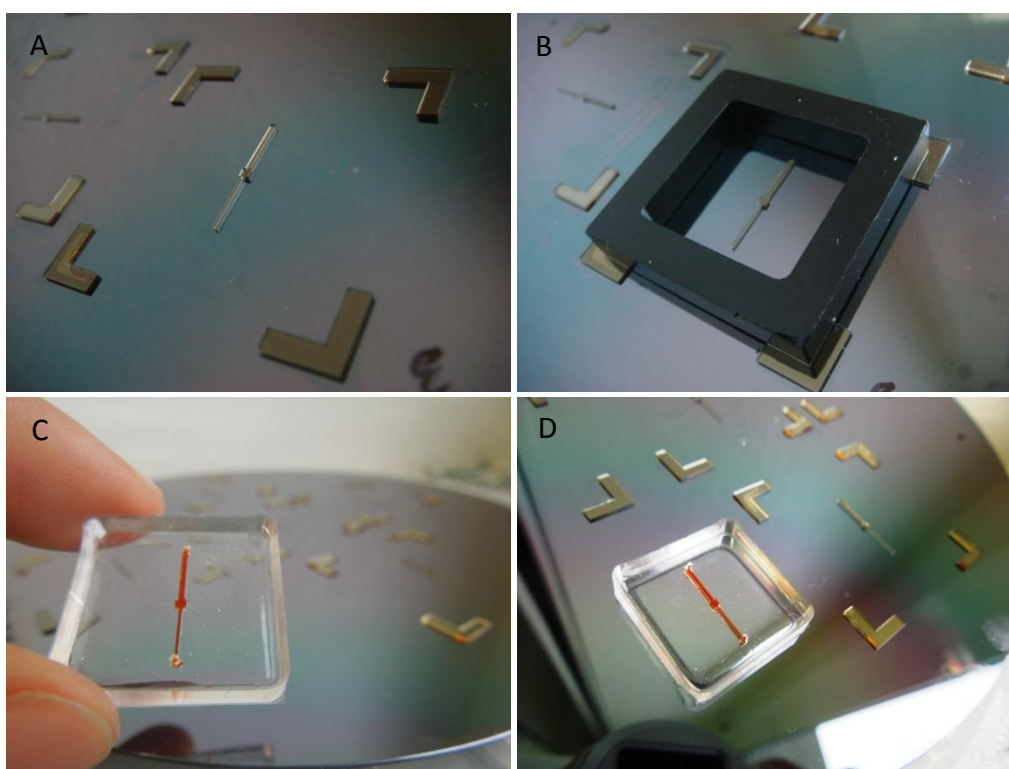


Figure 40: Silicon wafer with SU-8 photoresist silicon wafer (A), the frame for soft lithography (B) and the plasma bonded PDMS chip filled with orange liquid (C, D).

Due to the plasma treatment the microchannel is hydrophilic. Since the hydrophilic state of the PDMS is reversible the channel has to be filled with water to preserve this state. This tube-less microfluidic PDMS chip can be filled with any liquid by passive pumping. First, the channel is filled with water with the help of a pipette by forming a drop at the outlet. Once the channel is filled with the first liquid the second liquid can be filled by passive pumping as shown in Figure 41.

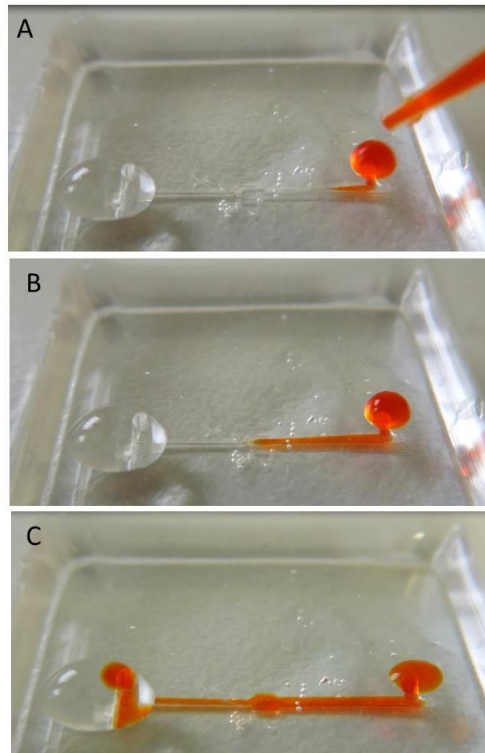


Figure 41: Passive pumping inside a microfluidic channel. (A) With the help of a pipette the channel is filled with liquid (clear) and a drop is formed at the outlet port (left). A smaller drop of a second fluid (orange) is introduced on top of the inlet port (right). (B) Subsequently the passive pumping starts and the orange liquid flows into the channel. (C) Finally the orange liquid is transferred into the channel and displaces the first liquid (clear)

Any liquid can be filled by using this method which is based on surface tension effects. The unequal drop volumes have different curved surfaces which results in a pressure difference inside drops. This pressure difference drives the flow inside the channel.⁸⁰ Without the use of additional equipment or material such as pumps and tubing the reagents, media etc. can be loaded through the inlet port and can be delivered through the channel to the outlet port.

Elastomeric materials and other polymers like PDMS and PMMA are easy to fabricate and are biocompatible. They were shown to be suitable for biological samples like cells. For instance the permeability for gases is an advantage for keeping the cells alive

(O₂, CO₂ exchange etc.).⁶⁵ As it can be seen in Figure 42 the HT29 cells adhere and grow to a 2D monolayer inside the PDMS chip.

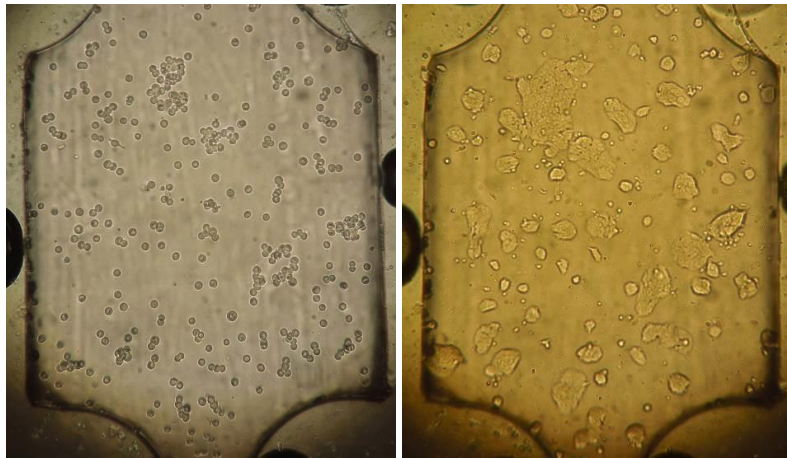


Figure 42: Cell growth inside the PDMS chip. Single cells adhere at the PDMS surface after 24 hours (A). Cells grow to 2D monolayer (picture taken after 4 days). Media was exchanged every 2 days.

The chip is not only designed to grow 2D cell monolayers but also to capture a spheroid inside the chamber which is in the center of the microchannel. The spheroid is inserted through the inlet of the bigger channel at the top. The spheroid is captured in the chamber because the following channel is smaller and the spheroid cannot pass this small channel (Figure 43).

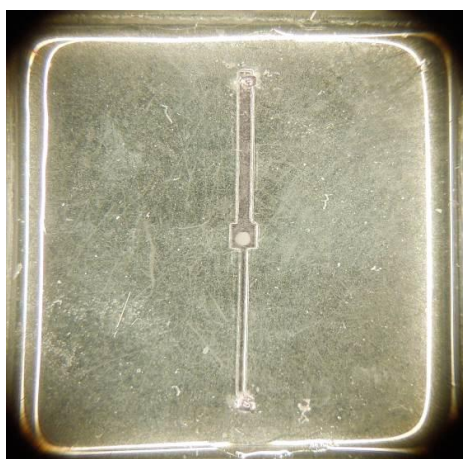


Figure 43: A spheroid is captured inside the chamber with a flanking microchannel.

However, the strong inherent signals of the polymer methyl groups are a big disadvantage for NMR measurements with PDMS. Our aim was to suppress the PDMS signal with different pulse techniques. For this purpose a 5 mm NMR tube was filled with cured PDMS and D₂O. The ¹H-NMR spectra of PDMS is shown before and after suppressing the PDMS signal with the spin echo pulse technique (Figure 44)

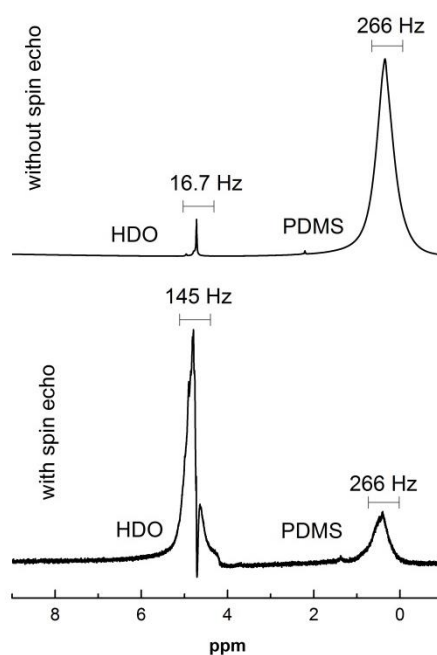


Figure 44: ¹H-NMR spectra of the PDMS chip before and after applying the spin echo technique

As it can be seen clearly the spin echo pulse technique did not show a successful suppression of the PDMS signal. Since many metabolites with methyl groups appear at the range of the PDMS signal and since the suppression was not sufficient enough we refrained from the use the PDMS chip for metabolomics analysis with NMR.

Glass was found out to be the best NMR compatible material. However, elastomeric materials like PDMS and PMMA are easy to fabricate, are biocompatible and suitable for cell samples. Therefore, the PDMS still offers many advantages. Our aim for the future is to fabricate a PDMS – Glass hybrid chip in order to take advantage of both materials. The chip may consist of a glass piece or capillary which is in contact with the NMR detection area while the rest of the chip consist of PDMS.

4.3.3 Microfluidic glass device

Since glass turned out to be the best material for NMR analysis we have designed and constructed a U-shaped microfluidic glass device (Figure 45).

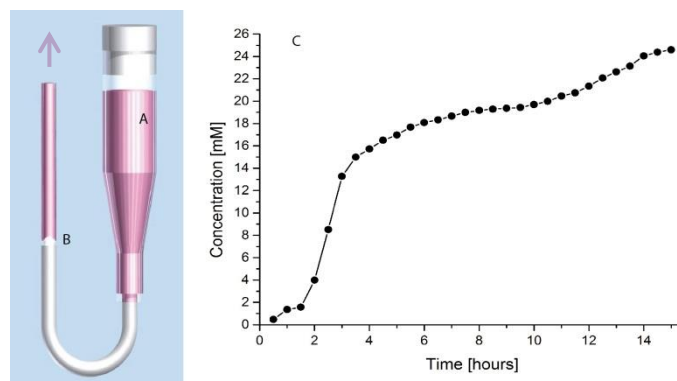


Figure 45: Microfluidic glass device as NMR sample holder. U-shaped microfluidic glass device is filled with cell culture medium (A) and one spheroid with 500 μm diameter. The spheroid (B) is trapped at a defined position with a Teflon tubing (shown as white tubing) which acts as a filter. (C) Graph is showing the time dependent transport of the acetate from the reservoir towards the capillary which is governed by diffusion and evaporation. The arrow on the left picture is indicating the evaporation and thus the flow direction.

The reservoir (A) is connected to the capillary with Teflon tubing (white tubing in Figure 45). The spheroid (B) which is filled at the top of the capillary is captured at the Teflon/capillary interface due to the smaller diameter of the Teflon tubing. Here the Teflon tubing acts as a filter to trap the spheroid at one defined position. Later the spheroid inside the device will be installed directly at the top of the microslot NMR detector which is the most sensitive area for detection (as shown in chapter 3.2.1 and 3.4.5). Additionally, the Teflon tubing ensures the flexibility of the device which is useful during the installation of the microfluidic device onto the NMR microslot detector. The integration of the microfluidic device with the NMR detector will be discussed in chapter 6 and shown in Figure 75).

In order to control the flow in the microfluidic glass device, we have pipetted acetate inside the reservoir and installed the capillary of the device directly on top of the

microslot NMR detector. Due to diffusion, evaporation and capillary action a transport of acetate from the reservoir towards the capillary is observed.⁸¹ At the beginning, diffusion is observed along the concentration gradient from the reservoir towards the capillary. Once the concentration equilibrium is reached around 16 mM (approx. after 6 hours) only the effect of the evaporation driven transport of the component is visible in the figure. The velocity of evaporation was figured out to be 6.5 μl /hour by volume measurements. In summary, by diffusion and evaporation controlled perfusion of the cells with nutrients, oxygen and by accurately controlled temperature, the viability of the cells is guaranteed at near physiological conditions for the long-term *in vitro* studies.

Evaporation driven liquid flow is an alternative pumping method to transport liquids through micro channels/capillaries. The transport is based on the combination of evaporation and capillary forces without the use of external pumps and valves. With this method a smooth and continuous flow velocity can be achieved.⁸¹ In this referred article it has been shown that even particles of the same size can move with different velocities within the channel. This is because some particles move close to the channel/capillary wall while others move in the center of the capillary. Therefore, we do not expect that the transport is similar for all nutrients (different diffusion coefficients etc.). With this experiment we wanted to simply show that there is a transport of nutrients from the reservoir towards the capillary. Since the transport is smooth and continuous we predict that the perfusion of the cell with nutrients is ensured as it can be seen in the results of a different experiment shown in Figure 46. Here the device is filled with water and a colored liquid is added into the reservoir. The transport of nutrients from the reservoir towards the capillary based on diffusion, evaporation and capillary action can be observed here as well.

4 Microfluidics and LOC

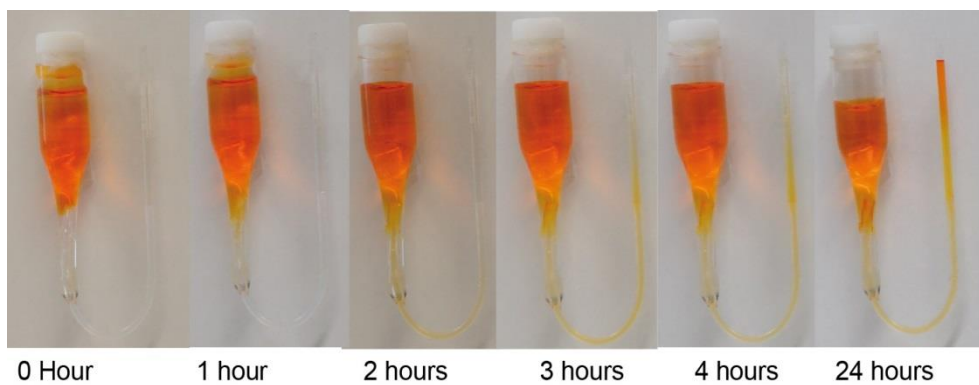


Figure 46: Microfluidic glass device filled with water. Orange colored dye is added into the reservoir. The transport of liquid from the reservoir towards the capillary based on diffusion, evaporation and capillary action can be observed.

5 Cells

This thesis deals with the development of a new NMR technique for the metabolic analysis of living cells. Before we start our analysis a short introduction to cell biology and the essential functions of the cell should be given as an overview. For a better understanding of the complex cell metabolism and the corresponding biochemical pathways which will be discussed in chapter 6 it is necessary to know the basics of the cell structure and the location and function of the organelles.

5.1 Introduction

5.1.1 Cell

Cells are the smallest living unit and the building blocks of organisms. Bacteria are the simplest organisms and their cells are called prokaryotic because their genome is not enclosed by a membrane. All other organisms (like the cells of plants, animal, human etc.) whose genome is enclosed by a membrane (nucleus) are called eukaryotes. While viruses are not always considered as a living object since they have little or no metabolism of their own.⁶⁰ Compared with prokaryotes eukaryotes are much more complex and their cell is compartmentalized with several organelles and all of these components are communicating within a network. For instance, the human body consists of approximately 3.72×10^{13} cells⁸² and the size of each cell is ranging from 10-100 μm . Figure 47 shows a typical human cell with its organelles and a brief description of their functions. However, we will discuss only some selected organelles because a detailed explanation would go beyond the scope of this work.

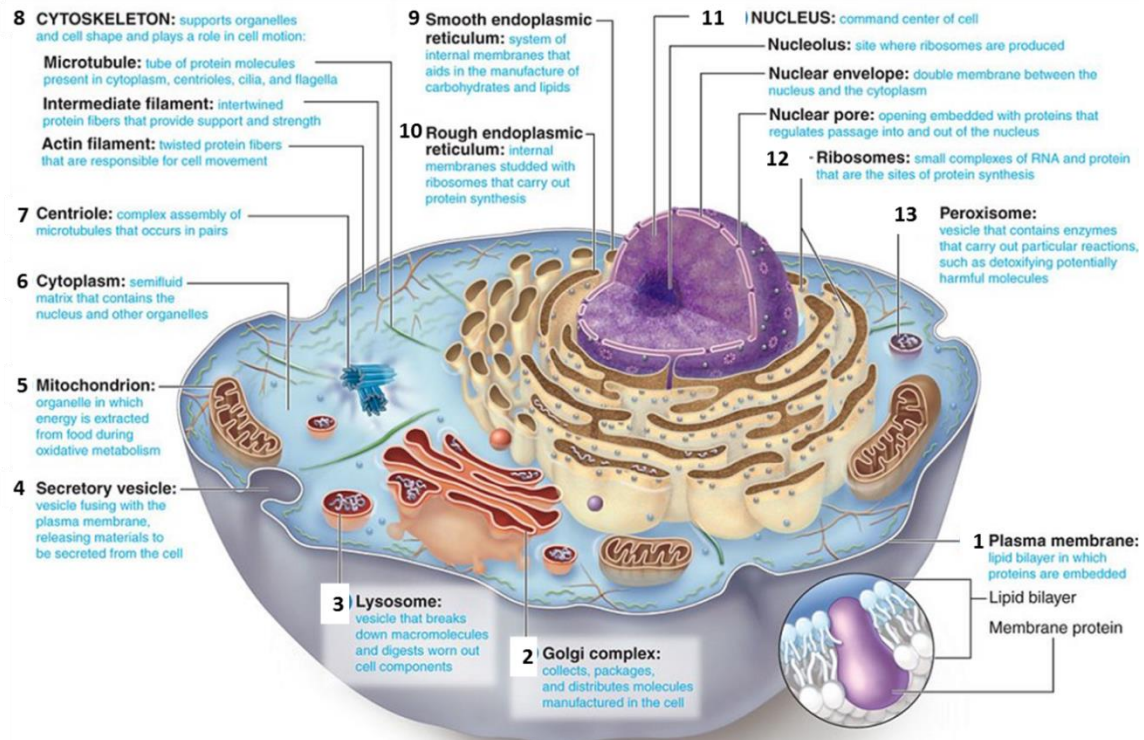


Figure 47: Human cell 3D Model⁸³ with the organelles and their functions.

Each human cell consists of a nucleus (Figure 47, 11) which contains almost the complete DNA of the human being. The DNA strand of about 2 m is densely packed as chromosomes and compressed inside the nucleus ($\sim 5 \mu\text{m}$ diameter).^{60, 84} In regards to the central dogma of the molecular biology, the DNA makes RNA and RNA makes protein.⁸⁵ As shown in Figure 48 a gene on the DNA strand encoding the information for a specific protein is transcribed into a mRNA. Afterwards, the mRNA leaves the nucleus and enters the cytoplasm towards the rough endoplasmic reticulum (Figure 48, 10). Here, ribosomes perform the assembly of a sequence of amino acids following precisely the sequence of the mRNA. After this translation process the long chain of amino acids undergoes post-translational modifications and folds into a full functioning protein.

Another very important process inside the nucleus is the replication of the DNA by which the cell makes a copy of its own DNA. For instance during the initial stages of mitosis or meiosis the DNA is copied via replication. After the cell division two daughter cells identical to the parent cell are formed each containing the chromosomal complement.

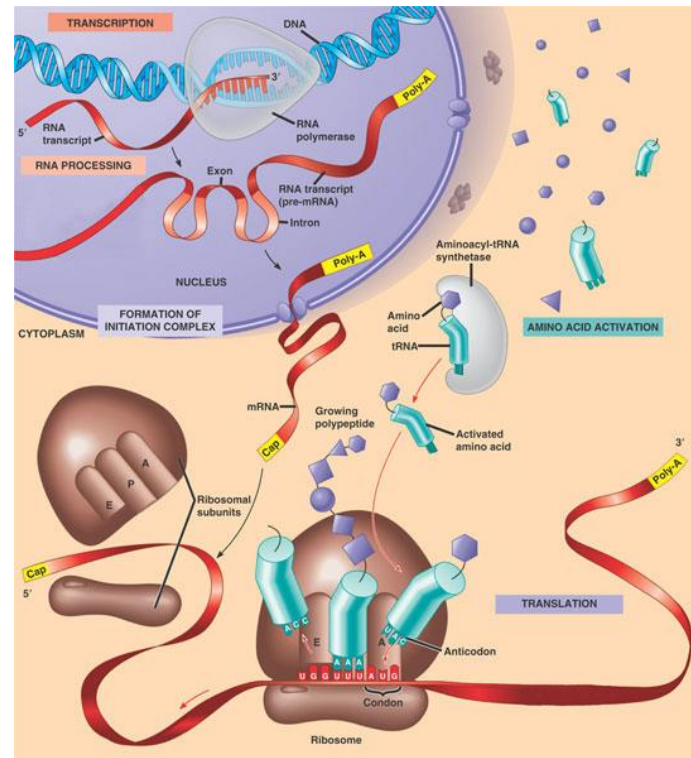


Figure 48: Information flow from DNA to protein ⁸⁶

Another organelle worth to mention is the mitochondria (Figure 47, 5), which is the energy plant of the cell. They are responsible for the adenosine triphosphate (ATP) production of eukaryotic cells during the oxidative metabolism. Without the mitochondria the cells would use the anaerobic glycolysis for energy production. However, the conversion of glucose to pyruvate via glycolysis would release only a small part of the energy which glucose usually provides. But with the help of the mitochondria 15 times more ATP is produced than with glycolysis only. Hereby, pyruvate enters the mitochondria and is further metabolized in the TCA cycle and via

the oxidative phosphorylation ATP is produced. Not only pyruvate but also fatty acids are used as fuel by the mitochondria in order to generate energy in form of ATP.⁸⁴

Also the plasma membrane (Figure 47, 1) plays an important role in cell biology and has to be mentioned here. The organelles and cytoplasm of the cell are surrounded by a ~5 nm thick plasma membrane consisting of lipids and proteins. The hydrophobic chains of the phospholipid bilayer are faced to each other, while the hydrophilic parts are facing the cytosol and extracellular milieu. The mammalian membrane mainly consists of phosphatidylcholine (lecithin), phosphatidylserine, phosphatidylethanolamine and sphingomyelin. Further components are cholesterol and several membrane proteins with essential functions varying from material transport to signal transduction. Also the secretory vesicles (Figure 47, 4) are important in material transport. By fusing with the plasma membrane the components secreted by the cell are released into the extracellular milieu. In summary, the plasma membrane defines the borders of the cell, allows the signal transduction, controls the material flow into and out of the cell, and is involved in cell-cell communication. Not only the outer cell membrane but also the membrane of the above mentioned mitochondria is essential and plays an important role during ATP generation. Therefore, the membrane sustains essential processes which are needed to keep the cell viable.

5.1.2 Metabolism

The field of study in which all of the genes (genomics), proteins (proteomics) and metabolites (metabolomics) are analyzed is called omics research. In a recent review article the metabolomics is stated as the apogee of the omic trilogy⁸⁷ and its relation to the central dogma of molecular biology is illustrated in the following picture (Figure 49).

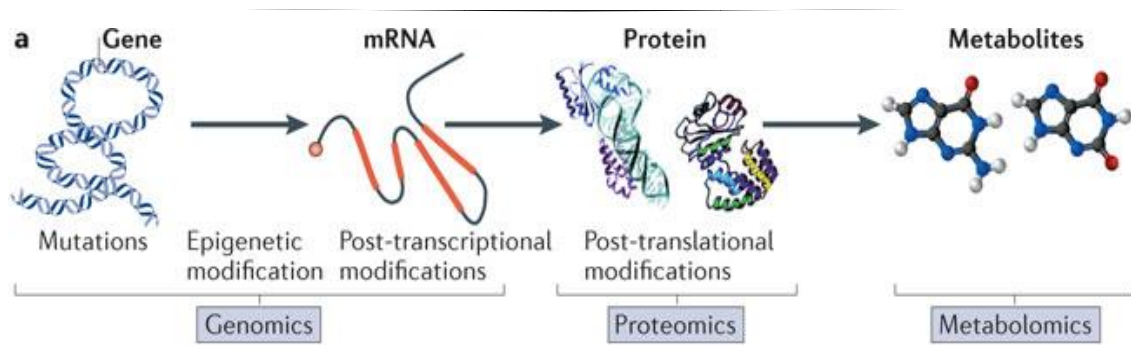


Figure 49: Illustration of the central dogma of molecular biology (transcription of DNA into mRNA and translation of mRNA into protein) and its relation to the omics cascade.⁸⁷

The central dogma of molecular biology describes the information flow via transcription of the gene to mRNA and finally the translation of the mRNA into protein. The metabolites are downstream biochemical end products of this information flow.⁸⁷ As it can be seen the metabolites are small molecules which are synthesized and chemically transformed by specific proteins (enzymes) which are encoded in the structural genes of the cell. Without enzymes many of the chemical reactions inside the cells will not be possible at physiological temperature (37°C). Enzymes not only catalyze the reactions they also control them. For each reaction a specific enzyme is responsible. In general, enzyme catalyzed reactions are interconnected with each other. For instance, the product of one enzyme is the substrate of the next enzyme and so on. And each of these reactions within this linear reaction chain is connected again with other reaction chains so that a complex metabolic network arises. Additionally, one metabolite can act as inhibitor (e.g. competitive, non-competitive etc.) or regulator (e.g. allosteric) of the same or another enzyme. Thus, all these components interact via a feedback regulation. Therefore, the metabolic pathways are complex, branched and interconnected networks⁶⁰ as it can be seen in Figure 50. Each pathway requires an in depth and detailed analysis since each of them contributes to sustain the essential life processes of the cell.

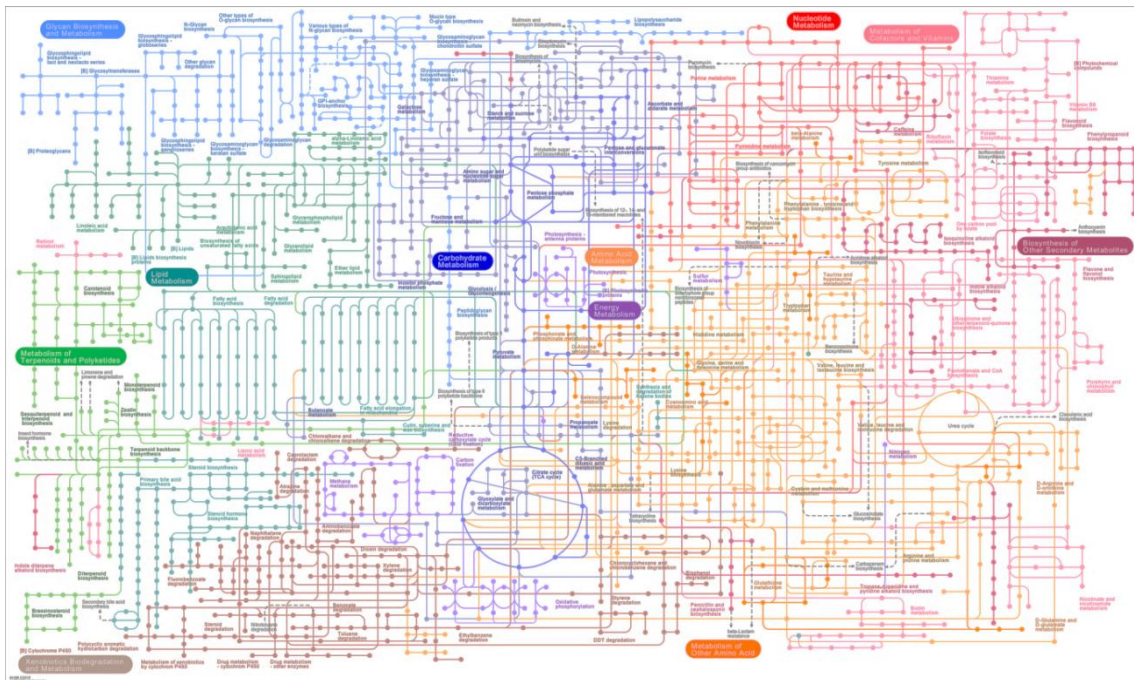


Figure 50: Map of metabolic pathways in humans⁸⁸

But the main characteristic for all metabolic pathways is that they can be divided into two main chemical transformation processes, namely catabolic and anabolic processes. The material taken up by the cells are not only used to synthesize macro- and small molecules (anabolize) but also to break down these material (catabolize). A continues turnover of the components provides support for the three basic needs of dividing cells:

- to generate energy (usually in form of ATP) in order to maintain the high degree of order inside the cell (low entropy)
- to increase the biosynthesis of macromolecules (e.g. for proteins, nucleic acids, lipid membrane etc.)
- to maintain a suitable redox status of the cell

In summary, the metabolism is essential for the cells to live, to grow and to divide and therefore metabolism and the associated biochemical pathways have been in the focus of research since the nineteenth century. Although much is known about the cells' metabolic pathways, its link to pathogenic conditions and especially metabolic

reprogramming in cancer is still a challenging task. Therefore, metabolomics analysis has received huge interest within the last decade.⁵

Compared with genomics and proteomics analysis metabolomics analysis reveals direct evidence about the biochemical activity of the cell and it can be correlated to the phenotype (cells' observable characteristics). Whereas genes are subjected to epigenetic regulations, like the changes in the transcriptional behavior of the cell without changing the DNA sequence. These changes can be observed only in the phenotype but not in the genotype which is problematic when doing genomics analysis. Also post-translational modifications of proteins make the proteomics analysis and its correlation with the phenotype difficult.⁸⁷ Therefore, the metabolite concentrations and the dynamic process of the metabolite production and degradation rates give direct information about the fundamental cellular functions, thus the status of the cell.¹ Furthermore, the metabolism shows the fastest and most sensitive response of the cell to the changes in the environment. Due to this reason, the cells' response to physical, chemical stimuli (e.g. from neighboring cells) can be studied via metabolomics (Figure 49). Additionally, the effect of toxins, pharmaceuticals, drugs etc. can be observed directly and time-resolved with the help of appropriate analytical techniques (see chapter 6).

At a glance, the metabolism

- gives direct information about the status of the cell
- allows direct correlation with the phenotype
- shows the fastest and most sensitive response of the cell to the changes in the environment

Therefore, not only the concentrations and content of the metabolites but also their metabolic activity has to be analyzed as well. But, the metabolome has high turnover rates, a large chemical diversity and a lower mass content¹ what makes the metabolomics analysis a challenging task and emphasizes the need for non-invasive and time resolved analytical tools like miniaturized NMR detectors as we introduced in chapter 3. For instance, a single yeast cell has an ethanol production rate of about

$6 \text{ fmol cell}^{-1} \text{ s}^{-1}$.⁸⁹ When the yeast cell is supposed to be captured in a $0.1 \mu\text{l}$ micro chamber, the ethanol concentration would be about 0.2 mM after 1 hour. This issue highlights the importance of the sampling strategy and the sample volume so as to minimize the loss and dilution of the analyte.¹ As a consequence, not only a suitable detector for mass and volume limited samples is required but also an appropriate sample holder is necessary for metabolomics analysis. Beside the low abundance of the analytes also the size of the sample poses another problem. As already mentioned above a typical human cell is about $10\text{-}100 \mu\text{m}$ diameter in size while bacteria cells are even much smaller (*E. coli* about $1 \mu\text{m}$). Consequently, the handling of sample turns out to be difficult. To overcome all these shortcomings LOC and μTAS technologies seem to provide all necessary bases to handle the small cell sample, to sample the low abundant metabolites within a small volume and to keep the cells viable and thus their metabolism upright during analysis which we introduced in chapter 4.

5.1.3 Cell culture and *in vivo* vs *in vitro*

For detailed biochemical analysis a huge number of cells are required e.g. for isolation of the DNA, RNA and Proteins or for metabolite analysis via cell extraction. Or to perform metabolomics analysis, by analyzing the response of the organism to external stimuli like drugs etc.⁹⁰ First of all the cells from the organism (animal, plant etc.) have to be removed. Usually tissues, like in a biopsy, are removed which consist of a heterogeneous cell population. In order to analyze the different cell types separately they have to be disaggregated. For this purpose usually proteolytic enzymes (e.g. Trypsin) are used in order to digest the extracellular matrix which keeps the cells together. Usually these trypsin solutions contain ethylenediaminetetraacetate (EDTA) which is chelating the Ca^{2+} .⁸⁴ This Ion is required for cell-cell adhesion and its absence and the proteolysis of the enzyme will lead to the disaggregation of the cells. These *ex vivo* cultures of the cells are usually grown in flat, hydrophilic and polymer (usually polystyrene) cell culture flasks (Figure 51) mostly with a gas permeable cap.

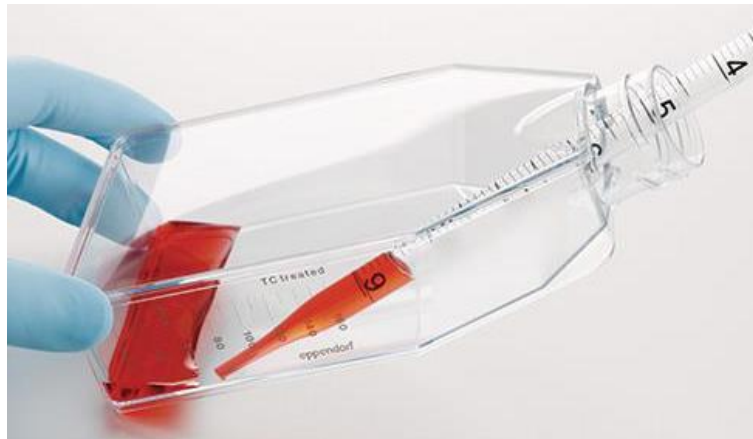


Figure 51: Cell culture flask⁹¹

After the isolation from the tissue, the first culture grown in culture flask is called primary culture. Afterwards, the cells are subcultured (passaged) by transferring them into a new flask. The passaged cultures are now called cell lines. Also for passaging Trypsin/EDTA is used to release the cells which are adhering on the bottom of the cell culture flask. A schematic view for passaging the subcultures is shown in Figure 52.

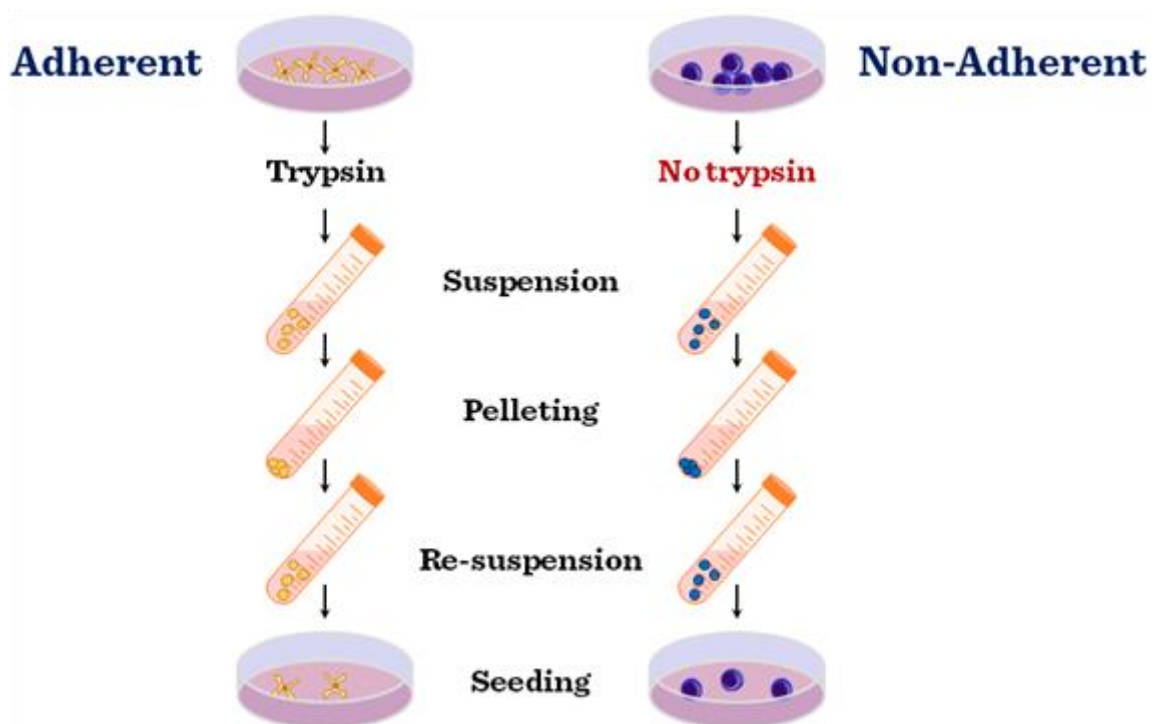


Figure 52: Standard procedure in cell culture⁹²

Unlike cancer cells, normal cells do not proliferate indefinitely and can perform only a limited number of cell divisions in culture (finite cell line). This event was observed the first time in culture and later confirmed *in vivo* and is called cellular senescence (state of permanent cell-cycle arrest). It is known to suppress the malignant progression of tumors on the one hand and to contribute ageing on the other hand.^{65, 93, 94} For biochemical analysis, the so called finite cell lines are usually immortalized via transformation which can be induced chemically or virally.⁹⁵ These now continuous cell lines are grown under favorable conditions and can be used for several biochemical analyses. Typically, and also in this work we will call the experiments with living cell cultures *in vitro* and experiments with living organisms (e.g. animal, human etc.) *in vivo*. But these terms can sometimes lead to confusion, because in some biochemistry labs it is called *in vitro* when an experiment is conducted in test-tubes/flasks without living cells. Whereas all experiments conducted with living cells (even in culture flask) are called *in vivo*.⁸⁴

5.1.4 Cancer / Tumor

Cancer is a disease in which the cells grow abnormally and have the ability to invade other tissues. Cancer cells can be described by two heritable characteristics:

- Cancer cells and their daughter cells can grow without the usual limitation of cell division.
- They can spread within the full organism and invade other tissues⁸⁴

First of all, the uncontrolled abnormal cell growth (neoplasia) leads to a neoplasm also called tumor (Figure 53). As long as the tumor is circumscribed and remains together as a cluster it is called benign. In this case, the tumor can grow bigger but it is localized and does not spread and invade within the body. At this state the tumor can be removed by surgery. But when the cells get the ability to detach from the tumor and to spread and invade other parts of the body than they are called malign. The invasive cancerous cells get into the blood circulation and built secondary tumors in distant

parts of the body (metastasis).⁸⁴ At this state a therapy is very difficult or even impossible.

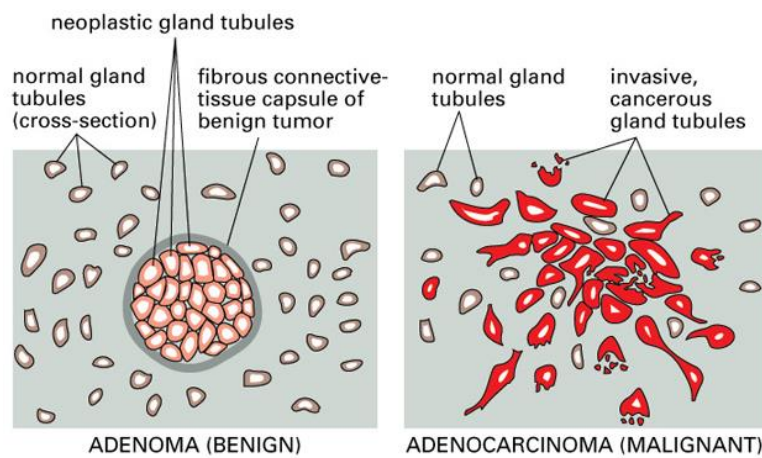


Figure 53: Benign and malignant tissue⁸⁴

Most of the tumors arise from a single abnormal cell. Even when the cancer has made metastasis the primary tumor can be traced back for instance by chromosome analysis. These findings indicate that the abnormal cell is able to inherit the aberration. Therefore, cancer probably involves alterations in the cell's DNA or chromosomal aberrations like the translocation between two chromosomes. Mostly, genetic aberration and also in some cases heritable epigenetic changes are supposed to play a role in cancer.^{60, 84} But as mentioned a tumor can arise from a single cell, but cancer as a result of a single mutation can be excluded. Recent evidence states that several mutations in a single cell are required to result in cancer. Regarding the precision of the DNA repair mechanism, the statistical probability for a mutation in human is approximately 10^{-6} per gene and per cell division. Additional external factors like carcinogenic reagents, ionizing radiation and viruses can enhance the probability for mutations. Probably within several years, an accumulation of several errors in DNA replication (mutations, translocation or deletion of chromosome parts etc.) is converting a mutated cell into a cancer cell.^{60, 84, 96, 97} Within the signaling pathways of cancer, two important types of cancer-critical genes are known which are categorized according to the increased or decreased activity of the gene product. The first type of genes consists of specific segments of the DNA, called proto-oncogenes, which are

5 Cells

coding for a protein. These proteins are usually involved in control of growth and differentiation of the cell. But a mutation converts (activates) these proto-oncogenes to oncogenes and drives the cell towards cancer. Oncogenes like ras and myc are found to be overexpressed in many types of cancer.^{60, 98} The second type of genes are the tumor-suppressor genes in which a mutation can cause a loss-of-function.⁸⁴ A deactivation of these genes, like p53 or rb1, drives cancer forward. For instance p53 is known to check DNA for damage at the cell cycle checkpoint (G1 to S-phase). When a massive damage is recognized the cell cycle is stopped at this phase and the programmed cell death - apoptosis - can be initiated. In over 50% of all human cancers the protein p53, also called the 'guardian of the genome', has been found deactivated (e.g. mutation).^{60, 99}

The Figure 54 summarizes the key signaling pathways involved in tumorigenesis and tumor progression in humans.

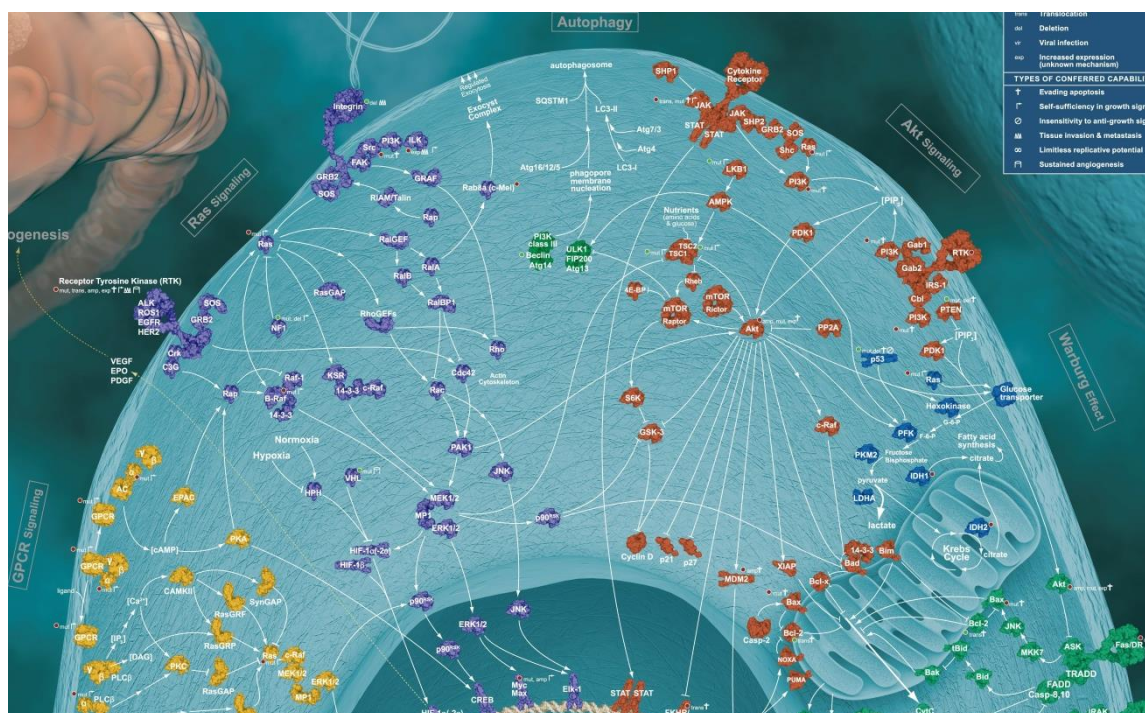


Figure 54: Some pathways in human cancer¹⁰⁰

Each pathway is color coded. For instance, Ras signaling pathway is purple, Warburg effect (see chapter 6.3.4) is dark blue, Akt signaling with mTOR (see chapter 6.3.4 and

6.3.6) is brown etc. The gene products known to be mutated in human tumors are coded with colored dots (oncogene red, tumor-suppressor gene green) and with information on types of genetic alterations (mut: point mutation etc.) and conferred capabilities to the tumor.

5.1.5 2D and 3D *in vitro* cell models vs animal models

Traditional cell culture experiments are conducted with cells grown in flat cell culture flasks. These two-dimensional (2D) *in vitro* models are suitable to study many biological mechanisms and provide several advantages like the enabling of cheap, rapid, simple and well controlled experiments in huge numbers (several batches). For instance, in cell culture the drug uptake and the mechanisms of action can be analyzed under well-controlled conditions. Furthermore, all components inside the cells like metabolites, nucleic acids, proteins, organelles etc. can be isolated with the help of the cell extraction method and further analyzed with reproductive outcome. Furthermore, when compared with *in vivo* assays *in vitro* assays are ethically uncritical when appropriate cell lines are used. Additionally, they are more cost effective and the analysis is usually rapid and has an easier readout. But the characteristic for *in vitro* assays is the fact that the cells are kept under artificial conditions. These assays are approximate reconstructions of the environment and processes which might be found *in vivo* (e.g. tissues). Due to this fact, the disadvantage of the 2D *in vitro* assays is that the environment and the homeostatic pathways found in animals, human etc. are not present.¹⁰¹⁻¹⁰³ Therefore, the 2D *in vitro* assays are not authentic analysis models and they are not always mirroring the cells state *in vivo*. Furthermore, the cells grown in 2D environment have often changed morphologies and cell-cell interaction and no tissue-specific architecture. Therefore, cells in 2D environment differ from cells grown in a 3D environment and emphasize the need for 3D *in vitro* models which mimic the functions of tissues in living organisms.¹⁰³⁻¹⁰⁵ As shown in the example in Figure 55, 3D models mirror the organotypic arrangement which is found in real tissues.

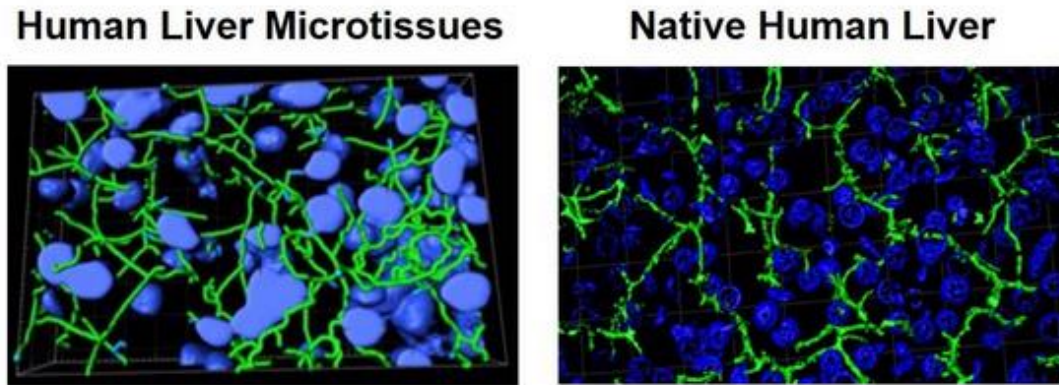


Figure 55: Comparison of 3D human liver microtissues with native human liver tissue. Organotypic arrangement of the polarized hepatocytes (blue nuclei) form bile canaliculi networks (green) like found in native human liver.¹⁰⁶

Compared with 3D *in vitro* assays *in vivo* animal models seem to be more authentic and effective analysis objects. But animal models are a controversial issue not only regarding the ethical concerns but also whether the animal models can mimic human diseases or not.^{12, 107} More than 80% of the potential therapeutics which were tested on animal models fail or have even a toxic effect when tested on human. In most cases the animal model experiments are not rigorously designed in the preclinical phase.^{13, 108, 109} Furthermore, animal models are highly complex systems which cannot be controlled as good as e.g. 3D *in vitro* models. The lack of appropriate preclinical tools, adequate cancer-cell-lines and mouse models makes the discovery of potential drug candidates a challenging task.^{109, 110} To overcome these limitations, 3D *in vitro* model systems are suggested to reduce the gap between 2D *in vitro* models and animal models.^{14, 111} As shown in Figure 56 some 3D culture models are suggested. Here, the most authentic 3D *in vitro* models are *ex vivo* tissue slices dissected from organs (Figure 56 a). These tissue slices preserve the cytoarchitecture and the cellular differentiation of the original tissue.¹⁴ However, this *ex vivo* model goes along with high cost, limited viability of the living tissue and the low availability of human organs for dissection. Consequently, it is difficult to implement these models for wide range molecular cell biology studies or as a standard preclinical analysis system. Therefore,

other 3D *in vitro* test models have been developed and some of them are shown in Figure 56 b-e. The spheroids are discussed in detail in the following section while the other 3D cell culture models will not be discussed in this work. The readers are referred to the review article of Pampaloni et al.¹⁴ for detailed information.

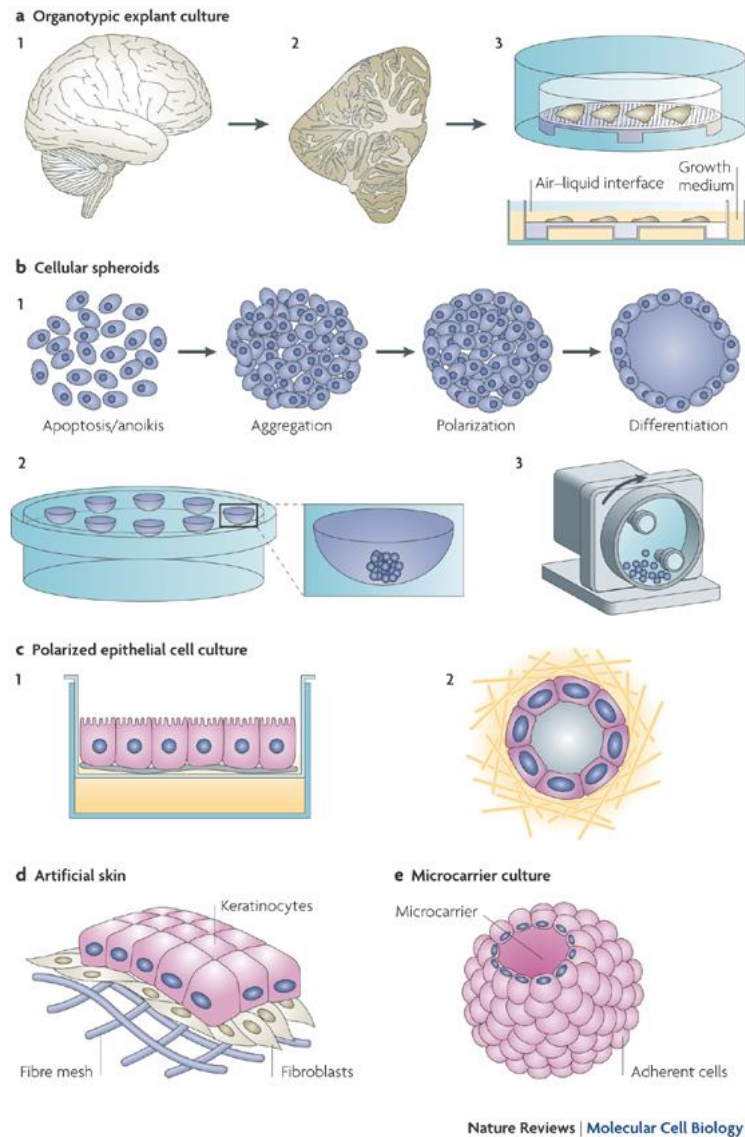


Figure 56: 3D cell culture models. a) dissected organ slices can be kept alive on semi porous membranes with air-liquid medium interface (b).¹⁴

As a conclusion, 3D *in vitro* test models have turned out to be authentic model systems which successfully bridge the gap between 2D cell culture and live tissue or animal models.¹⁴ 3D models, especially tumor spheroids (will be explained more in detail in

5.1.6) are mimicking the pathophysiological gradients inside tumor tissues and provide deeper knowledge about cell-cell interactions, cell adhesion and migration. Not only these biochemical properties but also the easy, rapid and cost effective analysis system can shrink the number of animal testings and makes 3D models a fundamental analytical tool for biochemical studies in omics research, high throughput screenings and preclinical studies. For instance, the Registration, Evaluation, Authorization and Restriction of Chemicals (REACH) program is an extensive and strict regulation of the European Union about the use of chemicals and their effect on human and environment. A recent article estimates that the REACH program will require 54 million animals and will cost 9 billion Euros over the next 10 years. The feasibility of the program is under threat without the investment into high-throughput methodologies¹¹² and without new approaches for toxicology screenings.

5.1.6 Spheroids (3D *in vitro* cell model)

Not only the evaluation of the effect of chemicals on humans like in the REACH program but also the development of new drugs and their trials on animals and humans is always a hot topic. The processes from drug development until the approval and the process for evaluation and authorization of chemicals are time consuming and cost intensive. Therefore, the improvement of fast, cheap and reproducible alternatives and high-throughput processes has received a substantial amount of interest over the past years. The most promising alternative is the use of spheroids which started with tumor spheroids from cancer cell lines. Nowadays a huge variety of spheroids also from non-cancer cell lines are gaining more and more interest and are actually commercially available for research purposes. Spheroids are popular 3D *in vitro* test models for basic biochemical studies, biomedical^{113, 114} and preclinical studies for drug screenings, toxicological studies^{9, 115} and of course biotechnology approaches.¹¹⁶ Additionally, the simple spherical shape of the spheroid allows an easy modeling and simulation of dynamic processes like growth and invasiveness of solid tumors.^{14, 117}

5 Cells

Usually the effect of chemicals and drugs are tested on the cheap and simple 2D *in vitro* cell culture assays. Most of cells which grow in monolayer have equal contact to the surrounding media (50% contact area for each cell) and the added chemicals/drugs as it can be seen in Figure 57.

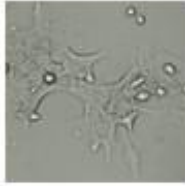

	2D Monolayer	3D Spheroids
		
Cell shape	Flat (3 μm thick)	Ellipsoid/polarized (10-30 μm thick)
Cell interface	50% cell-plastic (matrix) 50% cell-liquid	80% cell-cell & cell-matrix 20% cell-liquid
Cell junctions	Integrin-ECM	Adhesion junctions Desmosomes Gap junctions Tight junctions Integrin-ECM

Figure 57: Comparison of 2D monolayer with 3D spheroids at a glance ¹⁰⁶

This means that the drug can penetrate easily without any barriers into the majority of the cells which is not the case when applied on *in vivo* assays. Many anti-cancer drugs cannot fully penetrate into solid tumors and therefore cannot reach all the cells within the tumor. This results in poor efficiency of drug treatment which can lead to cancer recurrence or even fail in therapy.^{118, 119} The 2D cultures do not mirror the complex *in vivo* tissue architecture like cell-cell and cell-matrix contacts and interactions, pathophysiological gradients and genetic profiles.^{9, 10, 118, 120} *In vivo* assays with animal models are expensive, time-consuming, complex and ethically questionable and do not represent a suitable alternative. In the past years spheroids (3D *in vitro* model) have shown to successfully bridge the gap between 2D *in vitro* models and animal models

(*in vivo*) and are a powerful tool to study e.g. the effect of drug penetration.^{14, 118} As it can be seen in Figure 58 the spheroid consists of an outer layer with proliferating cells with good access to oxygen and nutrients mirroring vascularized cells in tumor and tissues. The middle layer consists of quiescent cells with moderate oxygen and nutrients availability. The core consists of necrotic and dead cells due to low or no oxygen and nutrients mirroring the avascularized areas of tumors.

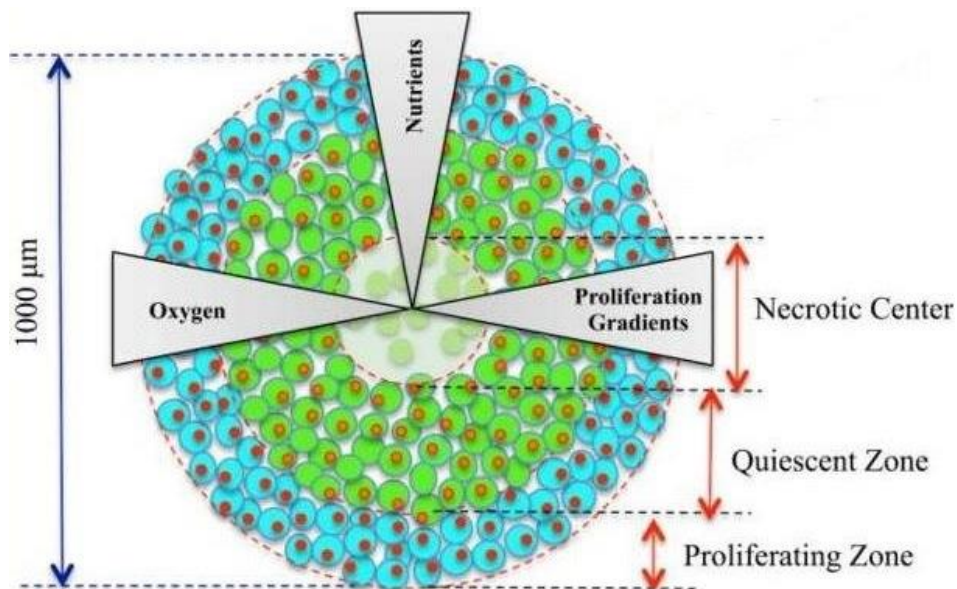


Figure 58: Schematic illustration of the spheroid. The complexity of the tissue specific architecture and the physiological gradients are shown which display the natural barriers for drugs.¹¹⁸

The decreasing concentrations of oxygen and nutrients display the pathophysiological gradients inside tumors. An illustration of the experimental data regarding the physiological gradients and metabolic profile inside the spheroid is shown in chapter 6.3.4 in Figure 81.

The concentric arrangements and the different subgroups of cells as well as the gradients inside the spheroid mirror the complexity of the tissue specific architecture and therefore it mimics the natural barriers for drugs. The drug penetration and distribution can be studied with cheap, fast, easy and reproducible spheroids assays

under *in vivo* like conditions. With traditional methods like fluorescence microscopy or more sophisticated and powerful approaches like matrix-assisted laser desorption/ionization (MALDI) mass spectrometry imaging (MSI) the time dependent drug penetration can be studied.^{118, 121} Not only the efficiency of drugs but also the effect of any type of chemical, toxin etc. on cells can be studied. With the help of spheroids toxic or weak drug candidates at pre-animal and pre-clinical trials can be eliminated. The effect of chemicals and toxins can be studied on genomics, proteomics and metabolomics level and can be eliminated also prior to the test on animals. Depending on the impact of the analysis it can even replace animal models and thus can contribute to shrink the number of animal testing. The overall goal is the full replacement of the 2D *in vitro* models and also animal models by 3D *in vitro* models which is of big interest in the society, research and industry.

Not only spheroids consisting of one cell line but also spheroids co-cultured with a second or even more cell lines can be used for *in vitro* assays. Depending on the application field co-culturing e.g. with immune cells or endothelial cells is possible (see 5.1.7). Usually for anti-cancer research monocultures of cancer cell lines were shown to be a suitable tool to study the tumor physiology and its metabolic response to therapy.¹²²

Spheroids are the most common and simple 3D *in vitro* test model, which utilizes the natural behavior of some cells to aggregate under specific conditions (Figure 56 b). Hereby, the hanging drop method is the most popular technique which provides spheroids from single- or co-culture cells (mono- or multicellular spheroids).^{123, 124} Recently, more sophisticated 3D cell culture platforms (kits)^{106, 125, 126} are available for a better coupling with automated systems and for high-throughput screenings.^{127, 128} Unlike the hanging drop method a new approach based on PDMS microarray technology was developed at the ISAS Miniaturization department by Hardelauf et al. in order to enable the scalable production of uniform tumor spheroids for high throughput toxicology screenings and also for anti-cancer research.¹¹ The PDMS microarray spheroid formation assay based on cell proliferation results in more dense

packed spheroids which are supposed to mimic real tissue samples better than hanging drop spheroids which are obtained by aggregation and proliferation. In this work we will use this PDMS microarray^{11, 105} and the InSphero hanging drop platform¹⁰⁶ for the formation of spheroids. The results of both methods are shown and discussed in chapter 5.3. Later, both types of spheroids will be used in chapter 6 for metabolomics studies with the help of the homebuilt microslot NMR detector and the metabolic performance of these spheroids will be compared.

5.1.7 Hanging drop Spheroid Platform

The hanging drop method is a very common technique which is in use in cell biology and protein crystallography since 100 years. Especially in cell culture the ability of adherent cells to aggregate is used by this simple technique. One drop of cell culture is given onto the lid of a petri dish and turned upside down. The bottom of the petri dish is filled with water to avoid the evaporation of the hanging drops (Figure 59).

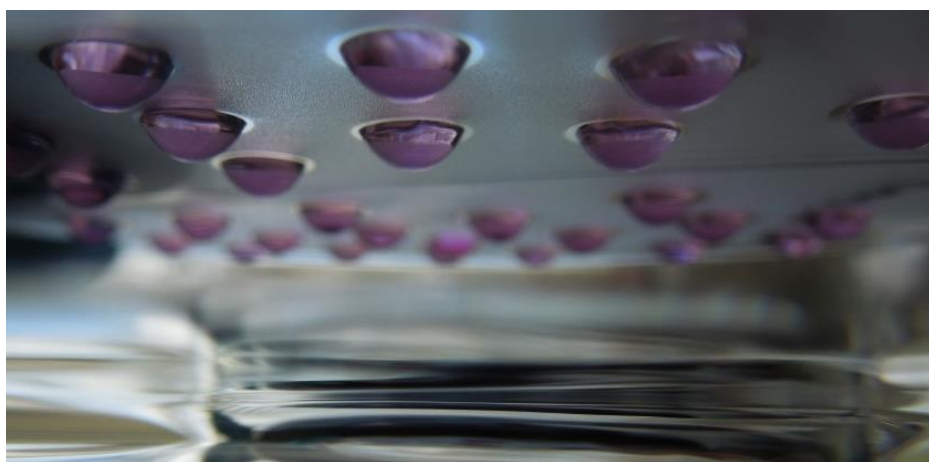


Figure 59: Hanging drop cell culture on petri dish

Inside a volume ranging from 10-30 μL the cells have no surface where they can adhere and start aggregating. At the liquid gas interface the cells are fed with nutrients and gases and start building cell-cell contacts and form a tissue like architecture.¹²⁹ With the improvement of new spectroscopic and microscopic techniques and with the availability of new high-throughput techniques, spheroids received a substantial

amount of interest. Since then this underestimated tool is catching up again.⁹ But the traditional hanging drop method inside a petri dish is not sufficient to meet the requirements. For instance, most of the cell aggregates do not form truly spherical shapes and must be transferred onto agarose coated plates until the cells form a uniform spheroid as it can be seen in Figure 60. Also the change of the media is difficult by this type of hanging drop technique.

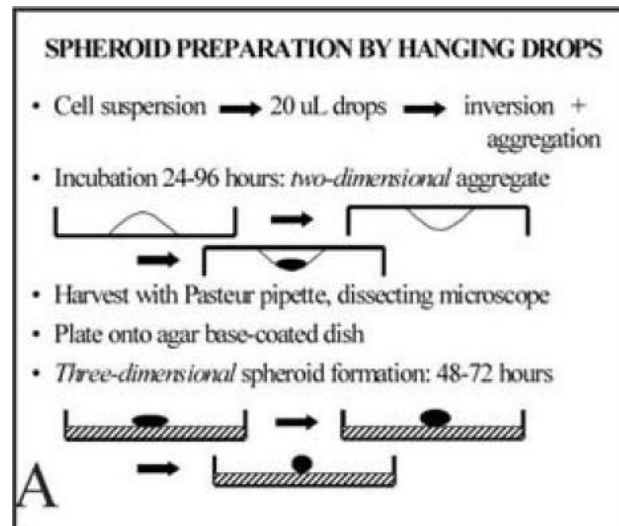


Figure 60: Traditional hanging drop method for spheroid preparation.¹²⁴

Together with the increasing interest on spheroid based assays the improvement of new and more advanced spheroid preparation techniques became possible. Especially the automated system for mass production of uniform spheroids is currently a hot topic and many small companies started to put their focus on these automated platforms which are of big importance for research and pharma industry. As shown in Figure 61 the most common automated platform consists of a 96-well or 384-well plate (made of e.g. polystyrene). The special design of each well allows the efficient formation of uniformly shaped spheroids.

5 Cells

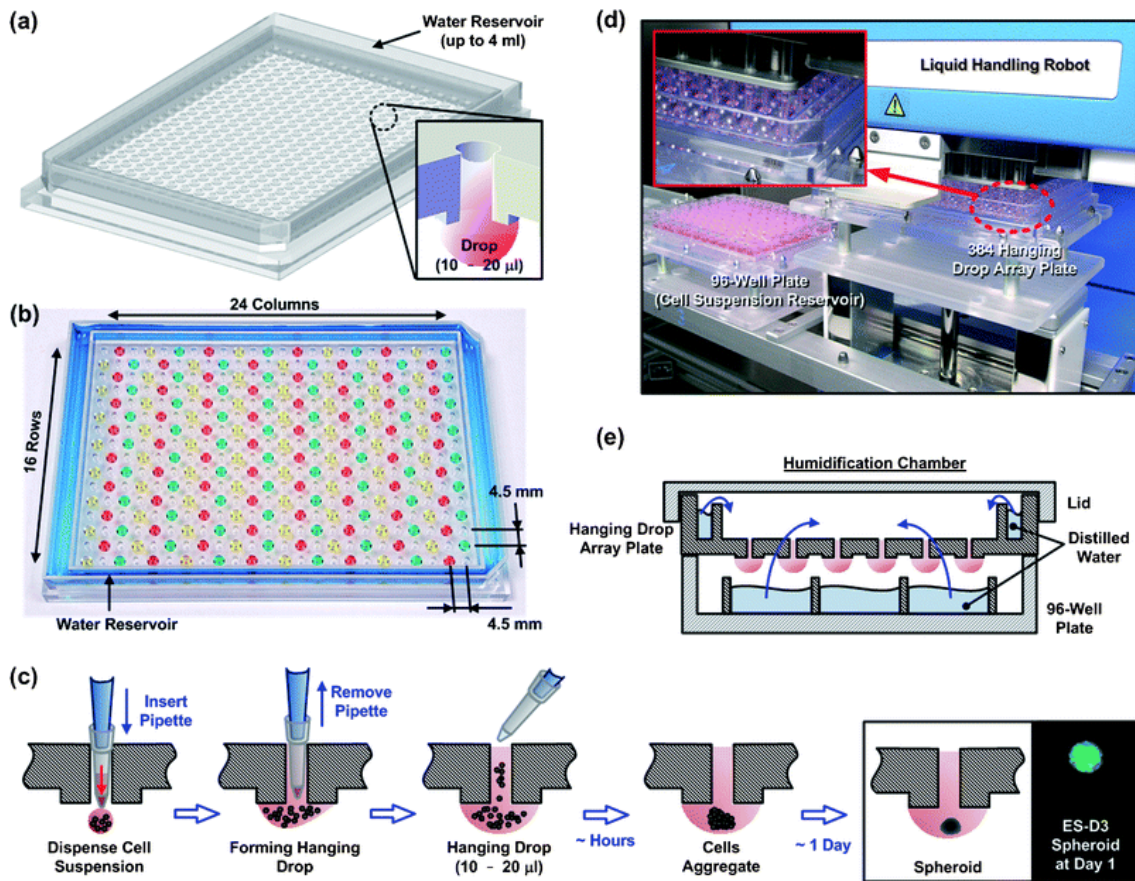


Figure 61: Illustration of the hanging drop spheroid culture on a 384 array plate .¹²⁵

With the help of automated pipettes or multichannel pipettes the cell suspension is pipetted from the top into the notch (cavity). The hydrophilic surface of the notches attracts the cell suspension and a hanging drop is formed and confined within the plateau (Figure 61 c and e). The cells start to aggregate and spheroids are formed usually within 2 – 4 days. The hanging drops are kept inside a humidification chamber as illustrated in Figure 61 e. Here, the array plate is sandwiched between the bottom plate filled with water and the lid.

As mentioned in chapter 5.1.6 the spheroids can be obtained from one cell line or it can be co-cultured with one or several other cell lines. The configuration possibilities of co-culture spheroids are shown in Figure 62.

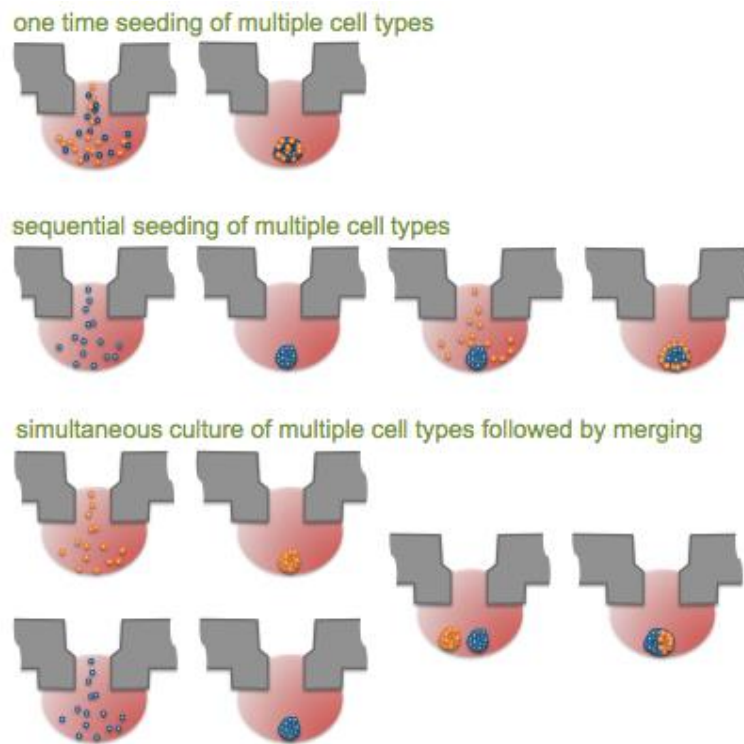


Figure 62: Configuration possibilities of co-culture spheroids. ¹³⁰

These automated platforms with uniform and reproducible spheroids will enhance the use of *in vitro* assays for basic biochemical studies as well as for drug testing and toxicological screenings.

5.1.8 PDMS Spheroid Microarrays by μ CP

Besides the most known hanging drop method new approaches were being developed to optimize the spheroid formation process. The aim is to improve more authentic spheroids which mimic the real tissue samples better than hanging drop spheroids. One of them was developed at the ISAS institute and was used in this work. This new approach comprises the PDMS microarray for the mass production of scalable and uniform tumor spheroids for metabolic and toxicological high-throughput screenings.^{11, 105}

The PDMS microarrays for spheroid formation were obtained by microcontact printing (μ CP). With this method one can provide areas on a substrate (like glass or polystyrene) on which the cells can adhere and grow (e.g. into spheroids). This method works as follows: a PDMS stamp (obtained by soft lithography, see 4.1.3) which has recessed spot structures is inked by contact with a thin liquid PDMS film (see Figure 63 and Figure 64). Prior to this step the thin liquid PDMS is spin coated onto a substrate to obtain a homogeneous and thin PDMS film. In a process which is called contact printing the structure on the inked PDMS stamp is transferred onto a substrate by subtle pressure of the stamp onto the substrate.

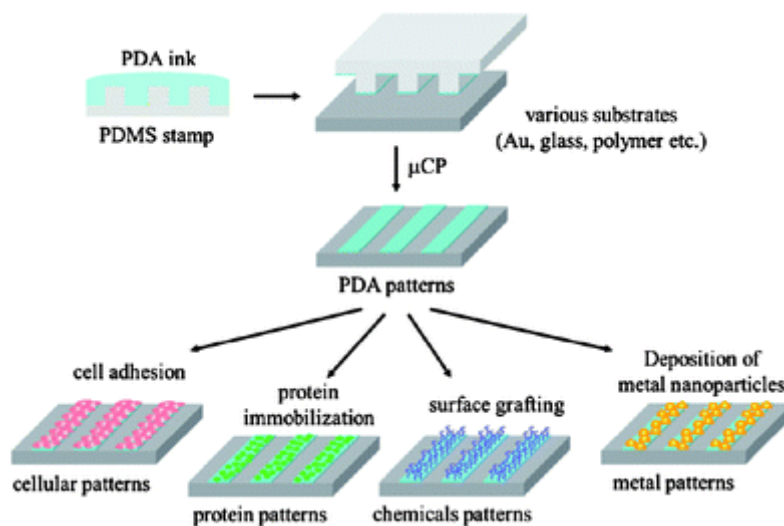


Figure 63: Microcontact printing (μ CP) for the production of tunable micropatterned substrates for biochemical assays.¹³¹

As shown in Figure 63 the μ CP technique is not only used for the fabrication of spheroid PDMS microarrays, this fast and easy method is for instance used to pattern substrates with functional groups like Polydopamine (PDA). These surfaces can be used for controlled cell adhesion, protein immobilization, surface grafting and the deposition of metal nanoparticles which can be used for various applications.¹³¹

μ CP printing is a very simple and cheap method for the reproducible patterning of substrate surfaces for various biochemical and chemical applications and the reproducibility will lead to statistically relevant data e.g. in high-throughput screenings.

5.2 Materials and Methods

5.2.1 Cell culture

Human colon adenocarcinoma cells HT29 were purchased from DSMZ (Germany) (kindly provided by the West lab). All consumables like cell culture flasks and sterile pipettes etc. were ordered from Sarstedt (Germany). Cell culture media and all other supplement, reagents and sera were purchased from (PAA, Germany). The Dulbecco's modified Eagle media (DMEM) with low glucose (1000 mg/L) was supplemented with 10% (v/v) foetal bovine serum (FBS) and 1% (v/v) penicillin and streptomycin. The cells were cultured in a humidified 5% CO₂ incubator (Thermo Fisher Scientific, Germany) at 37°C.

When the cell confluence was about 80% the adherent cells were harvested using 1 ml trypsin/EDTA for a 25 cm² cell culture flask. The trypsinization was stopped with 9 ml DMEM and the cells were transferred into a conical tube and centrifuged by 1200 rpm for 3 min. After discarding the supernatant the cells were resuspended in DMEM and passaged into a new cell culture flask or used for further experiments.

5.2.2 Spheroid formation with InSphero hanging drop

To conduct experiments on microtissue like model systems spheroids of HT29 cell line were prepared with the help of an InSphero GravityPLUSTM (InSphero, Switzerland) system. 5 ml PBS buffer is placed into the bottom reservoir of the InSphero 96-well plate to avoid evaporation of the spheroid drops inside the incubator. The cell solution is prepared by trypsinizing cells expanded in cell culture flask according to standard protocols. The cells are counted using a Neubauer cell counter (VWR, Germany), the number of cells required for the experiment is adjusted and the media is mixed

carefully. HT29 cells are plated at 1000 cells in total of 40 μl aggregation media consistent of DMEM supplemented with 10% (v/v) FBS and 1% (v/v) penicillin and streptomycin. 40 μl of the cell suspension is gently applied in each well by ensuring a tight contact of the multichannel pipette tip with the well inlet by subtle pressure. After closing the 96-well plate with the lid the Insphero gravityPlus system is placed in a humidifier CO₂ incubator at 37°C. Microtissue/spheroid formation is controlled with an inverted bright field microscope. After four days the media is changed. For this purpose 20 μl of the spheroid drop is aspirated with the multichannel pipette at lowest speed. Then 20 μl of fresh media is added. These steps are repeated twice. The change of the media is repeated every 3rd day. The spheroids are ready for further experiments usually after four or five days.

5.2.3 Spheroid formation with a PDMS microarray

The stencil for the PDMS stamp was fabricated by molding SU-8 resist coated silicon masters by using standard photolithography as described in 4.1.2 (400 μm pitch size with 150 μm spot diameter was used). The SU-8 mold consists of protruding circular structures which cause recessed structures in the PDMS stamp. For the fabrication of the PDMS stamp, the Sylgard 184 Silicone Elastomer Kit (Dow Corning Corporation, USA) was used. The base reagent was mixed with curing agent at a 10:1 (w/w) ratio. After thoroughly mixing, the prepolymer was degassed for 30 min inside a vacuum chamber. The mixture was then poured onto the master bordered by a frame. The viscous polymer was allowed to cure on an 80°C heater for 5-10 min. The protruding channel structures on the master create recessed structures on the PDMS. A thin and liquid PDMS film was prepared by spin coating 500 μL PDMS in chloroform (1:10, w/w) on a glass slide for 30 seconds at 6000 rpm. Before this step the PDMS base reagent was mixed with curing agent at a 5:1 (w/w) ratio and then mixed with chloroform and spin coated. As shown in Figure 64 the PDMS stamp was inked by conformal contact with the thin and liquid PDMS for about 10 seconds.

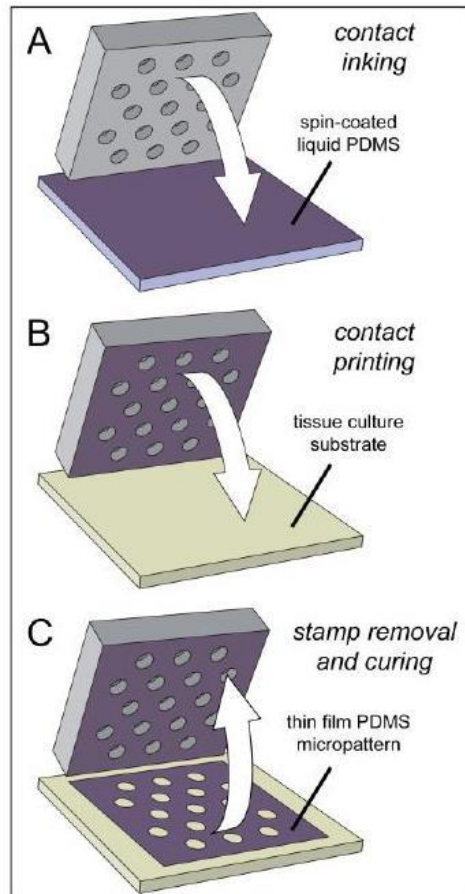


Figure 64: Schematic illustration of the μ CP. The PDMS stamp with recessed spot structures is inked by contact to liquid PDMS which is spin coated on a glass substrate (A, contact inking). The PDMS stamp with the liquid PDMS ink is transferred to a glass substrate or any other cell culture substrate (B, contact printing). The PDMS stamp is removed and the liquid PDMS ink is cured by heating. The printed PDMS structure (spots) remains on the glass substrate (C).¹³²

A preprint on a glass slide was done with the inked PDMS stamp in order to remove excessive PDMS on the stamp. Finally the second print on a second glass slide was done by subtle pressure of the PDMS stamp. Always the second print was used because it showed a higher structure resolution. Finally, the thin film PDMS micropattern on the glass substrate was cured by heating at 70°C for 10 minutes.

The cell culture was handled as described in chapter 5.2.1. The PDMS microarray was placed inside a petri dish. Afterwards, 1 mL of cell suspension in cell culture media

5 Cells

containing 2×10^5 cells was carefully pipetted onto the PDMS microarray. The cells were allowed to adhere on the glass exhibiting spots on the PDMS microarray. The lid of the petri dish was closed and placed inside the incubator at 37°C with 5 % CO₂. The media was exchanged every 2-3 days by using 6 mL media. The spheroids were harvested by pipetting after 14 days.

5.3 Results and Discussion

We have used the InSphero hanging drop platform and the PDMS microarray for the formation of spheroids. The results of both methods are shown and discussed in chapter 5.3. Later, both types of spheroids will be used in chapter 6 for metabolomics studies with the help of the homebuilt microslot NMR detector and the metabolic performance of these spheroids will be compared.

5.3.1 InSphero hanging drop spheroids

In the beginning the hanging drop method on petri dishes was tested. For this purpose 30 μ l of a cell suspension containing 1000 and 2000 cells was dropped onto a sterile petri dish lid and turned upside down. The drops inside a humidified chamber were incubated at 37°C for 4 days. The spheroids were controlled with the help of an inverted light microscope by turning the spheroids using an injection needle. However, the cell aggregates never reached a spherical shape and were looking like flat platelets. The reason for this might be the drop shape as shown in Figure 65.

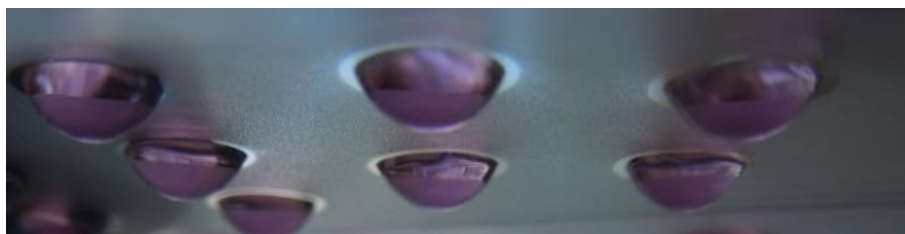


Figure 65: Hanging drop on a petri dish

When compared with the drop shape of the InSphero platform (Figure 66) the drops on the petri dish seem to have a lower contact angle and were consequently less spherical (elliptical) than the InSphero drops. The cells in the suspension precipitate at the bottom of the drop and distribute on the big drop surface and aggregate on a bigger surface which leads to a flat and rather 2D shape of the spheroid.

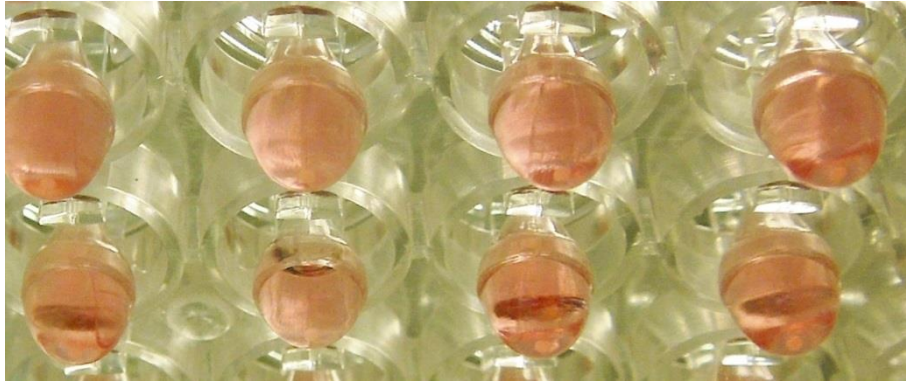


Figure 66: Hanging drops on an InSphero platform

On the contrary, the drops of the InSphero platform seem to have a bigger contact angle. The cells in the suspension precipitate at the bottom of the drop and distribute on the smaller drop surface where they can aggregate into a truly spherical shape.

The patented GravityPlus systems consist of 96 arrays with cavities looking like inverse funnels (side view) as shown in Figure 67. The cell suspension can be loaded from the top (pipette tip fits into the cavity) and the drop gets in contact with the funnel surface while the corners prevent spreading of the drop volume and ensure a spherical drop shape. Medium exchange can be performed by aspirating the old medium with the help of a pipette and adding fresh medium.

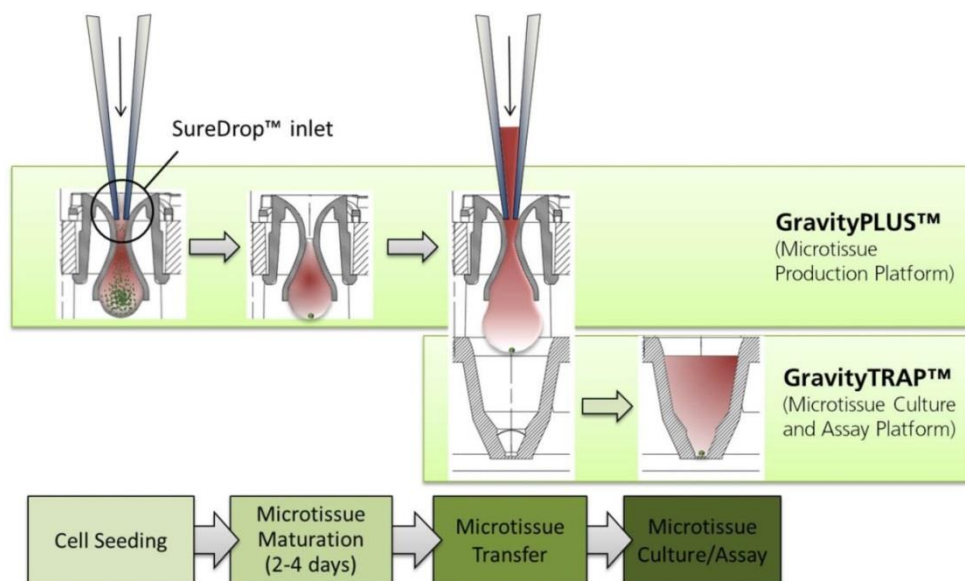


Figure 67: Insphero GravityPlus platform for spheroid formation by hanging drop. The spheroids can be transferred into a well plate for further assays.¹⁰⁶

The spheroids are ready for further experiments usually after 2-4 days. Before conducting an experiment the spheroids were transferred into fresh media and were controlled with a light microscope with the help of a needle. By turning the spheroid with the needle all three axes can be controlled. Once the shape is truly spherical and the size is as expected (see Figure 68) the spheroids can be used e.g. for long-term metabolomics analysis by NMR which is the main focus of this work and will be described in chapter 6.

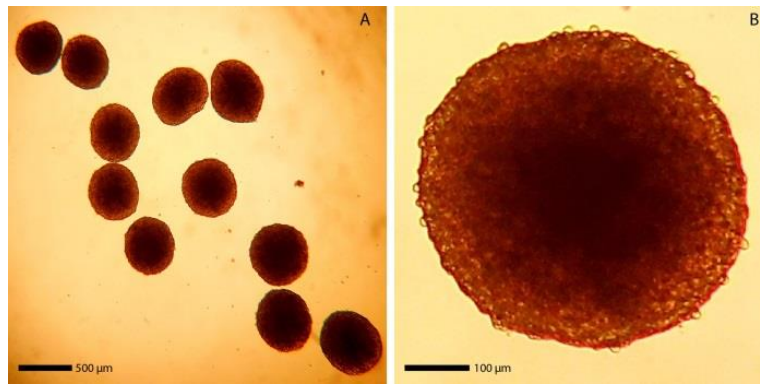


Figure 68: Microscopy image of uniformly sized tumor spheroids of HT29 adenocarcinoma cells (A) obtained by the Insphero gravityPlus system. Enlarged view of one spheroid (B).

Not only the size and shape was controlled but also some of the spheroids were sliced with a sharp injection needle in order to control the inner core. As expected the spheroids with diameters larger than 500 μm revealed a necrotic core with dead cells. As it can be seen in Figure 69 a white powder like material (necrotic core) flowed out of the spheroid during the slicing with the needle.

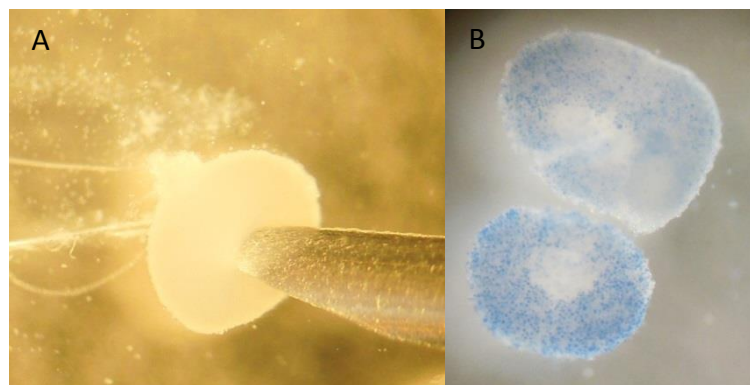


Figure 69: Microscopic image taken during the cutting of a spheroid with a sharp injection needle (A) to show the inner core of a spheroid with 600 μm diameter (B). In picture B the spheroid was stained with Trypan Blue solution. The dead cells are blue while the viable cells appear white. As expected the cut surface shows the largest number of dead cells caused by the mechanical force of the needle.

Afterwards, the spheroid slices were stained with Trypan Blue 0.4 % solution which stains selectively dead cells into blue. As expected the cut surface exploits more dead cells than on the rest of the spheroid which is caused by the mechanical force of the needle (Figure 69 b). The spheroid slices look like empty vessels after the necrotic core is removed.

It is well known from the literature that spheroids reveal a secondary necrosis in the core when they reach sizes of about 500 μm which is clearly visible in Figure 70.¹³³ The larger the spheroid is the bigger is the necrotic core.

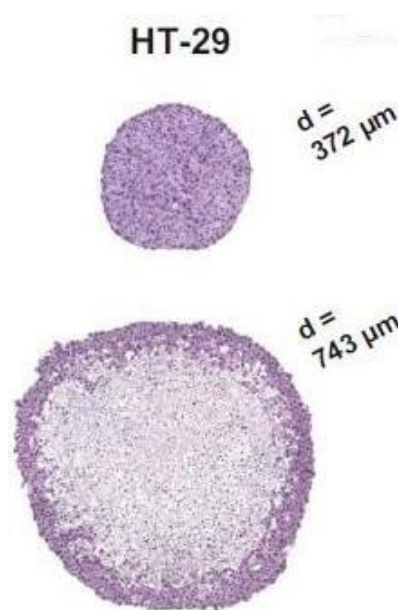


Figure 70: Microscope images of the median section of HT29 spheroids. Two spheroids with 372 μm and 743 μm diameters were embedded in paraffin and the median section was hematoxylin/eosin (H&E)-stained. Only the big spheroid revealed secondary necrosis (light pink).¹³³

The hypoxic conditions inside the spheroid are increasing the probability of cell death called necrosis. The cell death is always followed by the elimination of the cellular integrity and by the loss of cell's identity ending up with the heterolytic degradation of the cellular components into smaller fragments.¹³⁴ This is the reason why a powder like material flowed out of the spheroid which had no cell identity (Figure 69 a). This

aspect will be discussed again later in chapter 6.3.6. In this chapter we observed inside the spheroids a concentration increase of essential amino acids which cannot be synthesized within the mammalian cell metabolism. We assumed that the source of these essential amino acids are other proteins, which are broken down for instance as a result of necrosis and autophagy.

Reusing the InSphero plate

The InSphero platform consists of polystyrene with microstructure elements which are not suitable for sterilization inside an autoclave at 121°C.

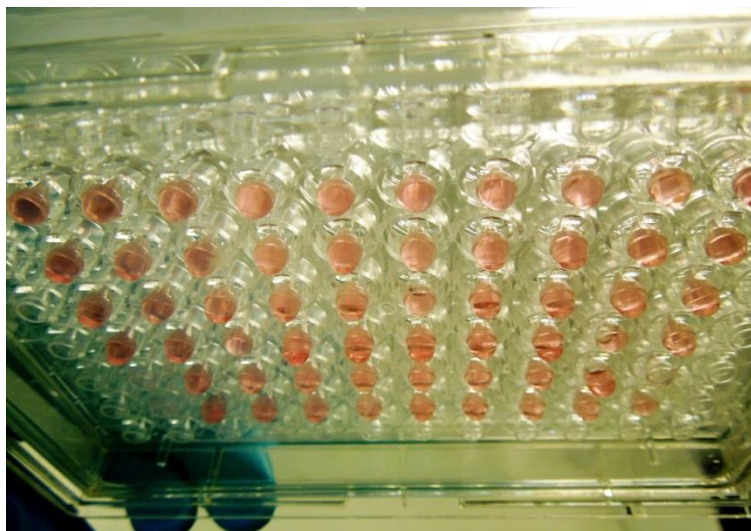


Figure 71: Bottom view of the 96-array InSphero hanging drop platform which is sandwiched between a bottom plate filled with water (for humidity) and a lid. The concave drop surface forces the cells to aggregate in spherical shape.

Therefore, the plate is designed for single use only. However, the price for each plate is around 80-100 € and not every experiment results in uniform and spherical spheroids so that the single use of the expensive plates is not effective. To overcome this problem, we improved a method to re-use the InSphero plate. For this purpose the plate is washed thoroughly with distilled water after the first use. The plate is then immersed into a 70 % Ethanol/Water (sterile) bath overnight. The plate is again rinsed with sterile and distilled water and dried under nitrogen stream. The plate is then

placed under a homebuilt plasma generator which was shown in chapter 4.3.1. Here, the cleaned and dried InSphero plate is placed inside the plasma generator and treated on both sides with O₂ plasma for 10 minutes. The plasma has here two positive effects. On the one hand plasma makes the polystyrene surface of the plate hydrophilic and on the other hand it sterilizes the plate which cannot be autoclaved. The hydrophilic surface attracts the hanging drop and the sterilization enables a contamination of the cells/spheroids with yeast or other bacteria. With this method the expensive InSphero plate can be used several times. But the cells/spheroids inside the hanging drops have to be monitored more often under the microscope to be sure to exclude any type of infection.

5.3.2 PDMS Microarray Spheroids

In this chapter the PDMS microarrays were used for the mass production of uniformly sized spheroids. The traditional hanging drop method utilizes the natural behavior of some cells to aggregate inside a drop without a surface for adhesion. Unlike this method, the microarray method consists of spots exposing a glass surface where the cells can adhere (Figure 72). Hydrophobic surfaces like PDMS prevent the deposition of extracellular matrix proteins causing the denaturation of the adhesion proteins.¹³⁵

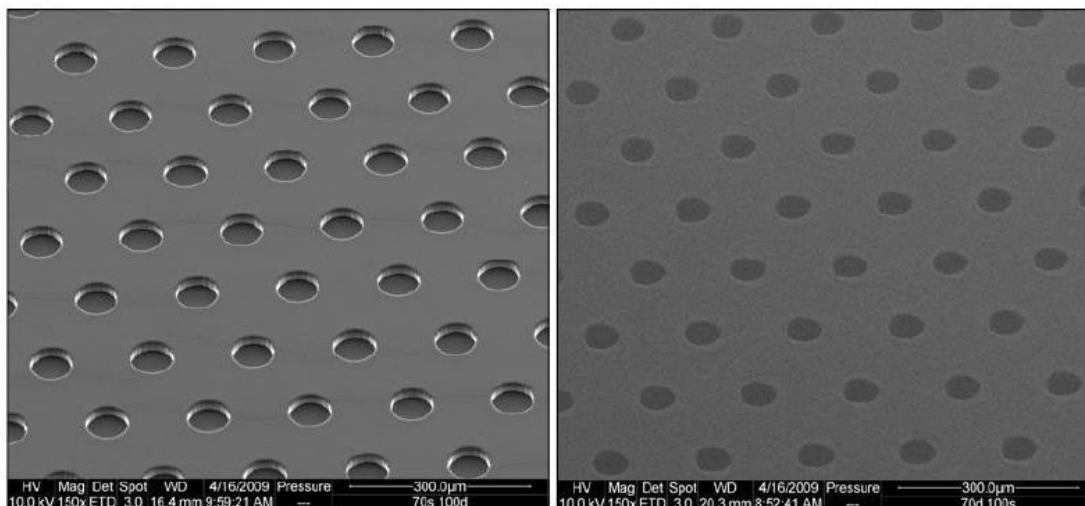


Figure 72: (A) SEM images of the PDMS stamp with recessed structure of the spots. (B) Complementary PDMS film with spots uncovering the underlying glass wafer where the cells will adhere.¹⁰⁵

The microarrays were seeded with 2×10^5 HT29 human colon adenocarcinoma cells in 1 mL cell culture media. The cells sediment, assemble and adhere inside the spots. After 3 days the non-adhering cells were removed and 6 ml fresh media was added and exchanged every 2-3 days. After 24 hours approximately 40-50 cells assemble and adhere inside each spot as shown in Figure 73 a and grow into a monolayer during the next 24 hour (b). After covering the full area of the spot the cells start growing into the top direction and building a hemisphere after 96 hours (C). Usually after 10 -14 days the spheroids reach their uniform spherical shape and can be harvested (see Figure 74).

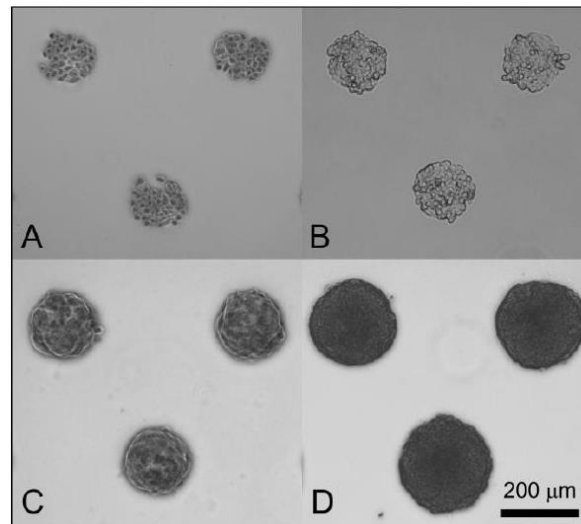


Figure 73: Microscopy image of the time dependent development of the spheroids. (A) After 24 hours the cells assemble inside the spot. (B) The cells grow into a monolayer. (C) After 96 the hemisphere is forming. (D) After 10 days the spheroid is fully developed.¹⁰⁵

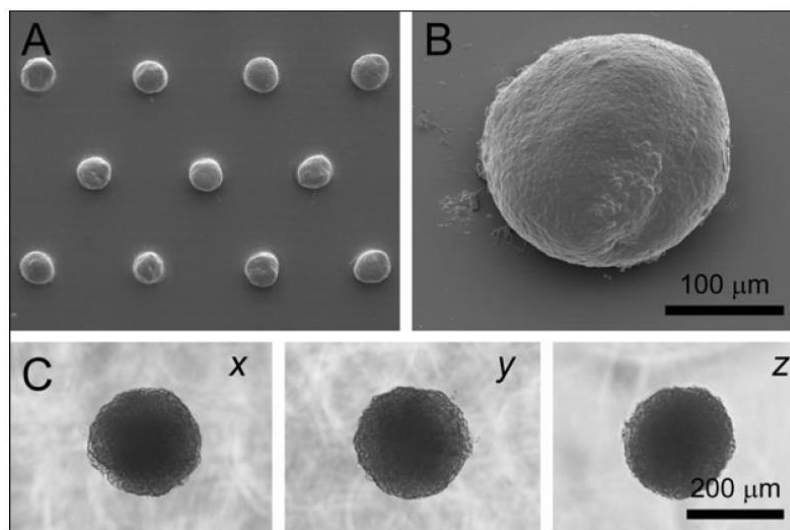


Figure 74: (A) SEM image of the formaldehyde-fixed (A) spheroids and (B) a single spheroid grown on the PDMS microarray showing the truly spherical shape. (C) Microscopy 3-axis image of an agarose embedded spheroid. Circularity measurements showed $x = 91\%$, $y = 93\%$, $z = 94\%$ circularity.¹⁰⁵

Several studies suggest that a small subpopulation within the proliferating cells is responsible for the sphere shaped development of tumors. The growth from 2D flat monolayers into 3D spherical structure is supposed to mimic the lineage expansion during *in vivo* development. Also the spheroid's cell density is similar to the density of *in vivo* tissues.^{105, 135} The physical characterization and spheroid number analysis from the referred work resulted in 2009 ± 153 cells with a density of $1044 \pm 7 \text{ kg/m}^3$ at a spheroid diameter of $200 \pm 11 \text{ }\mu\text{m}$.¹⁰⁵ The density of about 1044 kg/m^3 is comparable with tissue densities of e.g. brain 1020 kg/m^3 and skeletal muscle 1040 kg/m^3 . Taken together, the spheroid formation based on cell proliferation and the dense packed microarray spheroids are supposed to mimic real tissue samples better than hanging drop spheroids which are obtained by aggregation and proliferation. Both spheroids will be used in chapter 6 for metabolomics studies with the help of the homebuilt microslot NMR detector.

6 Hyphenation of NMR + LOC + Cells for long-term metabolomics

6.1 Introduction

In this chapter the results of chapter 3-5 which have been proven to be successful (microslot NMR detector with on-board heater, microfluidic glass device and spheroids) will be hyphenated. The miniaturized microslot NMR detector enables the analysis of ultra-small samples and the planar geometry of the detector allows the hyphenation with versatile LOC technology. The microfluidic glass device is not only a suitable NMR sample holder it ensures also the viability of spheroids under almost physiological conditions. With this set-up 3D *in vitro* cell culture models (spheroids) will be analyzed because they have turned out to be authentic model systems which successfully bridge the gap between 2D cell cultures and live tissue or animal models. Several long-term metabolomics studies on living cells will be conducted in order to elucidate the cellular functions and their corresponding biochemical pathways.

6.2 Materials and Methods

The NMR measurements were carried out at 600.35 MHz on a Bruker AVANCE III NMR spectrometer equipped with a homebuilt planar microslot waveguide probehead. In some cases comparison measurements with a conventional NMR Probe (Bruker PABBO 5 mm inverse probe) were performed. Proton NMR spectra were acquired using a simple pulse-acquisition sequence. The relaxation delay was 2 s. The excitation pulse angle was 60 degrees. The spectral range was 9652 Hz. 1024 scans were accumulated for each spectrum of the time series. The free induction decays were digitized into 16k points, followed by zero filling to 64k prior to Fourier transform. An exponential line broadening of 0.3 Hz was applied. Baseline corrections were performed using cubic splines.

The temperature was controlled with an on-board non-magnetic planar heater. The spheroids were placed inside a U-shaped capillary which contains a Teflon-filter to trap the spheroid and a reservoir filled with media. The analysis of the metabolite signals

were performed with the help of data available in the literature and on databases like Kyoto Encyclopedia of Genes and Genomes (KEGG), Human Metabolome Database (HMDB), Biological Magnetic Resonance Data Bank (BMRB) and by using the software Topspin, Chenomx, MestReNova and Origin9. The metabolite signals were assigned by using one-dimensional ^1H -NMR spectra. Chemical shift values are given relative to the water signal at 4.7 ppm. No standard was added in order to avoid perturbation of the natural metabolism of the cells. For a better assignment multiplicity and J-values were taken into account, if resolution was sufficient. If J-splittings could not be resolved, assignment was performed using shift values that were obtained from reference measurements with selected metabolites at concentrations ranging from 0.05 mM to 50 mM and at pH values ranging from 6 to 9 at a temperature of 37°C.

6.3 Results and Discussion

As the signal interference from macromolecules was at a low level, there was just a background of broad signals superimposed on the spectrum of the metabolites. In order to avoid signal losses due to spin-spin relaxation, we refrained from the use of a spin echo technique which is commonly employed for the attenuation of protein signals. Instead, the spectral response of macromolecules was eliminated by baseline correcting the spectra. As the one-dimensional proton NMR spectra showed a broad water signal in the range of 4.5-5.5 ppm, only the low-field and high-field range of the spectra were analyzed. Dynamic range problems because of the presence of a water signal did not occur: The dynamic range of the signals is not as big as the range of water vs. metabolite concentrations (55 M vs. 0.05 mM) suggests, as the signals of the metabolites are narrow (FWHM of 2 Hz) whereas the water signal is wide (FWHM around 50 Hz). So even for the samples of the lowest concentration (0.05 mM), the metabolite signals are digitized into at least 4 bits. For the 50 mM samples at least 13 bits are used for digitization.

Working with living cells requires measurements at a somewhat elevated temperature (37°C), which turned out to be even advantageous: Higher Temperatures increase the exchange of protons and molecular flipping, which gives rise to narrower resonance lines. Though elevated temperatures reduce the signal intensities due to the less

6 Hyphenation of NMR + LOC + Cells for long-term metabolomics

favorable Boltzmann distribution with more spins in the spin-up state, the decrease in line-broadening turns out to be more important, as the J-splittings are better visible allowing for an easier signal assignment.

6.3.1 Microslot NMR detector integrated with a microfluidic device.

The homebuilt planar microslot waveguide probehead (also called microslot NMR detector) and an on-board non-magnetic planar heater is shown in Figure 75.

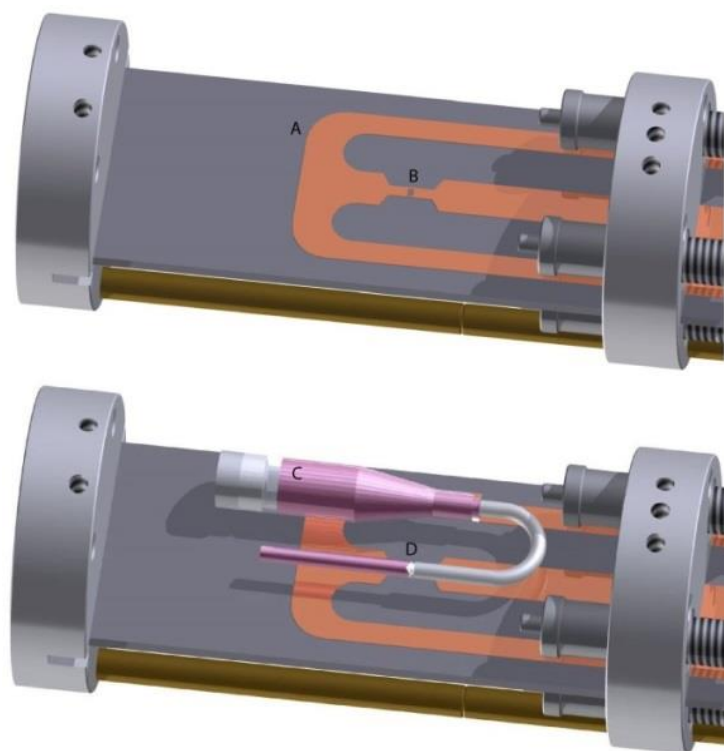


*Figure 75: **Microslot NMR detector integrated with a microfluidic device.** Schematic drawing of the planar waveguide microslot NMR probehead (A) with on-board non-magnetic planar heater (backside). The small slot (100 x 200 μm) in the copper strip (B) confines a homogenous magnetic field when electric current is applied. The dimensions of the slot can be adjusted to the size of the sample under investigation, thus samples with nano liter volume can be measured. The probehead is here hyphenated with a U-shaped microfluidic glass device (C) which is filled with cell culture medium and one spheroid with 500 μm diameter. The spheroid (D) is placed above the microslot of the probehead which is the most sensitive area for detection. During the course of the experiment the probehead and microfluidic device are in a vertical position and not horizontal as shown here.*

6 Hyphenation of NMR + LOC + Cells for long-term metabolomics

Two different experimental set-ups were used as it can be seen in Figure 76: Experiments in which the living cells were kept inside the incubator (called off-chip experiments in which only the medium was analyzed) are compared to experiments in which the living cells were kept inside the NMR (called on-chip experiments). This term is used because the cells within the NMR are placed inside a microfluidic device/chip during the course of the experiment. In another on-chip experiment the microfluidic device was filled with cell culture medium without living cells and measured for 24 hours. This experiment served as a control to analyze the components and their concentrations inside the cell culture medium.

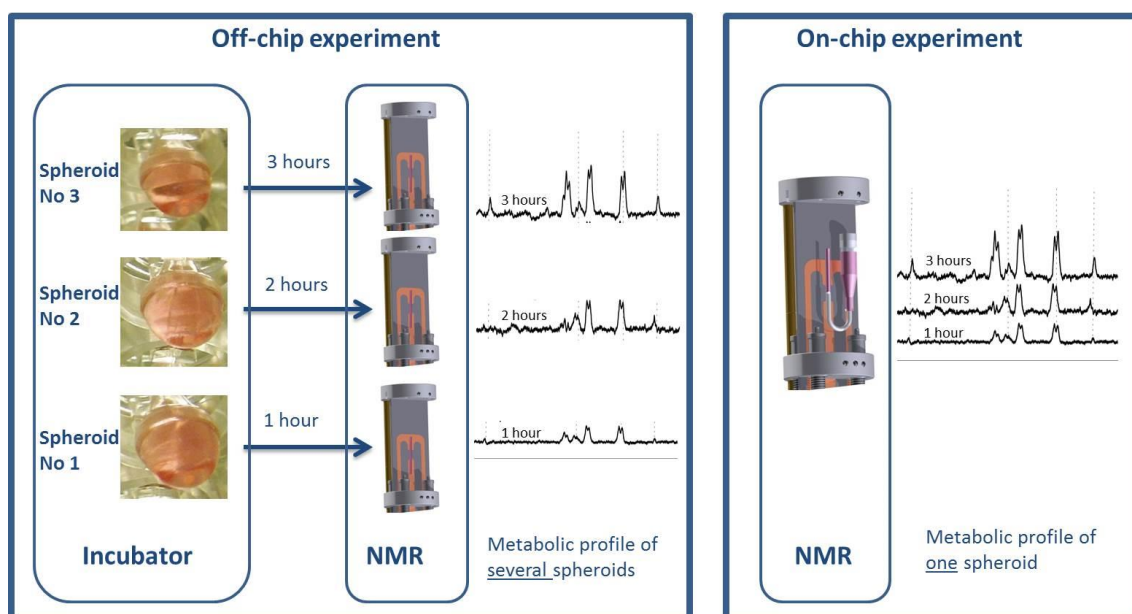


Figure 76: Off-chip and on-chip experiments at a glance.

Off-chip: Several hanging drops (cell culture medium) each containing one spheroid were placed inside the incubator. The physiological pH inside the cell culture medium was maintained using an incubator with 5% CO₂ supply. Every hour one drop was transferred into a glass capillary and was analyzed with the help of the microslot NMR detector and was discarded after each measurement.

On-Chip: A single spheroid was placed inside a U-shaped capillary which contains a teflon-filter to trap the spheroid at a defined position (Figure 75 D). Additionally, the

6 Hyphenation of NMR + LOC + Cells for long-term metabolomics

capillary is connected to a reservoir filled with media (Figure 75 C). By diffusion and evaporation controlled perfusion of the cells with nutrients and oxygen and accurately controlled temperature, the viability of the cells is ensured at near physiological conditions for the long-term *in vitro* studies. Since the cells were outside the incubator (no 5% CO₂ atmosphere) the physiological pH inside the cell culture medium was maintained by using 4-(2-hydroxyethyl)-1-piperazineethanesulfonic acid (HEPES). Viability assays showed no influence of HEPES on the cell growth and viability.

6.3.2 Spheroid vs media on chip for 24 hours.

For the on-chip experiments the microfluidic glass device was filled with cell culture medium (DMEM, 10% FBS, 25 mM HEPES). Afterwards, one HT29 spheroid at day 4 in culture with a size of approximately 500 μm consisting of about $0.9 \cdot 10^4$ cells and with necrotic/apoptotic core¹³³ was transferred into the capillary of the device. The production and degradation rates of the metabolites were observed online for 24 hours at 37°C. Figure 77 shows the ¹H-NMR spectra of the cell culture medium with spheroid.

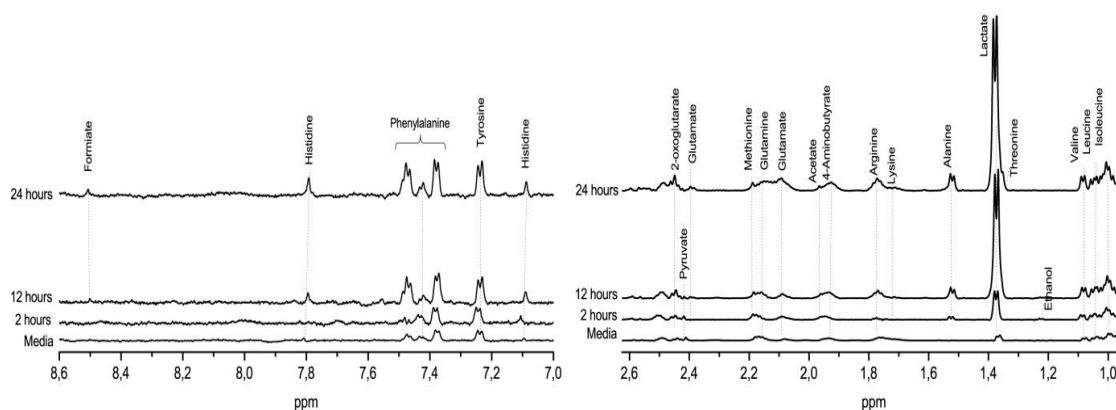


Figure 77: High resolution ¹H-NMR spectra (600 MHz) obtained with the microslot probehead. The microfluidic device is filled with media and one spheroid (on chip experiment). The dynamic process of metabolite production and degradation is observed at 37°C for 24 hours. For a better visibility of the signals the spectra on the left are enlarged tenfold compared to the spectra on the right.

The signal intensities are correlated with the concentration of the metabolites which were determined by integration of each peak relative to the solvent peak (As no external standard had been added, the known water concentration was used as a concentration reference). The assigned metabolite signals and their concentrations in mM were plotted as a function of time in Figure 78. As the flow of liquid and the components inside the capillary is not only governed by diffusion and capillary action, but also by evaporation, the concentration of the components inside the medium is likely to increase with time, even in the absence of a spheroid. For this reason, two experiments were conducted inside the microfluidic device, one without (control) and one with spheroid in the cell culture medium. As shown in the charts (Figure 78) the effect of the aforementioned concentration increase is, however, negligible: While in the control experiment without spheroid (Figure 78 B, D) the concentrations of the components inside the medium were found to remain almost constant over time, the experiment with spheroid (Figure 78 A, C) revealed a dynamic process of metabolite production and degradation within the 24 hour measurement time. For instance the alanine concentration inside the medium remains almost stable during a 24 hours measurement. But in presence of the spheroid the alanine concentration is clearly increasing within the same time. Not only the concentration increases but also the consumption or degradation of some metabolites like ethanol by the cells can give hints regarding the preferred metabolic pathways inside the cells. Taken together, the increasing signals in Figure 78 are a result of metabolite production of the living cells. Therefore, the temporal dynamics of cellular metabolite levels can be observed with this novel technique.

6 Hyphenation of NMR + LOC + Cells for long-term metabolomics

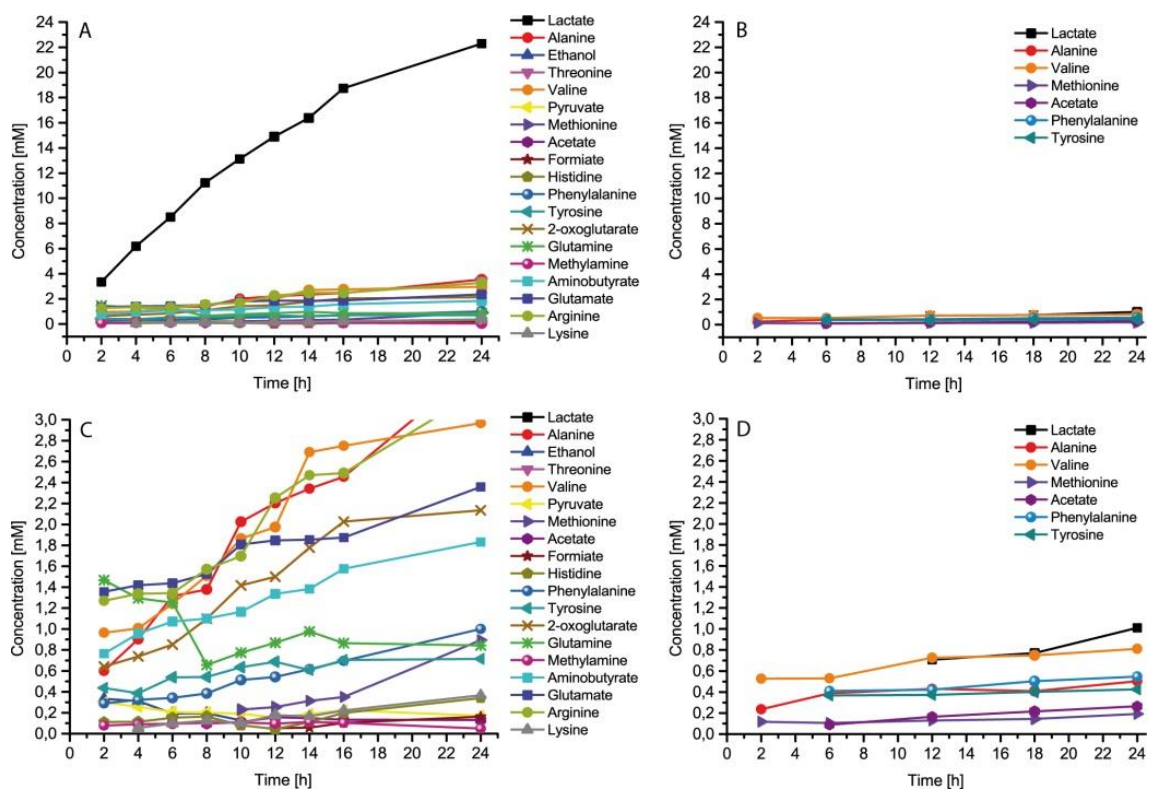


Figure 78: Metabolite concentrations in mM are plotted as a function of time. The graphs are showing the metabolite concentration levels inside the microfluidic device filled with media and one spheroid (A) and media only (B). The temporal dynamics of metabolite concentration levels can be observed. For a better comparison and analysis graph C shows the enlarged view of the low concentration range (up to 3 mM) of the graph A. Graph D shows the enlarged view of the low concentration range (up to 3 mM) of graph B.

6.3.3 Off-chip vs on-chip experiment.

For the off-chip experiments several drops (each 30 μ l drop consists of DMEM, 10% FBS) were pipetted on the lid of the petri dish. One spheroid of 500 μ m diameter was placed in each of these drops. The bottom of a petri dish was filled with 5 ml PBS buffer to avoid evaporation of the drop containing the spheroid. Finally, the lid was turned upside down, placed on the bottom piece of the petri dish and transferred inside the incubator (humidified 37°C incubator with 5% CO₂ atmosphere). Every one

6 Hyphenation of NMR + LOC + Cells for long-term metabolomics

hour one drop (without spheroid) was transferred into a capillary (same like the microfluidic device capillary) and measured with the microslot detector. The assigned metabolite signals and their concentrations in mM were plotted as a function of time in Figure 79, which shows metabolite profiles of the off-chip (A, C) and on-chip (B, D) experiments. For a better comparison of the metabolites in the low concentration range (up to 1 mM) the graphs in Figure 79 A and B are shown enlarged in the charts C and D, respectively.

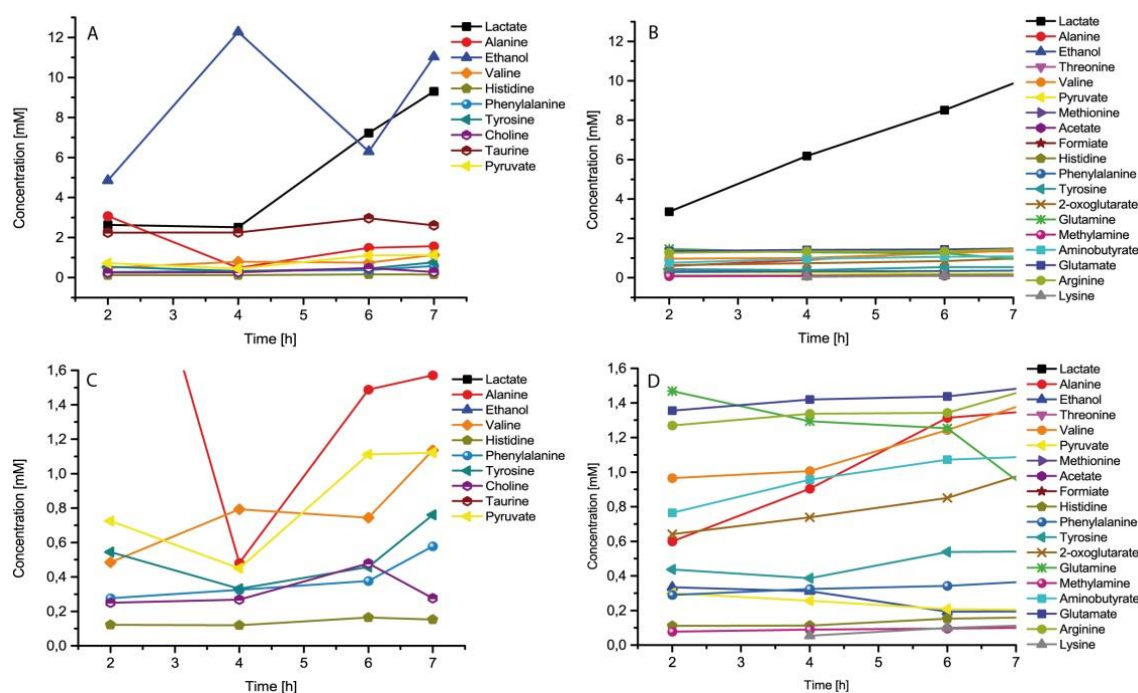


Figure 79: Comparison of the metabolite production rates of the off-chip (A) and on-chip (B) experiment for 7 hours. The off-chip experiment shows the metabolite profile of several spheroids at different time points while the on-chip experiment shows the metabolite profile of the same spheroid at different time points. C and D: Enlarged view of the low concentration range (up to 1.6 mM) of the charts A and B, respectively.

The off-chip experiment (Figure 79 A, C) showed highly fluctuating values when compared with the on-chip experiment (Figure 79 B, D). This is due to the different contribution of the individual spheroids which were used for each time point (off-chip). The off-chip experiment shows the metabolite profile of several spheroids at different

time points while the on-chip experiment shows the metabolite profile of the same spheroid as a function of time. This highlights the importance of the on-chip experiment in which the metabolite production and degradation of a single spheroid could be observed online for several hours. Even though the spheroid formation is a highly reproducible technique, not every spheroid is exactly the same. Small fluctuations in total cell number, diameter and shape of the spheroid are possible which give rise to these fluctuating values as shown in Figure 79 A, C. In addition stochastic biological processes can also influence the results in these cell populations.¹⁶ On the other hand, the smooth progress observed in the on-chip experiment Figure 79 B, D is promising for future applications of this novel analysis technique, as e.g. perturbations of metabolic pathways due to drugs and the corresponding cellular response can be observed online. The observed fluctuations for the off-chip experiment, on the other hand, complicate data analysis and can even mask the result of the perturbation. Furthermore, the off-chip experiment shows only the metabolites which were released by the cells to the extracellular milieu, whereas the on-chip experiment shows both the intracellular and the extracellular metabolites. Unfortunately, the signals of some metabolites like those of taurine and choline are superimposed by the HEPES signals in the on-chip experiment. To overcome this problem, we are currently designing a new microslot probehead with controlled 5 % CO₂ and O₂ supply acting as an incubator like environment during the course of long time measurements. Apart from the highly fluctuating values for the off-chip experiments and some differences in the detected metabolites, the on-chip and off-chip experiments presented above resulted in similar metabolic profiles (see Table 2). These findings indicate that the cells kept inside the NMR (on-chip) are exposed to similar conditions like cells grown inside the incubator (off-chip). The measurement uncertainty for the on-chip experiment is shown in chapter 6.3.7.

6 Hyphenation of NMR + LOC + Cells for long-term metabolomics

Table 2: Comparison of the metabolite concentrations of the on-chip and off-chip experiment [in mM].

	Off chip		On-chip			Notes
	1 hour	7 hours	2 hours	7 hours	24 hours	
Lactate	2.63	9.30	3.34	9.08	22.29	
Alanine	3.08	1,57	0.59	1.76	3.54	
Ethanol	4.86	11.03	0.33	0,19		Disappears after 10 hours
Threonine					3.41	Visible after 16 hours, Quantification after 24 hours
Valine	0.49	1.14	0.96	1.82	2.96	
Pyruvate	0.73	1.12	0.29	0.15	0.17	
Tyrosine	0.54	0.76	0.43	0.57	0.71	
Phenylalanine	0.28	0.58	0.28	0.48	1.00	
Histidine	0.12	0.15	0.11	0.19	0.34	
Choline	0.25	0.28				
Taurine	2.25	2.60				
Methionine					0.89	Appears after 10 hours with 0.22
Acetate					0.13	Appears after 8 hours with 0.09
Formiate				0.09	0.16	Appears after 12 hours with 0.05
2-oxoglutarate			0.64	1.08	2.13	
Glutamine			1.46	0.20	0.84	
Glutamate			1.36		2.36	
Methylamine			0.07	0.08	0.04	
Leucine						
Isoleucine						
Aminobutyrate			0.76		1.83	
Arginine			1.27		3.28	
Lysine					0.37	Quantification after 4 hours with 0.05

6.3.4 The role of lactate and alanine

The high accumulation of lactate is an indication of hypoxic conditions within the avascularized areas⁸ of the spheroids, which mimic tumor conditions. Hypoxic conditions and high lactate accumulation within the spheroid core are observed and shown in many studies^{9, 10} and are an indicator for a glycolytic metabolism (Figure 7). Nevertheless, it is well known that the metabolic profiles of cancer cells are remarkably different from those of normal cells.¹³⁶ But it is not yet fully understood whether these altered metabolic properties are specific to tumor/spheroid cells due to a genetic lesion or just mirror adaptation of the cells to their microenvironment like hypoxia. In a recent study lactate and alanine were used as metabolic biomarker of prostate cancer of biopsy tissues. Low concentrations of lactate (0.61 mmol/kg) and alanine (0.14 mmol/kg) were observed in benign biopsy tissues while high concentrations of lactate (1.59 mmol/kg) and alanine (0.26mmol/kg) were found in malignant tissues.⁶ Hence the explanation of high lactate accumulation within tumor tissues/spheroids as an indicator of hypoxia does not seem fully conclusive, especially as recent studies^{9, 136-139} assign a more important key role to lactate in cancer metabolism.

At this point, the hypoxia related and the best characterized example for metabolic reprogramming in tumor cells, the Warburg effect, has to be mentioned. It describes the shift from oxidative phosphorylation to glycolysis in order to produce ATP. It has been proposed that the shift to glycolytic metabolism is an adaptation of the avascular cells to hypoxia during the early stage of tumor growth.^{7, 140} This allows ATP production in the absence of oxygen. Some tumor cells keep their glycolytic metabolism even when oxygen is available again. Moreover, the metabolic switch from oxidative phosphorylation towards glycolysis is driven by multiple oncogenic signaling pathways such as PI3K, AKT, mTOR, HIF1, MYC. Interesting is also the switch to the pyruvate kinase M2 (PKM2), an isoform of pyruvate kinase which is usually present in stem cells and over expressed in many cancer cells. This enzyme catalyzes the conversion of phosphoenolpyruvate to pyruvate and generation of ATP. By slowing the glycolysis, PKM2 allows the conversion of pyruvate to lactate, alanine and other

6 Hyphenation of NMR + LOC + Cells for long-term metabolomics

molecules rather than allowing pyruvate to enter the oxidative pathway (see figure 5).⁷ Although the glycolytic pathway can result in much faster ATP generation, compared to the oxidative pathway (34 ATP molecules per glucose molecule) it results in 2 ATP molecules per glucose molecule. This shift indicates that the glycolytic pathway provides a biosynthetic advantage for tumor cells.

Furthermore, Sonveaux et al. pointed out that lactate, the end-product of glycolysis plays an important role in the metabolic symbiosis between glycolytic and oxidative cells within a tumor. They proposed that lactate, produced by glycolytic tumor cells, fuels oxidative tumor cells for energy exploitation as shown in Figure 80.

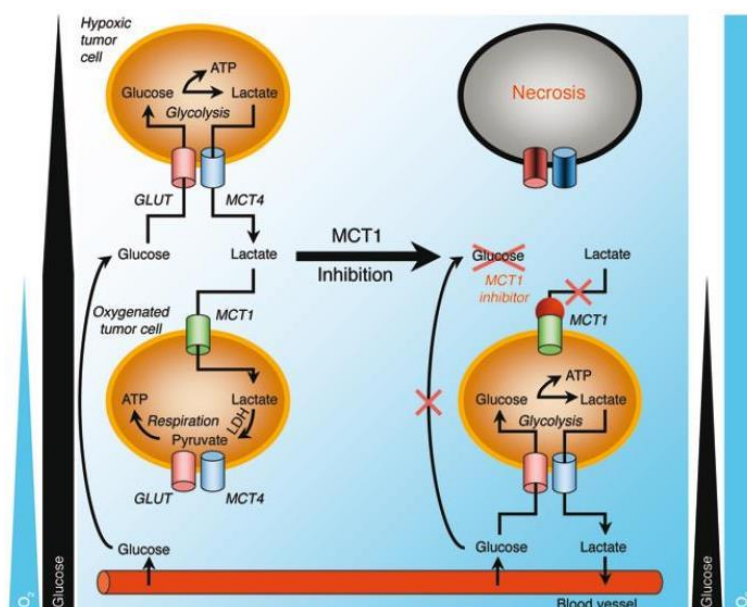


Figure 80: Illustration of the lactate-based metabolic symbiosis in tumors. Lactate produced by cells under hypoxic conditions fuels the oxidative metabolism of tumor cells which have access to oxygen. A model for therapeutic targeting of this symbiosis is given via MCT1 inhibition.

In this symbiosis lactate is shuttled via monocarboxylate transporter 4 (MCT4) outside the membrane by the glycolytic cells in the hypoxic area. Afterwards, the oxidative tumor cells in oxygenated regions import the lactate via MCT1 and metabolize it through oxidative phosphorylation to ATP¹³⁷. This symbiosis between glycolytic and

6 Hyphenation of NMR + LOC + Cells for long-term metabolomics

oxidative tumor cells may explain why the global ATP concentrations in tumors are rarely different from normal tissues although glycolysis provides 2 ATP molecules whereas oxidative phosphorylation provides 38 ATP molecules (as discussed above).¹³⁷ The high lactate accumulation within the hypoxic areas and the pathophysiological gradients inside a spheroid is shown in Figure 81.

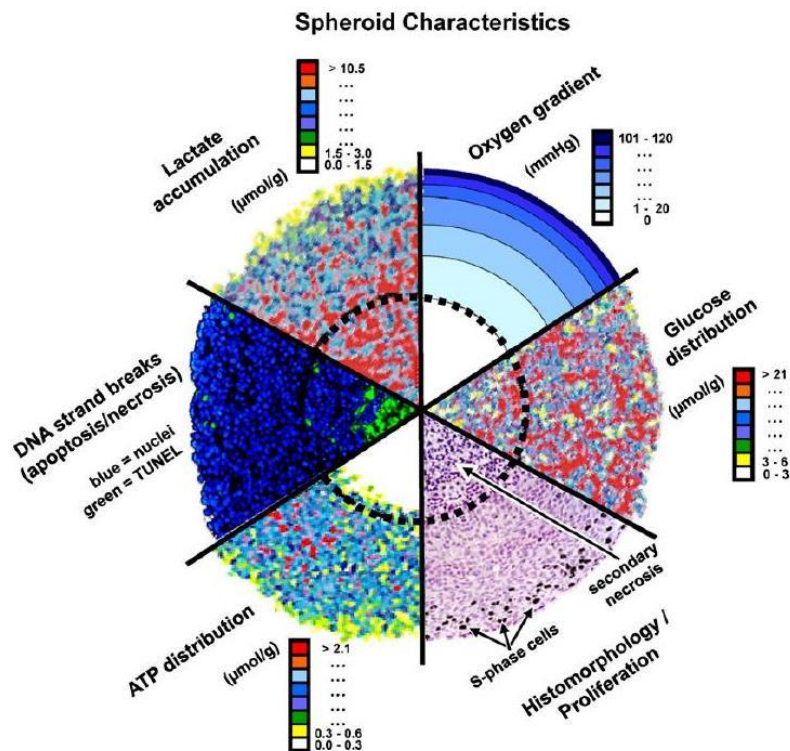


Figure 81: Median section of the spheroid showing the pathophysiological gradients inside the spheroid. The results of different analytical techniques were combined: autoradiography, the tunnel assay, bioluminescence imaging, and probing with oxygen microelectrodes.⁹

Another study by Rodriguez-Enriquez et al. published in the same year revealed also insights regarding the unusual energy metabolism in tumor cells. It has been shown that the glycolytic metabolism which is expected under hypoxic tumor conditions is not the only predominant energy pathway found in tumor cells. During the early stages of spheroid formation, young-spheroids reveal besides glycolytic metabolism also an active oxidative phosphorylation pathway. Almost 60% of the ATP was produced via

oxidative phosphorylation despite the hypoxic conditions of the tumor microenvironment. Also the change in expression levels of proteins involved in glycolysis and oxidative phosphorylation is an indicator for the adaptation of the cells to the tumor microenvironment. The new strategies in shifting the energy metabolism and the symbiosis of the different subgroups of cells with each other are indicators why tumors show a good survival and persistence.¹²² This might explain the poor therapeutic success of many anti-cancer drugs which are usually targeting one type of biochemical pathway or one type of subgroup. While the target/drug kills one subgroup of cells the others can switch their metabolism or keep up symbiosis with other subgroups and the consequence is the tumor recurrence. One has to reveal the different subgroups and target each of them, thus a combined therapy is here suggested.

Additionally, there is also evidence that a high lactate concentration is influencing the tumor cell migration and metastasis and is correlated with resistance to radiotherapy and anticancer drug therapy^{8, 9, 136} Considering these findings the role of lactate can be further analyzed with this novel microslot NMR detector e.g. by targeting the lactate transporting enzymes and observing the metabolic changes online.

6.3.5 The role of ethanol and acetate.

Compared with the off-chip experiments the on-chip experiments showed lower ethanol concentrations. The initial ethanol concentration of 0.33 mM decreased and ethanol was not observed after 10 hours. Acetate, however, was observed after 8 hours and reached concentrations of 0.13 mM after 24 hours. On the contrary, the off-chip experiments showed no acetate but high concentrations of ethanol.

In the CO₂ buffered off-chip experiment inside the incubator the CO₂ reacts with the water of the medium and forms H₂CO₃ which is in equilibrium with the bicarbonate and carbonate ions.

6 Hyphenation of NMR + LOC + Cells for long-term metabolomics



This means that via the CO_2 reaction hydrogen ions are released which keep the pH of the medium at an acceptable level and prevent basic conditions. The proposed pathways for acetate and endogenous ethanol are given in Figure 7.

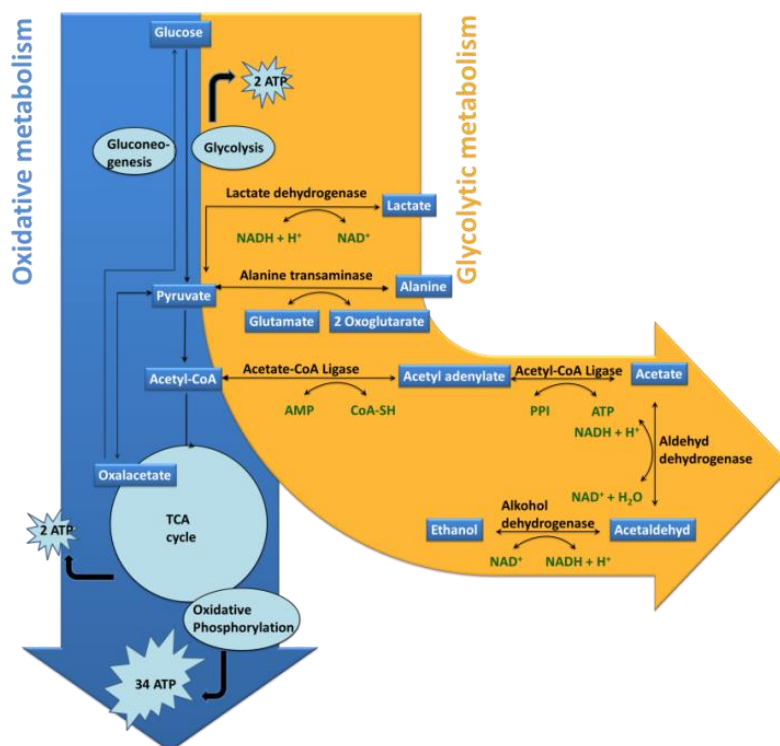


Figure 82: Section of a metabolic pathway map. The metabolic profiles of the multicellular tumor spheroid were investigated by using the microslot NMR probehead. The amounts and dynamics of the metabolites are indicating a shift from oxidative (blue) to glycolytic metabolism (yellow). Glycolytic metabolism appears usually at hypoxic conditions like found inside the spheroids.

The pyruvate dehydrogenase multienzyme complex catalyzes the oxidative decarboxylation of pyruvate to acetyl-coA which is converted to acetate. Aldehyde dehydrogenase catalyses the reduction of acetate to acetaldehyde by releasing nicotinamide adenine dinucleotide (NAD^+). Acetaldehyde is then reduced to

ethanol by alcohol dehydrogenase again by releasing NAD^+ . The high ethanol concentration within the off-chip experiment is an indicator for highly reductive conditions within the CO_2 buffered atmosphere inside the incubator, which support the reduction of acetaldehyde to ethanol, whereas the HEPES buffered on-chip experiment does not seem to provide high reductive conditions and the reaction probably stops with acetate. Almost at the same time ethanol disappears (after 10 hours), and acetate appears (after 8 hours) which underlines the above described idea. Therefore a new microslot probehead with controlled 5% CO_2 and O_2 supply is currently being designed.

6.3.6 The role of other amino acids

Valine, Isoleucine, Leucine, Methionine, Histidine, Phenylalanine, Tyrosine, Threonine.

Amino acids play an important role in catabolic and anabolic processes within the metabolism. Within the off-chip and on-chip experiments the increased biosynthesis of the amino acids is mirroring again the need for fast growing cells for energy, macromolecules and the maintenance of the cells' redox status.^{7, 141} There is also a remarkable concentration increase of essential amino acids which cannot be synthesized within the mammalian cell metabolism. The sources of these essential amino acids are presumably other proteins, which are broken down for instance as a result of autophagy, apoptosis, necrosis etc. as shown in Figure 70 in chapter 5.3.1. In this chapter we showed that the necrotic core consists of death cells with no cellular integrity. The degradation and decomposition of the cellular fragments was clearly visible. The hypoxic conditions inside the spheroid are increasing the probability of necrosis and programmed cell death. Within this context, the mechanistic target of rapamycin complex 1 (mTORC1) senses growth factors, cellular stresses, oxygen abundance, nutrient availability and energy levels. For instance, amino acids must be present in the cellular environment for mTORC1 to be active.¹⁴²⁻¹⁴⁵ When activated, mTORC1 phosphorylates substrates that potentiate anabolic processes, such as lipid

synthesis, and limit catabolic ones, such as autophagy. This means less oxygen or nutrient availability deactivates mTORC1 which increases autophagy.

6.3.7 Measurement uncertainty

Several separate measurements with different spheroids were carried out. But no error bars were calculated for the metabolite concentrations because we preferred to show the metabolic profiles of a single spheroid which gives only single data points. We tried to avoid generating statistical average values for the metabolic profiles of the different spheroids.

Under otherwise quantitative conditions like fully relaxed spectra, sufficient digital resolution, use of zero filling and exponential weighting as well as careful phase and baseline correction, the following two topics have to be discussed as sources limiting the accuracy, one source of uncertainty is the limited signal to noise ratio (S/N) of the spectra. With a S/N value of x , the corresponding uncertainty is given by $(1/x)*100\%$. As the currently available technical setup does not allow for a more extended signal averaging, these uncertainties appear to be unavoidable at the moment.

In order to investigate the quality of our measurements and the resulting experimental data we preferred to carry out several separate experiments like reference measurements with selected metabolites at concentrations ranging from 0.05 mM to 50 mM and at pH values ranging from 6 to 9 at a temperature of 37°C (see 6.2). These measurements were used for the assignment of the metabolite signals and to control the reliability of our concentration calculation via integration. The measurement uncertainty for the on-chip experiment (see Figure 78) was calculated with the help of the signal to noise for lactate (high concentrated compound) and valine (low concentrated compound) and is shown in Table 3.

However, the idea to compare the profiles of different spheroids might be very interesting after establishing this new method. A huge variety of biochemical analysis can be conducted to investigate the metabolic profiles of several spheroids. For

instance one may determine the effect of the spheroid shape, diameter and cell number to the overall metabolic profile of the spheroid.

Table 3: The measurement uncertainty of the on-chip experiment

Lactate	Exp No	S/N	Error (%)	Valine	Exp No	S/N	Error (%)
	1	101.2	0.98		1	10.7	9.3
	2	110.6	0.90		2	14.4	6.9
	3	137.0	0.72		3	16.9	5.9
	4	149.5	0.66		4	18.2	5.5
	5	169.9	0.58		5	54.0	1.9
	6	181.2	0.55		6	58.3	1.7
	7	255.1	0.39		7	64.2	1.6
	8	365.9	0.27		8	89.9	1.1

6.3.8 Comparison of two individual on-chip experiments

As mentioned above, several separate on-chip measurements were carried out. However we refrained to generate statistical average data out of these single measurements because in conventional metabolomics research analytical end-points show only statistical average response of several millions of cells. Instead, we will compare in this chapter the metabolic profiles of two uniform spheroids with 500 μm diameter each consisting of approx. 9.000 cells which were measured within the same conditions in two separate on-chip experiments. The production and degradation rates of the metabolites were observed online for 24 hours at 37°C inside the NMR. The assigned metabolite signals and their concentrations in mM were plotted as a function of time in Figure 83 A1 and B1. For a better optical analysis of the results the enlarged view of the 3 mM range was shown in graph A2 and B2 and the 1 mM range was shown in graph A3 and B3.

6 Hyphenation of NMR + LOC + Cells for long-term metabolomics

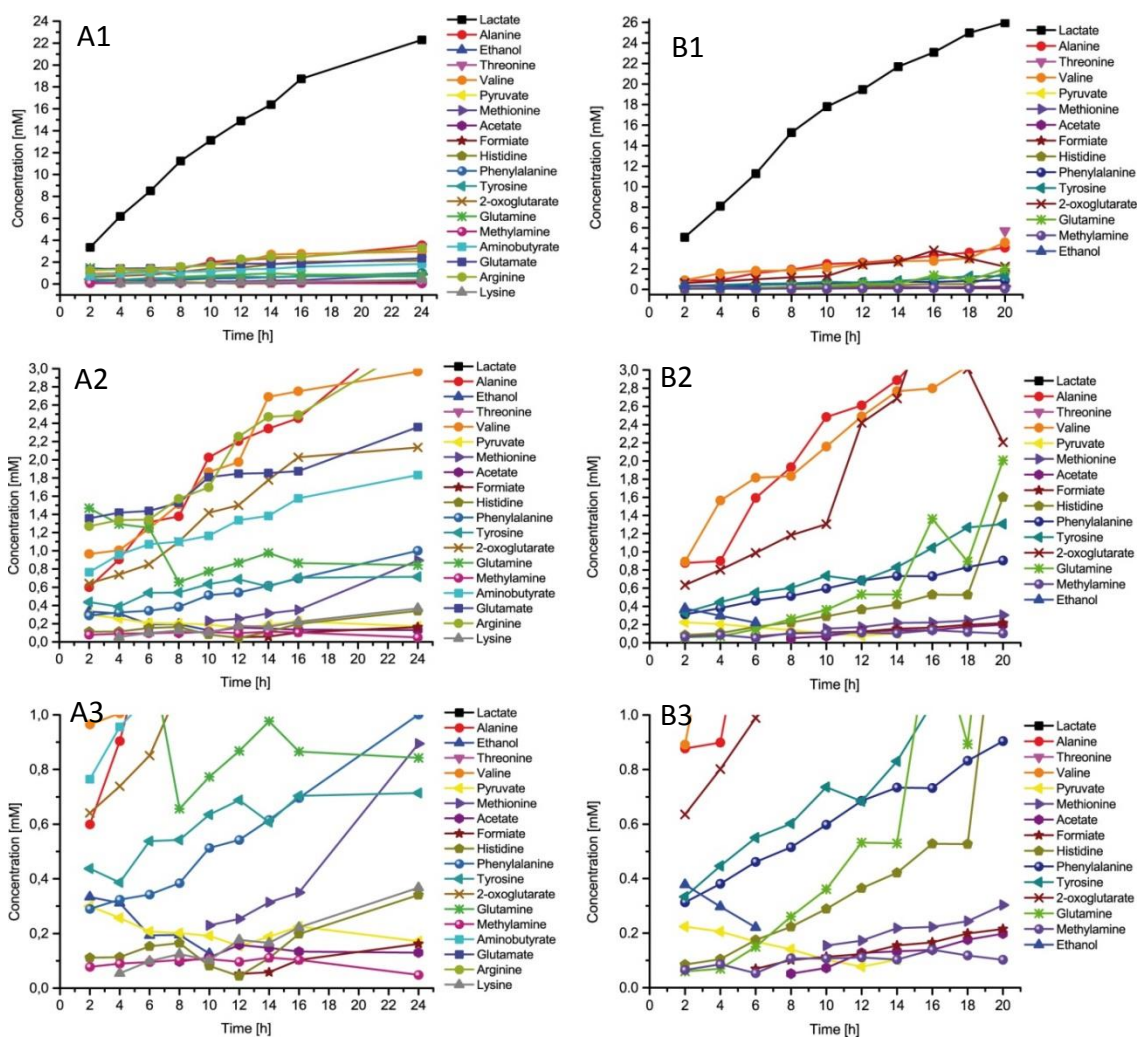


Figure 83: Comparison of the metabolite concentrations in mM which are plotted as a function of time. The graphs are showing the metabolite concentration levels inside the microfluidic device filled with media and one spheroid no. 1 (A1) and spheroid no. 2 (B1). The temporal dynamics of metabolite concentration levels can be observed. For a better comparison and analysis graph A2 (up to 3mM range) and A3 (up to 1mM range) are showing the enlarged view of the graph A1. B2 and B3 are the enlarged view of B1.

With slightly different concentrations most of the metabolites of both spheroids A1 and A2 show comparable dynamics. The different number of metabolites presumably depends on the quality of the shimming. Some low concentrated compounds are not visible or cannot be quantified due to a lower shimming quality which can slightly

differ from one experiment to another experiment. However, the metabolic profile for both spheroids is similar as expected. This is a very important result showing the reproducibility of this method and the reliability of the data. Especially for high-throughput toxicological screenings for per-animal and pre-clinical trials of drugs it is essential and of high importance to have a stable and highly reproducible method.

6.3.9 Metabolic profile of the PDMS microarray spheroids

In this chapter the metabolic profiles of spheroids obtained by the PDMS microarray method are analyzed. However, the Teflon tubing inside the capillary of the microfluidic glass device has an inner diameter of about 400 μm and one spheroid ($\sim 230 \mu\text{m}$) alone would clock the tubing. Therefore, 3 spheroids were used for one measurement. The triangle arrangement of the spheroids prevented the clocking of the tubing. Each spheroid consists of about 2500 cells¹⁰⁵ with a diameter of about 230 μm . The production and degradation rates of the metabolites were observed online for 24 hours at 37°C inside the NMR (on-chip). The assigned metabolite signals and their concentrations in mM were plotted as a function of time in Figure 84 A.

6 Hyphenation of NMR + LOC + Cells for long-term metabolomics

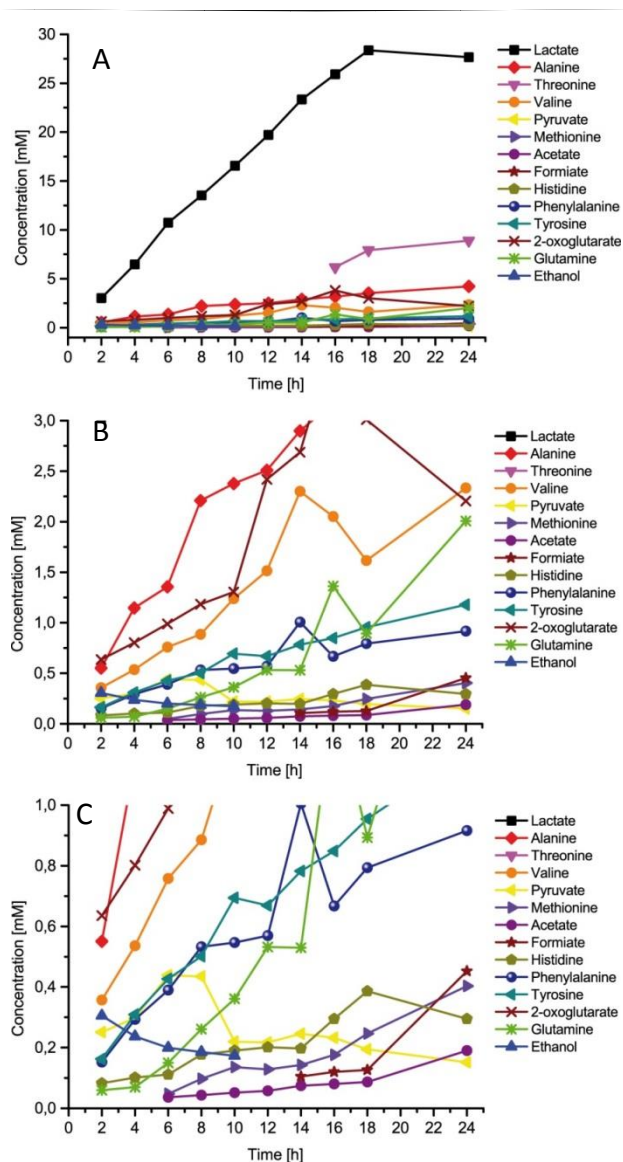


Figure 84: Metabolite profile of spheroids obtained with the PDMS microarray method. Metabolite concentrations in mM are plotted as a function of time. The graphs are showing the metabolite concentration levels inside the microfluidic device filled with media and 3 spheroids with diameters of about 230 μm .

The metabolic profile shows a slightly elevated concentration of the metabolites when compared with the InSphero hanging drop spheroids with 500 μm diameter. However, one has to take into account that 3 spheroids were used in this experiment. After 24 hours 30 mM lactate was produced. Each spheroid with 230 μm diameter and approx. 2500 cells produced 10 mM lactate (~ 0.004 mM / cell). The InSphero spheroid

6 Hyphenation of NMR + LOC + Cells for long-term metabolomics

with 500 μm diameter and approx. 9000 cells produced about 25 mM lactate ($\sim 0.003\text{mM} / \text{cell}$). Also the high concentration of threonine is remarkable. Spheroids with 230 μm produced 0.0012 mM / cell threonine while spheroids with 500 μm produced 0.0012 mM / cell threonine. The spheroids produced with the PDMS microarrays seem to be slightly more active producers of metabolites probably because of the different growth conditions when compared with the InSphero spheroids. However, the metabolic profile of both spheroid types appears to be in general similar and thus comparable with each other.

After the 24 hour measurement the spheroids were analyzed by microscope and it was observed that the 3 spheroids were merged together (Figure 85). This is another proof that the conditions inside the microfluidic device are suitable for cell growth and proliferation.

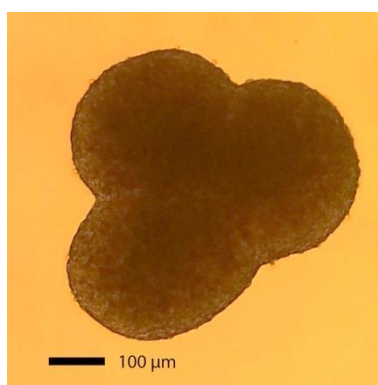


Figure 85: Microscopic image of 3 spheroids obtained with the PDMS microarray method are grown together inside the microfluidic device during the 24 hour measurements

6.3.10 On chip experiments with several spheroids

For experiments in which a higher concentration of the metabolites is needed (especially the very low concentrated ones) several spheroids can be used at the same time for one experiment. In this chapter 2 spheroids from the InSphero hanging drop method with 500 μm diameter were analyzed. The production and degradation rates

6 Hyphenation of NMR + LOC + Cells for long-term metabolomics

of the metabolites were observed online for 17 hours at 37°C inside the NMR (on-chip). The assigned metabolite signals and their concentrations in mM were plotted as a function of time in Figure 86. As expected the metabolite concentrations of 2 spheroids (each 500 μm) are visibly higher when compared with the concentration of 1 spheroid (500 μm).

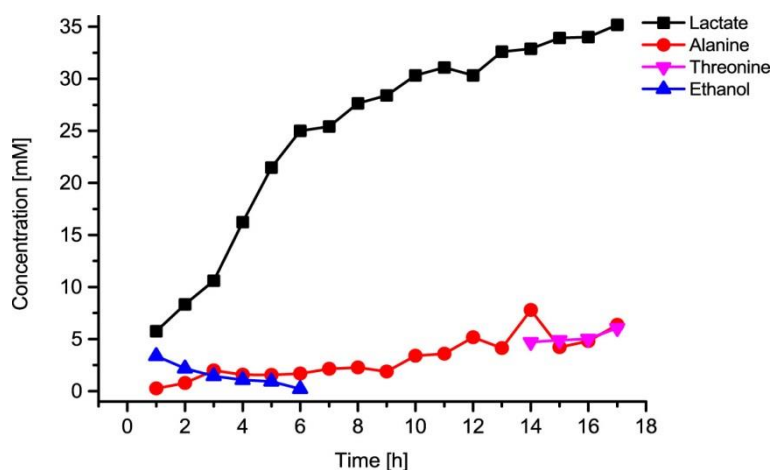


Figure 86: Metabolite concentrations in mM are plotted as a function of time. The graph is showing the metabolite concentration levels inside the microfluidic device filled with media and 2 spheroids with diameters of about 500 μm .

However, due to baseline roll in the NMR spectrum (see Spectra in Figure 87) most of the low concentrated components could not be detected or quantified. We assume that the reasons for oscillation are external factors like vibration caused by cars and trains close to the building in which the magnet is placed. Additionally, for a variety of reasons the high resolution magnets tend to drift. To adjust and to keep the magnetic field as stable as possible a field frequency lock was developed.¹⁴⁶ Usually deuterium is used as the lock nucleus as well as the reference substance. But since the homebuilt NMR probehead consists of only one channel and a second channel is required for D₂O detection, it is not possible to use D₂O in order to lock the magnetic field. Even if the lock would be possible we refrained from the use of D₂O in order not to perturb the metabolism of the cells.

6 Hyphenation of NMR + LOC + Cells for long-term metabolomics

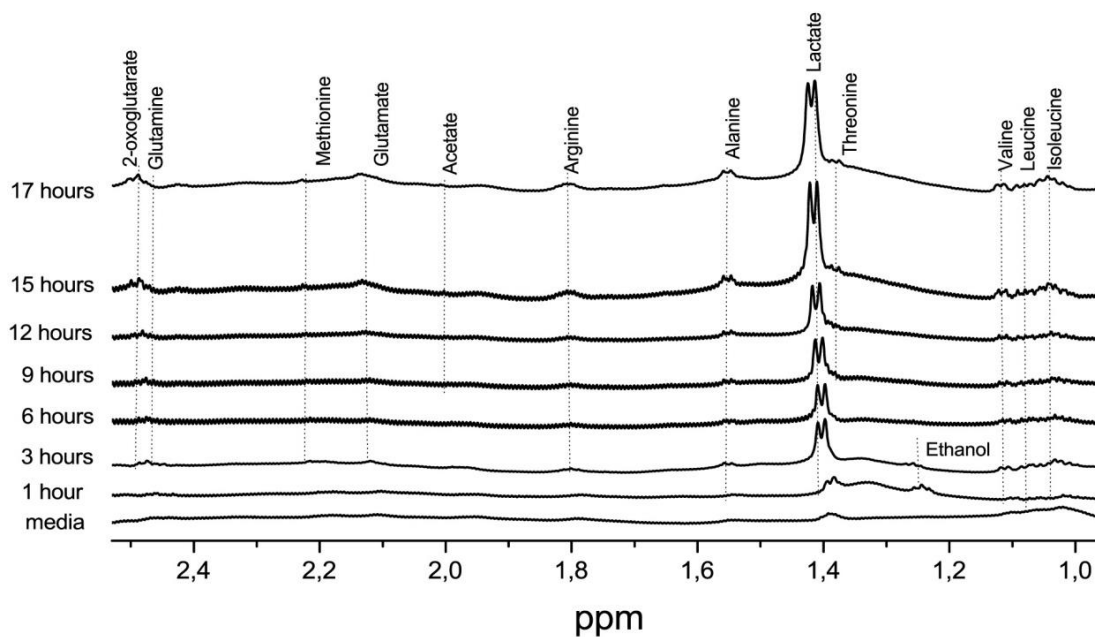


Figure 87: ¹H-NMR spectra (600 MHz) obtained with the microslot probehead. The microfluidic device is filled with media and two spheroids with 500 μm diameter (on-chip experiment). The dynamic process of metabolite production and degradation is observed at 37°C for 17 hours. Due to oscillation the low concentrated components could not be detected or quantified.

Also here, the spheroids were analyzed by microscope after the 17 hours measurement and it was observed that the 2 spheroids were merged together (Figure 88). The viability of the spheroids is ensured; they grow and proliferate inside the microfluidic device which is inside the NMR spectrometer.



Figure 88: Microscopic image of 2 spheroids obtained with the PDMS microarray method are grown together inside the microfluidic device during the 17 hour measurements

6.3.11 Metabolic profile of cells grown in 2D monolayer

As described in 5.2.1 the HT29 cells were passaged into a new cell culture flask. Starting after 24 hours every day 30 μl of the cell culture media was transferred into a capillary (same like the microfluidic device capillary) and measured with the microslot detector. The assigned metabolite signals and their concentrations in mM were plotted as a function of time in Figure 89.

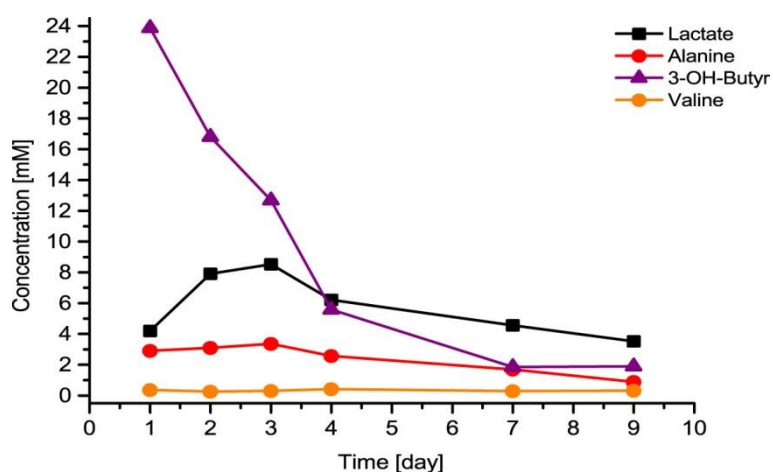


Figure 89: Metabolite concentrations in mM are plotted as a function of time. The graph is showing the metabolite concentration levels inside the cell culture flask filled with 10 mL media and cells grown in 2D monolayer.

6 Hyphenation of NMR + LOC + Cells for long-term metabolomics

The metabolic profile of the cells grown in 2D monolayer is obviously different from those from the spheroids. Since the cell metabolites are diluted in a 10 mL volume the number of metabolites which could be assigned or quantified is much lower when compared with the on-chip results of the spheroids. The alanine concentration is increasing slightly up to 3.5 mM and decreases after 3 days. The lactate concentration is increasing much faster up to 9 mM and decreases after 3 days. The valine concentration instead remains almost constant (0.5 mM) with a small increase after 3 days (0.7 mM). In traditional cell culture the media inside the cell culture flask is changed every 3 - 4 days because of the depletion of nutrients. Once the cell confluence of about 80 % is reached (after 7 – 10 days) the cells are harvested and passaged into a new cell culture flask otherwise the cells will die due to contact inhibition even when fresh media is added. In this experiment the media was not changed and the cells were not passaged in order to monitor the metabolism of the cells when they grow and when they start to be stressed and finally die. Within the first 3 days of excess nutrients and space the cells are growing and produce lactate and also small amounts of alanine. When the nutrients get depleted lactate and alanine start decreasing. The small increase of valine at this time point presumably arises from other proteins, which are broken down from dead cells for instance as a result of autophagy, apoptosis, necrosis etc. which was explained more in detail in chapter 6.3.6.

Remarkably is the initial high concentration of 3-hydroxybutyric acid (24mM) which is a ketone-body typically found in the metabolic state called ketosis. In this state ketone-bodies like acetoacetate and 3-hydroxybutyric acid are synthesized by breakdown of fatty acids or deamination of amino acids. In early stages of life in developing mammals or when glucose levels are low, ketone-bodies are the sources of energy. It serves also as a precursor for acetyl-CoA and can be used in TCA cycle or in the synthesis of fatty acids and complex lipids.^{147, 148}

After accommodation to the new environment and adhering on the surface of the cell culture plate, the cells start growing. The high concentration of the ketone-body 3-

6 Hyphenation of NMR + LOC + Cells for long-term metabolomics

hydroxybutyric acid is decreasing very fast at this stage which is presumably utilized for the synthesis of acetyl-CoA or for the synthesis of fatty acids and complex lipids in order to cover the need of fast growing cells for energy and macromolecules. Once the nutrients and glucose are depleted after 4 days, the cells reduce their growth rate and the utilization of 3-hydroxybutyric acid is reduced as well (slow decrease of the concentration). The same can be said about lactate which is the product of glucose. Once the glucose is depleted the lactate concentration is decreasing as well.

7 Conclusion

In this study, the design and fabrication of a novel miniaturized planar waveguide NMR probehead and its hyphenation with a microfluidic device for the non-invasive and online detection of living cells' metabolites was successfully demonstrated for the first time. The microfluidic device was employed as NMR sample holder and to preserve the *in vivo* like state of vascularized tumors. This device ensures the viability of cells at near physiological conditions by perfusion of the cells with thermally controlled media and gases to enable long-term *in vitro* studies. 23 intra- and extracellular metabolites of the HT29 adenocarcinoma cell line could be identified using ^1H NMR spectroscopy. Further, metabolite concentrations from off-chip and on-chip experiments were measured as a function of time. Due to high lactate, alanine and ethanol concentrations the results from both kinds of measurements were indicating a shift from oxidative to glycolytic metabolism in spheroids. The increased biosynthesis of amino acids mirrors the requirement of proliferating cells for macromolecules. The difference between both types of experiments presumably arise from the CO_2 buffered system of the off-chip experiment and HEPES buffered system of the on-chip experiment. Approaches to overcome this problem are already in progress.

Comparison of different on-chip experiments showed that this new analysis technique can provide highly reproducible results. During the course of the long-term experiments not only the viability of the cells is guaranteed but also the growth and proliferation of the cells was ensured as it was shown on the example of the merging spheroids.

Further, spheroids obtained by two different methods were analyzed with the microslot NMR detector and showed a comparable metabolic profile. Also the metabolism of 2D monolayer cell culture was analyzed and corresponding metabolic pathways could be explained.

Metabolic profiles of cancer cells are remarkably different from those of normal cells. But yet, it is not fully understood whether these altered metabolic properties are

7 Conclusion

specific to cancer cells or just mirror the increased proliferation of tumor cells⁵. Studies revealed that the metabolic profile of tumors depends on the genetic lesion as well as the tissue where they grow¹⁴⁹. Thus, the correlation between oncogenic signaling pathways and the metabolic reprogramming has emerged. But the metabolomics analysis is very complex and a challenging task, as many parameters have to be considered like the physiological gradients inside a tumor tissue, the distribution of heterogeneous cell populations, cell-cell interactions and their complex 3D network and the distribution and function of biomolecules within this network⁹. Additionally, the fast and sensitive reaction of the metabolism to the changes in the environment as well as the lack of appropriate analysis techniques made metabolomics research a challenging task. With our instrumental and methodological development the complex metabolic profiles as well as the metabolic adaptation of the cells to their microenvironment can be studied *in vitro*. The technique has no special sample requirements, i.e. tissues, tissue like samples (spheroids), cells grown in monolayers, and even cell organelles like mitochondria can be measured adequately. Labor-intensive sample preparations and pretreatments like metabolite extraction are not necessary. Depending on the biological sample more complex and more sophisticated microfluidic chips can be designed and employed, as the planar geometry of the probehead allows any kind of chip design. For instance a central cell cultivation chamber with flanking media and gas perfusion channels can be designed to ensure the long time viability of biological samples under incubator like conditions. Furthermore, this novel analysis technique can be used for metabonomic analysis⁵ to understand the molecular mechanism of anticancer drugs action. Thus, our future approach is a time resolved and *in vitro* investigation of cancer cells' metabolic response to targeted therapy with different anti-cancer drugs by using the homebuilt microslot NMR probehead. Not only in cancer research any type of cell line and their responses to external stress factors as in toxicological or pharmaceutical studies can be studied which has a high potential to replace tests on animal models.

8 Outlook

The microslot NMR detector opens a new window for metabolomics studies on living cells which can be implemented on tissue like samples and on 3D organ systems in future. However, not only the cells' metabolic response to toxins or pharmaceuticals but also the spatial distribution of the metabolites and drugs inside a sample (e.g. tissue, tumor etc.) is of high importance. The drug's absorption, distribution, metabolism, and excretion (ADME) defines the efficacy¹²¹ and thus the success of a clinical chemotherapy. Ineffective drugs as well as an inadequate drug treatment can lead to cancer recurrence. The gold standards to evaluate the drug efficacy are *in vitro* 2D cell culture assays. As already discussed in the previous chapters 2D cell culture models fail to mimic the typical metabolic and proliferative gradients in the tissue. 3D cell culture systems are therefore increasingly seen as essential tools to bridge the gap between 2D culture models and animal models, since they can simulate the microenvironment of a tumor in a realistic way. Being able to "look" inside a spheroid, tumor or tissue will enhance the knowledge about the metabolic pathways and the efficacy of drugs and the effect of toxins. Therefore, visualization techniques are needed also to complement the NMR based metabolomics analysis on living cells which we have improved in this work. For instance, microscopy is a prerequisite in cell analysis which makes essential cellular processes observable. However, it is restricted to phenotypical analysis and usually requires staining (e.g. in histology) or labeling with fluorescent markers.¹ In this chapter two label-free visualization approaches are introduced. While the matrix-assisted laser desorption/ionization (MALDI) mass spectrometry imaging (MSI) or MALDI-MSI is an invasive approach the miniaturized magnetic resonance imaging (miniaturized MRI) is a non-invasive technique.

MALDI-MSI is an invasive and label-free method to investigate the spatial distribution of molecules on surfaces. During the past years it became a powerful tool which has been used for the investigation of drug and metabolite distributions in various biological samples like cell-based models or real tissues.¹¹⁸ For this purpose biological

8 Outlook

samples like spheroids are sectioned into slices and each slice is analyzed by a mass spectrometer as shown in Figure 90.

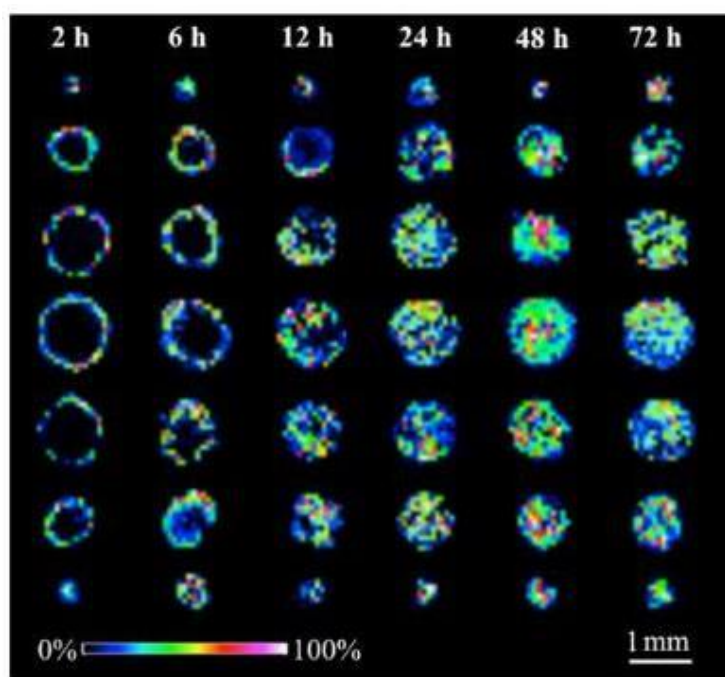


Figure 90: Image obtained by MALDI-MSI is showing the time dependent penetration of irinotecan into spheroids. 6 tumor spheroids were treated with irinotecan (20.6 μM) each for 2, 6, 12, 24, 48, and 72 h (from left to right). One spheroid was consecutively sliced into 7 pieces with each slice having a thickness of 12 μm . The time dependent distribution of irinotecan was measured and shown as a color gradient intensity map.¹¹⁸

The MALDI-MSI procedure is described as following: “sectioned biological specimens are placed in a mass spectrometer and an ordered array of mass spectra are acquired from a raster of positions across the sample surface. Ion density maps can then be reconstructed for any selected peak of a particular mass from the data set in which each pixel consists of a mass spectrum”.¹²¹

The high sensitivity of this method makes MALDI-MSI a powerful and popular tool for testing ADME processes inside 3D cell cultures and tissues. Connecting MSI technology with spheroid analysis (e.g. with microslot NMR detector) has a great potential to

become an informative platform not only for pharmaceutical and toxicological studies but also for the investigation of overall metabolic processes and pathways. However, the biggest disadvantage of the MSI technique and all other mass spectrometry approaches is its invasive (destructive) nature. The pictures obtained by MSI are snapshots of one specific time point and do not show the dynamic picture inside living cells/tissues. For instance the Figure 90 shows the results of seven different time points which are obtained by seven different spheroids. Therefore, a non-invasive analysis technique like Magnetic resonance imaging (MRI) is needed.

MRI is a non-invasive and label-free method to investigate the spatial distribution of molecules in 3D biological samples. It works on the same principle as the NMR spectroscopy, but imposes field gradients on the sample in order to achieve spatial resolution. MRI is a well-established and powerful technique commonly used in hospitals as a diagnostic tool for the visualization of anatomical and physiological diseases. However, the millimeter resolution is not sufficient to investigate the regional differences and distributions of drugs and metabolites in small samples like spheroids and tissues.¹⁵⁰ To overcome this problem our aim for the future is to establish a miniaturized MRI method based on the planar microstrip technology which was introduced in this thesis. This planar microslot NMR detector was improved and used in this work for the long-term non-invasive analysis of a tumor spheroid metabolism. The planar microstrip NMR detector shall in future be applied to measure spectroscopic imaging experiments, i.e. for taking high resolution NMR spectra as a function of spatial displacement. This will give valuable *in vitro* information on the distribution of metabolites and pharmaceuticals in 3D tumor model systems. As in the case of the microslot NMR detector, we here also want to integrate the miniaturized MRI detector with a microfluidic chip to ensure the functionality of the cell culture models. As in conventional MRI experiments the acoustic noise of the imaging gradients gives rise to spatial dislocations of the sample (i.e. the spheroid), we will use radiofrequency field gradients instead, which are free of mechanical interference with the sample. Moreover, this technique reduces the influence of susceptibility discontinuities in the samples, which blur the images and are a big problem in

8 Outlook

especially high field MRI. Moreover, imaging with a radiofrequency field gradient can be carried out on any standard liquid state NMR spectrometer without the requirement for additional dedicated hardware. To conclude, unlike MALDI-MSI, the proposed miniaturized MRI technique will preserve the anatomical and functional integrity of e.g. spheroids and will allow for a noninvasive mapping of the spatial distribution of metabolites and pharmaceuticals in spheroids. Additionally, one can mimic the microenvironment in patients by hyphenating the MRI detector with a microfluidic device which contains the 3D biological sample to be analyzed. Currently, the MRI probe has been manufactured and first experiments are on the way.

List of Abbreviations

μCP	Microcontact printing
μTAS	Micro Total Analysis Systems
ATP	Adenosine triphosphate
BMRB	Biological Magnetic Resonance Data Bank
DMEM	Dulbecco's modified Eagle media
DNA	Deoxyribonucleic acid
ECM	Extracellular matrix
EDTA	Ethylenediaminetetraacetic acid
FBS	Foetal bovine serum
FEM	Finite element method
FID	Free induction decay
FT	Fourier transformation
FWHM	Full width at half maximum
GND	Ground
H&E stain	Hematoxylin/eosin-stain
HEPES	4-(2-hydroxyethyl)-1-piperazineethanesulfonic acid ().
HMDB	Human Metabolome Database
KEGG	Kyoto Encyclopedia of Genes and Genomes
LOC	Lab-on-a-chip
MALDI	Matrix-assisted laser desorption/ionization
MCT4, MCT1, MCT2	Monocarboxylate transporters
MRI	Magnetic resonance imaging
mRNA	messenger Ribonucleic acid
MS	Mass spectrometry

List of Abbreviations

MSI	Mass spectrometry imaging
NAD+	Nicotinamide adenine dinucleotide
NMR	Nuclear magnetic resonance spectrometry
OD	Optical density
PDA	Polydopamine
PDMS	Polydimethylsiloxane
PKM2	Pyruvate kinase M2
PMMA	Poly(methyl methacrylate)
Ppm	Parts per million
PS	Polystyrene
PTFE	Polytetrafluoroethylene
r.f.	Radio frequency
REACH	Registration, Evaluation, Authorization and Restriction of Chemicals
S/N	Signal to noise
SEM	Scanning electron microscope
SWR	Standing wave ratio
TCA	tricarboxylic acid
TMS	Tetramethylsilane
UV	Ultra violet

References

- [1] Kortmann, H.; Blank, L. M.; Schmid, A., Single Cell Analytics: An Overview. In *High Resolution Microbial Single Cell Analytics*, Muller, S. B. T., Ed. Springer-Verlag: Berlin, 2011; Vol. 124, pp 99-122.
- [2] Schmid, A.; Blank, L. M., Hypothesis-driven omics integration. *Nat. Chem. Biol.* **2010**, *6* (7), 485-487.
- [3] Rubakhin, S. S.; Romanova, E. V.; Nemes, P.; Sweedler, J. V., Profiling metabolites and peptides in single cells. *Nat. Methods* **2011**, *8* (4), S20-S29.
- [4] Warburg, O., Origin of cancer cells. *Science* **1956**, *123* (3191), 309-314.
- [5] Schulze, A.; Harris, A. L., How cancer metabolism is tuned for proliferation and vulnerable to disruption. *Nature* **2012**, *491* (7424), 364-373.
- [6] Tessem, M. B.; Swanson, M. G.; Keshari, K. R.; Albers, M. J.; Joun, D.; Tabatabai, Z. L.; Simko, J. P.; Shinohara, K.; Nelson, S. J.; Vigneron, D. B.; Gribbestad, I. S.; Kurhanewicz, J., Evaluation of lactate and alanine as metabolic biomarkers of prostate cancer using H-1 HR-MAS spectroscopy of biopsy tissues. *Magn. Reson. Med.* **2008**, *60* (3), 510-516.
- [7] Cairns, R. A.; Harris, I. S.; Mak, T. W., Regulation of cancer cell metabolism. *Nat. Rev. Cancer* **2011**, *11* (2), 85-95.
- [8] Tatum, J. L.; Kelloff, G. J.; Gillies, R. J.; Arbeit, J. M.; Brown, J. M.; Chao, K. S. C.; Chapman, J. D.; Eckelman, W. C.; Fyles, A. W.; Giaccia, A. J.; Hill, R. P.; Koch, C. J.; Krishna, M. C.; Krohn, K. A.; Lewis, J. S.; Mason, R. P.; Melillo, G.; Padhani, A. R.; Powis, G.; Rajendran, J. G.; Reba, R.; Robinson, S. P.; Semenza, G. L.; Swartz, H. M.; Vaupel, P.; Yang, D.; Croft, B.; Hoffman, J.; Liu, G. Y.; Stone, H.; Sullivan, D., Hypoxia: Importance in tumor biology, noninvasive measurement by imaging, and value of its measurement in the management of cancer therapy. *Int. J. Radiat. Biol.* **2006**, *82* (10), 699-757.
- [9] Hirschhaeuser, F.; Menne, H.; Dittfeld, C.; West, J.; Mueller-Klieser, W.; Kunz-Schughart, L. A., Multicellular tumor spheroids: An underestimated tool is catching up again. *J. Biotechnol.* **2010**, *148* (1), 3-15.
- [10] Friedrich, J.; Seidel, C.; Ebner, R.; Kunz-Schughart, L. A., Spheroid-based drug screen: considerations and practical approach. *Nat. Protoc.* **2009**, *4* (3), 309-324.

References

- [11] Hardelauf, H.; Frimat, J.-P.; Stewart, J. D.; Schormann, W.; Chiang, Y.-Y.; Lampen, P.; Franzke, J.; Hengstler, J. G.; Cadenas, C.; Kunz-Schughart, L. A.; West, J., Microarrays for the scalable production of metabolically relevant tumour spheroids: a tool for modulating chemosensitivity traits. *Lab Chip* **2011**, *11* (3), 419-428.
- [12] Seok, J.; Warren, H. S.; Cuenca, A. G.; Mindrinos, M. N.; Baker, H. V.; Xu, W.; Richards, D. R.; McDonald-Smith, G. P.; Gao, H.; Hennessy, L.; Finnerty, C. C.; Lopez, C. M.; Honari, S.; Moore, E. E.; Minei, J. P.; Cuschieri, J.; Bankey, P. E.; Johnson, J. L.; Sperry, J.; Nathens, A. B.; Billiar, T. R.; West, M. A.; Jeschke, M. G.; Klein, M. B.; Gamelli, R. L.; Gibran, N. S.; Brownstein, B. H.; Miller-Graziano, C.; Calvano, S. E.; Mason, P. H.; Cobb, J. P.; Rahme, L. G.; Lowry, S. F.; Maier, R. V.; Moldawer, L. L.; Herndon, D. N.; Davis, R. W.; Xiao, W.; Tompkins, R. G.; Inflammation Host Response, I., Genomic responses in mouse models poorly mimic human inflammatory diseases. *Proc. Natl. Acad. Sci. U. S. A.* **2013**, *110* (9), 3507-3512.
- [13] Perrin, S., Preclinical research: Make mouse studies work. *Nature* **2014**, *507* (7493), 423-425.
- [14] Pampaloni, F.; Reynaud, E. G.; Stelzer, E. H. K., The third dimension bridges the gap between cell culture and live tissue. *Nat. Rev. Mol. Cell Biol.* **2007**, *8* (10), 839-845.
- [15] Zenobi, R., Single-Cell Metabolomics: Analytical and Biological Perspectives. *Science* **2013**, *342* (6163), 1201-+.
- [16] Altschuler, S. J.; Wu, L. F., Cellular Heterogeneity: Do Differences Make a Difference? *Cell* **2010**, *141* (4), 559-563.
- [17] Ibanez, A. J.; Fagerer, S. R.; Schmidt, A. M.; Urban, P. L.; Jefimovs, K.; Geiger, P.; Dechant, R.; Heinemann, M.; Zenobi, R., Mass spectrometry-based metabolomics of single yeast cells. *Proc. Natl. Acad. Sci. U. S. A.* **2013**, *110* (22), 8790-8794.
- [18] Fritzsche, F. S. O.; Dusny, C.; Frick, O.; Schmid, A., Single-Cell Analysis in Biotechnology, Systems Biology, and Biocatalysis. *Annu. Rev. Chem. Biomol. Eng.* **2012**, *3*, 129-155.
- [19] Kraly, J. R.; Holcomb, R. E.; Guan, Q.; Henry, C. S., Review: Microfluidic applications in metabolomics and metabolic profiling. *Anal. Chim. Acta* **2009**, *653* (1), 23-35.
- [20] Jacobson, S. C.; Hergenroder, R.; Koutny, L. B.; Warmack, R. J.; Ramsey, J. M., Effects of injection schemes and column geometry on the performance of microchip electrophoresis devices. *Anal. Chem.* **1994**, *66* (7), 1107-1113.
- [21] Manz, A.; Graber, N.; Widmer, H. M., Miniaturized total chemical-analysis systems - A novel concept for chemical sensing. *Sens. Actuators, B* **1990**, *1* (1-6), 244-248.

References

- [22] Janasek, D.; Franzke, J.; Manz, A., Scaling and the design of miniaturized chemical-analysis systems. *Nature* **2006**, *442* (7101), 374-380.
- [23] West, J.; Becker, M.; Tombrink, S.; Manz, A., Micro total analysis systems: Latest achievements. *Anal. Chem.* **2008**, *80* (12), 4403-4419.
- [24] deMello, A. J., Control and detection of chemical reactions in microfluidic systems. *Nature* **2006**, *442* (7101), 394-402.
- [25] Reisewitz, S.; Schroeder, H.; Tort, N.; Edwards, K. A.; Baeumner, A. J.; Niemeyer, C. M., Capture and Culturing of Living Cells on Microstructured DNA Substrates. *Small* **2010**, *6* (19), 2162-2168.
- [26] Reinholt, S. J.; Behrent, A.; Greene, C.; Kalfe, A.; Baeumner, A. J., Isolation and Amplification of mRNA within a Simple Microfluidic Lab on a Chip. *Anal. Chem.* **2014**, *86* (1), 849-856.
- [27] Wu, N. A.; Peck, T. L.; Webb, A. G.; Magin, R. L.; Sweedler, J. V., H-1-NMR spectroscopy on the nanoliter scale for static and online measurements. *Anal. Chem.* **1994**, *66* (22), 3849-3857.
- [28] Fratila, R. M.; Velders, A. H., Small-Volume Nuclear Magnetic Resonance Spectroscopy. *Annu. Rev. Anal. Chem.* **2011**, *4*, 227-249.
- [29] Olson, D. L.; Peck, T. L.; Webb, A. G.; Magin, R. L.; Sweedler, J. V., High-resolution microcoil H-1-NMR for mass-limited, nanoliter-volume samples. *Science* **1995**, *270* (5244), 1967-1970.
- [30] Serber, Z.; Selenko, P.; Hansel, R.; Reckel, S.; Lohr, F.; Ferrell, J. E.; Wagner, G.; Dotsch, V., Investigating macromolecules inside cultured and injected cells by in-cell NMR spectroscopy. *Nat. Protoc.* **2006**, *1* (6), 2701-2709.
- [31] Hoult, D. I.; Richards, R. E., The signal-to-noise ratio of the nuclear magnetic resonance experiment. 1976. *J. Magn. Reson.* **2011**, *213* (2), 329-43.
- [32] Krojanski, H. G.; Lambert, J.; Gerikalan, Y.; Suter, D.; Hergenroeder, R., Microslot NMR Probe for Metabolomics Studies. *Anal. Chem.* **2008**, *80* (22), 8668-8672.
- [33] Maguire, Y.; Chuang, I. L.; Zhang, S.; Gershenfeld, N., Ultra-small-sample molecular structure detection using microslot waveguide nuclear spin resonance. *Proc. Natl. Acad. Sci. U. S. A.* **2007**, *104* (22), 9198-9203.

References

- [34] Zhang, X. L.; Ugurbil, K.; Chen, W., Microstrip RF surface coil design for extremely high-field MRI and spectroscopy. *Magn. Reson. Med.* **2001**, *46* (3), 443-450.
- [35] van Bantum, P. J. M.; Janssen, J. W. G.; Kentgens, P. M., Towards nuclear magnetic resonance mu-spectroscopy and mu-imaging. *Analyst* **2004**, *129* (9), 793-803.
- [36] Bart, J.; Janssen, J. W. G.; van Bantum, P. J. M.; Kentgens, A. P. M.; Gardeniers, J. G. E., Optimization of stripline-based microfluidic chips for high-resolution NMR. *J. Magn. Reson.* **2009**, *201* (2), 175-185.
- [37] Markley, J. L., NMR analysis goes nano. *Nat. Biotechnol.* **2007**, *25* (7), 750-751.
- [38] Lambert, J., NMR Spektroskopie Vorlesung. In *NMR Spektroskopie Vorlesung*, Dortmund, 2013.
- [39] Telfah, A. Transport of Protonic Charge Carriers in Methyl-Sulfonic-Acid / Water Mixtures: A Model for Lowly Hydrated Sulfonic Acid Based Ionomers. Dissertation, 2008.
- [40] Hesse, M.; Meier, H.; Zeeh, B.; Editors, *Spectroscopic Methods in Organic Chemistry*. Thieme: 1995; p 364 pp.
- [41] Freude, D., NMR Spectroscopy. In *Spectroscopy*, Universität Leipzig, 2006.
- [42] Lacey, M. E.; Subramanian, R.; Olson, D. L.; Webb, A. G.; Sweedler, J. V., High-resolution NMR spectroscopy of sample volumes from 1 nL to 10 μ L. *Chem. Rev.* **1999**, *99* (10), 3133-+.
- [43] Selenko, P.; Wagner, G., NMR mapping of protein interactions in living cells. *Nat. Methods* **2006**, *3* (2), 80-81.
- [44] Spraul, M.; Freund, A. S.; Nast, R. E.; Withers, R. S.; Maas, W. E.; Corcoran, O., Advancing NMR sensitivity for LC-NMR-MS using a cryoflow probe: Application to the analysis of acetaminophen metabolites in urine. *Anal. Chem.* **2003**, *75* (6), 1536-1541.
- [45] Rinaldi, P. L., Three-dimensional solution NMR spectroscopy of complex structures and mixtures. *Analyst* **2004**, *129* (8), 687-699.
- [46] Webb, A. G., Microcoil nuclear magnetic resonance spectroscopy. *J. Pharm. Biomed. Anal.* **2005**, *38* (5), 892-903.

References

- [47] Webb, A. G., Radiofrequency microcoils in magnetic resonance. *Progress in Nuclear Magnetic Resonance Spectroscopy* **1997**, *31*, 1-42.
- [48] Peck, T. L.; Magin, R. L.; Kruse, J.; Feng, M., NMR microspectroscopy using 100- μ m planar rf-coils fabricated on gallium-arsenide substrates. *IEEE Trans. Biomed. Eng.* **1994**, *41* (7), 706-709.
- [49] Massin, C.; Boero, C.; Vincent, F.; Abenhaim, J.; Besse, P. A.; Popovic, R. S., High-Q factor RF planar microcoils for micro-scale NMR spectroscopy. *Sens. Actuator A-Phys.* **2002**, *97-8*, 280-288.
- [50] Leidich, S.; Braun, M.; Gessner, T.; Riemer, T., Silicon Cylinder Spiral Coil for Nuclear Magnetic Resonance Spectroscopy of Nanoliter Samples. *Concepts Magn. Reson. Part B* **2009**, *35B* (1), 11-22.
- [51] Anders, J.; Chiaramonte, G.; SanGiorgio, P.; Boero, G., A single-chip array of NMR receivers. *J. Magn. Reson.* **2009**, *201* (2), 239-249.
- [52] Maguire, Y.; Gershenfeld, N.; Chuang, I. L. Slitted and stubbed microstrips for high sensitivity, near-field electromagnetic radiation detection. US7560927B2, 2009.
- [53] Telfah, A.; Lambert, J.; Kalfe, A.; Hergenroder, R. Heizung für Mikrostreifenleiter. 10 2014 115 702.8, 2015.
- [54] Chichkov, B. N.; Momma, C.; Nolte, S.; vonAlvensleben, F.; Tunnermann, A., Femtosecond, picosecond and nanosecond laser ablation of solids. *Applied Physics a-Materials Science & Processing* **1996**, *63* (2), 109-115.
- [55] Mispelter, J.; Lupu, M.; Briguët, A.; Editors, *NMR Probeheads for Biophysical and Biomedical Experiments: Theoretical Principles and Practical Guidelines*. World Scientific Publishing: 2006; p 612 pp.
- [56] NIST Time and Frequency from A to Z. <http://tf.nist.gov/general/enc-q.htm> (accessed 2015).
- [57] Pearson, G. A. Shimming an NMR magnet. <http://nmr.chem.uiowa.edu/manuals/Shimming-GAP-NMR-magnet.pdf> (accessed 2015).
- [58] Anderson, W. A., Electrical current shim for correcting magnetic fields. *Rev. Sci. Instrum.* **1961**, *32* (3), 241-&.

References

- [59] Whitesides, G. M., The origins and the future of microfluidics. *Nature* **2006**, *442* (7101), 368-373.
- [60] Metzler, D. E.; Metzler, C. M., *Biochemistry: The Chemical Reactions of Living Cells*. Harcourt/Academic Press: 2001.
- [61] Quantification, G. Lab-on-a-chip. <http://www.gene-quantification.de/>.
- [62] Schlüter, M. Mikrofluidische Strukturen für biochemische Analysen. TH Aachen, 2004.
- [63] Kalfe, A. PMMA biosensor for nucleic acid isolation and amplification with NASBA in microfluidic channels. Master Thesis, TU Dortmund / Cornell University New York, Dortmund / New York, 2010.
- [64] Lee, S. J.; Lee, S. Y., Micro total analysis system (mu-TAS) in biotechnology. *Appl. Microbiol. Biotechnol.* **2004**, *64* (3), 289-299.
- [65] El-Ali, J.; Sorger, P. K.; Jensen, K. F., Cells on chips. *Nature* **2006**, *442* (7101), 403-411.
- [66] Goral, V. N.; Zaytseva, N. V.; Bäumner, A. J., Electrochemical microfluidic biosensor for the detection of nucleic acid sequences. *Lab Chip* **2006**, *6* (3), 414-421.
- [67] Sivaraman, A.; Leach, J. K.; Townsend, S.; Iida, T.; Hogan, B. J.; Stolz, D. B.; Fry, R.; Samson, L. D.; Tannenbaum, S. R.; Griffith, L. G., A microscale in vitro physiological model of the liver: Predictive screens for drug metabolism and enzyme induction. *Curr. Drug Metab.* **2005**, *6* (6), 569-591.
- [68] Powers, M. J.; Domansky, K.; Kaazempur-Mofrad, M. R.; Kalezi, A.; Capitano, A.; Upadhyaya, A.; Kurzawski, P.; Wack, K. E.; Stolz, D. B.; Kamm, R.; Griffith, L. G., A microfabricated array bioreactor for perfused 3D liver culture. *Biotechnol. Bioeng.* **2002**, *78* (3), 257-269.
- [69] Folch, A.; Toner, M., Microengineering of cellular interactions. *Annu. Rev. Biomed. Eng.* **2000**, *2*, 227-+.
- [70] Reyes, D. R.; Iossifidis, D.; Auroux, P. A.; Manz, A., Micro total analysis systems. 1. Introduction, theory, and technology. *Anal. Chem.* **2002**, *74* (12), 2623-2636.
- [71] Martynova, L.; Locascio, L. E.; Gaitan, M.; Kramer, G. W.; Christensen, R. G.; MacCrehan, W. A., Fabrication of plastic microfluid channels by imprinting methods. *Anal. Chem.* **1997**, *69* (23), 4783-4789.

References

- [72] Guerin, L. J.; Bossel, M.; Demierre, M.; Calmes, S.; Renaud, P. In *Simple and low cost fabrication of embedded micro-channels by using a new thick-film photoplastic* Solid State Sensors and Actuators, 1997. TRANSDUCERS '97 Chicago., 1997 International Conference, 1997.
- [73] School-of-Electrical-and-Computer-Engineering Photolithography. <http://www.ece.gatech.edu/research/labs/vc/theory/photolith.html>.
- [74] SnipView-Chemistry Photolithography. <http://www.snipview.com/q/Chemistry%20of%20Photolithography>.
- [75] Michel, B.; Bernard, A.; Bietsch, A.; Delamarche, E.; Geissler, M.; Juncker, D.; Kind, H.; Renault, J. P.; Rothuizen, H.; Schmid, H.; Schmidt-Winkel, P.; Stutz, R.; Wolf, H., Printing meets lithography: Soft approaches to high-resolution printing. *Ibm Journal of Research and Development* **2001**, 45 (5), 697-719.
- [76] Douvas, A.; Argitis, P.; Misiakos, K.; Dimotikali, D.; Petrou, P. S.; Kakabakos, S. E., Biocompatible photolithographic process for the patterning of biomolecules. *Biosens. Bioelectron.* **2002**, 17 (4), 269-278.
- [77] Whitesides, G. M.; Ostuni, E.; Takayama, S.; Jiang, X. Y.; Ingber, D. E., Soft lithography in biology and biochemistry. *Annu. Rev. Biomed. Eng.* **2001**, 3, 335-373.
- [78] Diener-Electronic Plasma generator. <http://www.plasma.de/>.
- [79] TUEindhoven, Microfluidics methods. **2014**.
- [80] Meyvantsson, I.; Warrick, J. W.; Hayes, S.; Skoien, A.; Beebe, D. J., Automated cell culture in high density tubeless microfluidic device arrays. *Lab Chip* **2008**, 8 (5), 717-724.
- [81] Goedecke, N.; Eijkel, J.; Manz, A., Evaporation driven pumping for chromatography application. *Lab Chip* **2002**, 2 (4), 219-223.
- [82] Bianconi, E.; Piovesan, A.; Facchin, F.; Beraudi, A.; Casadei, R.; Frabetti, F.; Vitale, L.; Pelleri, M. C.; Tassani, S.; Piva, F.; Perez-Amodio, S.; Strippoli, P.; Canaider, S., An estimation of the number of cells in the human body. *Annals of Human Biology* **2013**, 40 (6), 463-471.
- [83] Today, T. Cell organells and functions. <http://is.justrending.com/functions/functions-of-cell-organelles.html> (accessed 2015).

References

- [84] Alberts, B., *Molecular Biology of the Cell*. Garland Pub.: 1989.
- [85] Crick, F., Central dogma of molecular biology. *Nature* **1970**, 227 (5258), 561-&.
- [86] PBWorks Introduction and Basic Molecular Biology.
<http://compbio.pbworks.com/w/page/16252897/Introduction%20and%20Basic%20Molecular%20Biology> (accessed 2015).
- [87] Patti, G. J.; Yanes, O.; Siuzdak, G., Metabolomics: the apogee of the omics trilogy. *Nature Reviews Molecular Cell Biology* **2012**, 13 (4), 263-269.
- [88] KEGG Kyoto Encyclopedia of Genes and Genomes. <http://www.genome.jp/kegg/> (accessed 2015).
- [89] Blank, L. M.; Kuepfer, L.; Sauer, U., Large-scale C-13-flux analysis reveals mechanistic principles of metabolic network robustness to null mutations in yeast. *Genome Biology* **2005**, 6 (6).
- [90] Nicholson, J. K.; Lindon, J. C.; Holmes, E., 'Metabonomics': understanding the metabolic responses of living systems to pathophysiological stimuli via multivariate statistical analysis of biological NMR spectroscopic data. *Xenobiotica* **1999**, 29 (11), 1181-1189.
- [91] Eppendorf Cell culture flask. <http://www.eppendorf.com/DE-de/>.
- [92] Bartis, D.; Pongrácz, J., Three dimensional tissue cultures and tissue engineering. Pécs, 2011.
- [93] Rowat, A. C.; Bird, J. C.; Agresti, J. J.; Rando, O. J.; Weitz, D. A., Tracking lineages of single cells in lines using a microfluidic device. *Proc. Natl. Acad. Sci. U. S. A.* **2009**, 106 (43), 18149-18154.
- [94] Mata, A.; Fleischman, A. J.; Roy, S., Characterization of polydimethylsiloxane (PDMS) properties for biomedical micro/nanosystems. *Biomed. Microdevices* **2005**, 7 (4), 281-293.
- [95] Lifetechnologies Introduction to cell culture.
<http://www.lifetechnologies.com/de/de/home.html>.
- [96] Marx, J., Many gene changes found in cancer. *Science* **1989**, 246 (4936), 1386-1388.
- [97] Cavenee, W. K.; White, R. L., The genetic-basis of cancer. *Sci. Am.* **1995**, 272 (3), 72-79.

References

- [98] Yokota, J.; Tsunetsuguyokota, Y.; Battifora, H.; Lefevre, C.; Cline, M. J., Alterations of myc, myb, and rasha protooncogenes in cancer are frequent and show clinical correlation. *Science* **1986**, *231* (4735), 261-265.
- [99] Marx, J., How p53 suppresses cell-growth. *Science* **1993**, *262* (5140), 1644-1645.
- [100] Weinberg, R., *The Biology of Cancer, Second Edition*. Garland Science Taylor & Francis Group: 2013.
- [101] Nasr, A. H. In Vitro and in Vivo. <http://science.jrank.org/pages/3541/In-Vitro-in-Vivo.html>.
- [102] Lodish, H., *Molecular Cell Biology*. W. H. Freeman: 2008.
- [103] Gallo, M. In Vivo and in Vitro Testing. <http://www.encyclopedia.com/doc/1G2-3404000449.html>.
- [104] NationalResearchCouncil, *Methods of Producing Monoclonal Antibodies. Monoclonal Antibody Production*. National Academies Press (US): Washington (DC, 1999).
- [105] Hardelauf, H. Development and Characterization of in vitro Microarray Technologies for Cell Biology. TU Dortmund, Dortmund, 2013.
- [106] InSphero 3D cell culture and microtissues. <http://www.insphero.com/>.
- [107] Takao, K.; Miyakawa, T., Genomic responses in mouse models greatly mimic human inflammatory diseases. *Proc. Natl. Acad. Sci. U. S. A.* **2015**, *112* (4), 1167-1172.
- [108] Scott, S.; Kranz, J. E.; Cole, J.; Lincecum, J. M.; Thompson, K.; Kelly, N.; Bostrom, A.; Theodoss, J.; Al-Nakhala, B. M.; Vieira, F. G.; Ramasubbu, J.; Heywood, J. A., Design, power, and interpretation of studies in the standard murine model of ALS. *Amyotrophic Lat. Scler.* **2008**, *9* (1), 4-15.
- [109] Begley, C. G.; Ellis, L. M., Raise standards for preclinical cancer research. *Nature* **2012**, *483* (7391), 531-533.
- [110] Francia, G.; Kerbel, R. S., Raising the bar for cancer therapy models. *Nat. Biotechnol.* **2010**, *28* (6), 561-562.

References

- [111] Griffith, L. G.; Swartz, M. A., Capturing complex 3D tissue physiology in vitro. *Nature Reviews Molecular Cell Biology* **2006**, *7* (3), 211-224.
- [112] Hartung, T.; Rovida, C., Chemical regulators have overreached. *Nature* **2009**, *460* (7259), 1080-1081.
- [113] Sutherland, R. M., Cell and environment interactions in tumor microregions: the multicell spheroid model. *Science* **1988**, *240* (4849), 177-184.
- [114] Kim, J.-Y.; Mohanty, S.; Singh, P.; Hierlemann, A.; Fluri, D. A.; Kelm, J. M.; Marchan, R.; Hengstler, J. G.; Boonen, K.; Landuyt, B.; Hammad, S.; Frey, O., 3D spherical microtissues and microfluidic technology for multi-tissue experiments and analysis. *J Biotechnol* **2015**, (Copyright (C) 2015 U.S. National Library of Medicine.).
- [115] Gobel, U.; Ruffner, H.; Lichtenberg, J., 3D cell culture systems - towards primary drug discovery platforms: An interview with Heinz Ruffner (Novartis) and Jan Lichtenberg (InSphero). *Biotechnol. J.* **2012**, *7* (7), 833-834.
- [116] Kale, S.; Biermann, S.; Edwards, C.; Tarnowski, C.; Morris, M.; Long, M. W., Three-dimensional cellular development is essential for ex vivo formation of human bone. *Nat. Biotechnol.* **2000**, *18* (9), 954-958.
- [117] Stein, A. M.; Demuth, T.; Mobley, D.; Berens, M.; Sander, L. M., A mathematical model of glioblastoma tumor spheroid invasion in a three-dimensional in vitro experiment. *Biophys. J.* **2007**, *92* (1), 356-365.
- [118] Liu, X.; Weaver, E. M.; Hummon, A. B., Evaluation of Therapeutics in Three-Dimensional Cell Culture Systems by MALDI Imaging Mass Spectrometry. *Anal. Chem.* **2013**, *85* (13), 6295-6302.
- [119] Jain, R. K., Barriers to drug-delivery in solid tumors. *Sci. Am.* **1994**, *271* (1), 58-65.
- [120] Vinci, M.; Gowan, S.; Boxall, F.; Patterson, L.; Zimmermann, M.; Court, W.; Lomas, C.; Mendiola, M.; Hardisson, D.; Eccles, S. A., Advances in establishment and analysis of three-dimensional tumor spheroid-based functional assays for target validation and drug evaluation. *BMC Biol.* **2012**, *10*.
- [121] Liu, X.; Hummon, A. B., Mass Spectrometry Imaging of Therapeutics from Animal Models to Three-Dimensional Cell Cultures. *Anal. Chem.* **2015**.

References

- [122] Rodriguez-Enriquez, S.; Gallardo-Perez, J. C.; Aviles-Salas, A.; Marin-Hernandez, A.; Carreno-Fuentes, L.; Maldonado-Lagunas, V.; Moreno-Sanchez, R., Energy metabolism transition in multi-cellular human tumor spheroids. *Journal of Cellular Physiology* **2008**, *216* (1), 189-197.
- [123] Kelm, J. M.; Timmins, N. E.; Brown, C. J.; Fussenegger, M.; Nielsen, L. K., Method for generation of homogeneous multicellular tumor spheroids applicable to a wide variety of cell types. *Biotechnol. Bioeng.* **2003**, *83* (2), 173-180.
- [124] Del Duca, D.; Werbowetski, T.; Del Maestro, R. F., Spheroid preparation from hanging drops: characterization of a model of brain tumor invasion. *Journal of Neuro-Oncology* **2004**, *67* (3), 295-303.
- [125] Tung, Y.-C.; Hsiao, A. Y.; Allen, S. G.; Torisawa, Y.-s.; Ho, M.; Takayama, S., High-throughput 3D spheroid culture and drug testing using a 384 hanging drop array. *Analyst* **2011**, *136* (3), 473-478.
- [126] Hsiao, A. Y.; Tung, Y.-C.; Qu, X.; Patel, L. R.; Pienta, K. J.; Takayama, S., 384 hanging drop arrays give excellent Z-factors and allow versatile formation of co-culture spheroids. *Biotechnol. Bioeng.* **2012**, *109* (5), 1293-1304.
- [127] Ivascu, A.; Kubbies, M., Rapid generation of single-tumor spheroids for high-throughput cell function and toxicity analysis. *J. Biomol. Screen.* **2006**, *11* (8), 922-932.
- [128] Zhang, X. L.; Wang, W.; Yu, W. T.; Xie, Y. B.; Zhang, X. H.; Zhang, Y.; Ma, X. J., Development of an in vitro multicellular tumor spheroid model using microencapsulation and its application in anticancer drug screening and testing. *Biotechnol. Prog.* **2005**, *21* (4), 1289-1296.
- [129] Schulz, J. C., Adh rente Zellkultur im „h ngenden Tropfen“. *LaborWelt* **2012**, *3*.
- [130] Biomatrix Perfecta3D[®] Hanging Drop Culture Plates. <https://3dbiomatrix.com/>.
- [131] Chien, H. W.; Kuo, W. H.; Wang, M. J.; Tsai, S. W.; Tsai, W. B., Tunable Micropatterned Substrates Based on Poly(dopamine) Deposition via Microcontact Printing. *Langmuir* **2012**, *28* (13), 5775-5782.
- [132] Frimat, J.-P.; Sisnaiske, J.; Subbiah, S.; Menne, H.; Godoy, P.; Lampen, P.; Leist, M.; Franzke, J.; Hengstler, J. G.; van Thriel, C.; West, J., The network formation assay: a spatially standardized neurite outgrowth analytical display for neurotoxicity screening. *Lab Chip* **2010**, *10* (6), 701-709.

References

- [133] Friedrich, J.; Eder, W.; Castaneda, J.; Doss, M.; Huber, E.; Ebner, R.; Kunz-Schughart, L. A., A reliable tool to determine cell viability in complex 3-D culture: The acid phosphatase assay. *J. Biomol. Screen.* **2007**, *12* (7), 925-937.
- [134] Silva, M. T., Secondary necrosis: The natural outcome of the complete apoptotic program. *FEBS Lett.* **2010**, *584* (22), 4491-4499.
- [135] Carré, A.; Mittal, K. L., *Surface and Interfacial Aspects of Cell Adhesion*. Taylor & Francis: 2011.
- [136] Zhao, Y.; Butler, E. B.; Tan, M., Targeting cellular metabolism to improve cancer therapeutics. *Cell Death Dis.* **2013**, *4*.
- [137] Sonveaux, P.; Vegran, F.; Schroeder, T.; Wergin, M. C.; Verrax, J.; Rabbani, Z. N.; De Saedeleer, C. J.; Kennedy, K. M.; Diepart, C.; Jordan, B. F.; Kelley, M. J.; Gallez, B.; Wahl, M. L.; Feron, O.; Dewhirst, M. W., Targeting lactate-fueled respiration selectively kills hypoxic tumor cells in mice. *J. Clin. Invest.* **2008**, *118* (12), 3930-3942.
- [138] Le, A.; Cooper, C. R.; Gouw, A. M.; Dinavahi, R.; Maitra, A.; Deck, L. M.; Royer, R. E.; Jagt, D. L. V.; Semenza, G. L.; Dang, C. V., Inhibition of lactate dehydrogenase A induces oxidative stress and inhibits tumor progression. *Proc. Natl. Acad. Sci. U. S. A.* **2010**, *107* (5), 2037-2042.
- [139] Halestrap, A. P.; Meredith, D., The SLC16 gene family - from monocarboxylate transporters (MCTs) to aromatic amino acid transporters and beyond. *Pflugers Arch.* **2004**, *447* (5), 619-628.
- [140] Gatenby, R. A.; Gillies, R. J., Why do cancers have high aerobic glycolysis? *Nature Reviews Cancer* **2004**, *4* (11), 891-899.
- [141] Vander Heiden, M. G.; Cantley, L. C.; Thompson, C. B., Understanding the Warburg effect: the metabolic requirements of cell proliferation. *Science* **2009**, *324* (5930), 1029-33.
- [142] Chantranupong, L.; Wolfson, R. L.; Orozco, J. M.; Saxton, R. A.; Scaria, S. M.; Bar-Peled, L.; Spooner, E.; Isasa, M.; Gygi, S. P.; Sabatini, D. M., The Sestrins Interact with GATOR2 to Negatively Regulate the Amino-Acid-Sensing Pathway Upstream of mTORC1. *Cell reports* **2014**, *9* (1), 1-8.
- [143] Efeyan, A.; Zoncu, R.; Sabatini, D. M., Amino acids and mTORC1: from lysosomes to disease. *Trends Mol. Med.* **2012**, *18* (9), 524-533.

References

- [144] Kim, S. G.; Buel, G. R.; Blenis, J., Nutrient regulation of the mTOR Complex 1 signaling pathway. *Mol. Cells* **2013**, *35* (6), 463-473.
- [145] Yuan, H. X.; Xiong, Y.; Guan, K. L., Nutrient Sensing, Metabolism, and Cell Growth Control. *Mol. Cell* **2013**, *49* (3), 379-387.
- [146] Spectroscopy, C. f. N. The Lock. <http://nmr.chem.wsu.edu/tutorials/basics/lock/>.
- [147] Yeh, Y. Y.; Sheehan, P. M., Preferential utilization of ketone-bodies in the brain and lung of newborn rats. *Federation Proceedings* **1985**, *44* (7), 2352-2358.
- [148] Tanaka, J.; Ozawa, K.; Tobe, T., Significance of blood ketone body ratio as an indicator of hepatic cellular-energy status in jaundiced rabbits. *Gastroenterology* **1979**, *76* (4), 691-696.
- [149] Yuneva, M. O.; Fan, T. W. M.; Allen, T. D.; Higashi, R. M.; Ferraris, D. V.; Tsukamoto, T.; Mates, J. M.; Alonso, F. J.; Wang, C. M.; Seo, Y.; Chen, X.; Bishop, J. M., The Metabolic Profile of Tumors Depends on Both the Responsible Genetic Lesion and Tissue Type. *Cell Metab.* **2012**, *15* (2), 157-170.
- [150] Mehta, G.; Hsiao, A. Y.; Ingram, M.; Luker, G. D.; Takayama, S., Opportunities and challenges for use of tumor spheroids as models to test drug delivery and efficacy. *J. Controlled Release* **2012**, *164* (2), 192-204.

Acknowledgment

First and foremost I offer my sincerest gratitude to my supervisor, Dr. Roland Hergenröder, whose encouragement and patience from the initial to the final level enabled me to develop this project. Especially, I'm grateful for his support, for his trust in me and for giving me the opportunity to work in my own way.

I also owe my deepest thankfulness to Dr. Jörg Lambert (with his outstanding NMR knowledge) and Dr. Ahmad Telfah (for his brilliant ideas and hard work with the microslot NMR detector). Without their discussions, brainstorming, help and patience this thesis would not be possible.

I offer my gratitude to my Referees Prof. Dr. Jörg Tiller and PD. Dr. Joachim Franzke, who kindly agreed to support me to complete my thesis and who nicely spared time.

I offer my special gratitude to Hannes Raschke for his uncomplicated and flexible way to solve problems and to Dr. Alex von Bohlen for helpful discussions and motivations.

I am also thankful to many of my colleagues at the Interface Processes Maria Becker, Mikheil Gogiashvili, Dr. Astrid Jürgensen and Dr. Victoria Shpacovitch and all the members of the Hergenröder Group.

I offer my further regards to Günther Jestel and Jürgen Lonzynski for their support in probehead fabrication, to Michael Weil for the drawings, to Sarah Waide, Jan Hengstler, Cristina Cadenas, Sonja Vosbeck and Agatha Widera for cell culture and spheroid support, to Ulrich Marggraf for the silicon wafer and to Normal Ahlmann for the plasma generator.

Thanks the International Leibniz Graduate School "Systems Biology Lab-on-a-Chip" for financial support.

Lastly, I offer my regards and blessings to my family and friends who supported me in any respect during the completion of this project. Especially I'm thankful for their patience and understanding when I could not spent time with them.

Curriculum Vitae

Name Ayten Kalfe
Titel M. Sc. in Chemical Biology
E-mail ayten.kalfe@isas.de
Phone +49 231 1392 - 230

Education

Since 10/2011	Ph. D Student	Technical University Dortmund, Department of Biological and Chemical Engineering, Dortmund, Germany Leibniz-Institut für Analytische Wissenschaften – ISAS – e.V., Dortmund, Germany
2009 - 2010	Graduate Student, Masters Thesis	Cornell University, Department of Biological and Environmental Engineering, Ithaca, New York, USA
2007 - 2010	M. Sc. in Chemical Biology	Technical University Dortmund, Department of Chemistry, Dortmund, Germany
2003 - 2007	B. Sc. in Chemical Biology	Technical University Dortmund, Department of Chemistry, Dortmund, Germany
2003	Abitur	Theodor Körner Schule (High School), Bochum, Germany

Publications

A. Kalfe, A. Telfah, J. Lambert, R. Hergenröder. Looking into Living Cell Systems: Planar Waveguide Microfluidic NMR Detector for in Vitro Metabolomics of Tumor Spheroids. Anal. Chem. 87, 7402

A. Telfah, J. Lambert, A. Kalfe, A. Jürgensen, R. Hergenröder. Dielectric studies of Polyethylene oxide (PEO) as a model for morphological effect on ion transportation in the composite polymer electrolytes (Submitted)

S. J. Reinholt, A. Behrent, C. Greene, A. Kalfe, A. J. Baeumner. Isolation and Amplification of mRNA within a Simple Microfluidic Lab on a Chip. Anal. Chem. 86, 849 (Jan, 2014).

Patents

1. Deutsche Patentanmeldung 10 2014 107 296.0 (German Patent No.)
Doppelresonanz-Probenkopf auf Mikrostreifenleiterbasis (NMR Double Resonance Probehead based on microstrip waveguide technology for ultra-small samples like living cells).

2. Deutsche Patentanmeldung 10 2014 115 702.8 (German Patent No.)
Heizung für Mikrostreifenleiter (non-magnetic planar heater for NMR probehead based on microstrip waveguide technology. This heater should keep cells alive under physiological conditions in order to enable long-term measurements on living cells).

Work Experience

- Since 10/2011 Ph. D Thesis:
Technical University Dortmund, Department of Biological and Chemical Engineering, Dortmund, Germany
Leibniz-Institut für Analytische Wissenschaften – ISAS – e.V., Dortmund, Germany
Supervisor Dr. Roland Hergenröder
Looking into living cell systems: Planar waveguide microfluidic NMR detector for in vitro metabolomics of tumor spheroids
- 2009 - 2010 Master Thesis:
Cornell University, Department of Biological and Environmental Engineering, Ithaca, New York, USA
Supervisor USA: Prof. Antje Bäumner,
Supervisor Germany: Prof. C. M. Niemeyer, Prof. W. Blankenfeldt
PMMA biosensor for nucleic acid isolation and amplification with NASBA in microfluidic channels
- 2008 Research Internship:
Cornell University, Department of Biological and Environmental Engineering, Ithaca, New York, USA
Supervisor USA: Prof. Antje Bäumner
Investigations on microfluidic devices altering surface chemistries in order to enable a NASBA reaction in the microfluidic channels
- 2007 - 2008 Research Assistant:
Max Planck Institute of Molecular Physiology, Department of Physical Biochemistry, Dortmund, Germany
Supervisor: Prof. Dr. Wulf Blankenfeldt
- 2007 Bachelor Thesis:
Max Planck Institute of Molecular Physiology, Department of Physical Biochemistry, Dortmund, Germany
Supervisor: Prof. Dr. Wulf Blankenfeldt
Investigation of the substrate specificity of PhzM and PhzS, two enzymes involved in the pyocyanin biosynthesis of Pseudomonas aeruginosa

Grants and Fellowships

- 10/2015 - 12/2016 Postdoctoral position within context of the “Early Independence Strategy Fund” offered by the ISAS institute
- 10/2011 - 10/2015 PhD bursary paid by the International Leibniz Graduate School “Systems Biology Lab-on-a-Chip” (S-BLOC) bursary
- 08/2014 Travel grant paid by the Cold Spring Harbor Laboratory, New York, USA
Mechanisms & Models of Cancer meeting
- 2009 - 2010 Master studies bursary and Cornell University tuition fees paid by the Cornell University (\$ 30.000)

Awards

- 2015 Short listed for the LUSH prize for animal free testing
- 2015 Best Poster Award Environmental Toxicology (EnTox), Germany
- 2013 Best Poster Award ISAS Summer School 2013, Dortmund

Invited Talks

- 06/2014 Max-Planck-Institute for Intelligent Systems, Stuttgart; Germany
(broadcasted to University of Heidelberg)
- 10/2014 Charles University, Laboratory for Radiofrequency Spectroscopy, Prague, Czech Republic

Conference activity (Poster and Talks)

- 03/2012 ISAS In-house Seminar, Dortmund
- 06/2012 Doktorandenforum der Sektion D (Leibniz Gemeinschaft), Berlin
- 10/2012 ISAS Summer School 2012, Dortmund
- 10/2013 ISAS Summer School 2013, Dortmund
- 10/2013 3. Marktplatz bio.dortmund 2013, Dortmund
- 11/2013 Single cell and molecule analysis (SICA) conference, Münster
- 11/2013 ISAS In-house Seminar, Dortmund
- 04/2014 Humboldt Kolleg International Conference
Conference for enhancement of research in Jordan, Amman
- 08/2014 Mechanisms and models of cancer, Cold Spring Harbor Laboratory, New York, USA
- 10/2014 Science Night Ruhr (WissensNacht Ruhr am Dortmunder U)
- 05/2015 Environmental Toxicology (EnTox) in North Rhine-Westphalia, Germany

Media Coverage

- 11/2013 Ruhr Nachrichten, Dortmund D1 Süd, 13th November 2013 (newspaper)
- 09/2013 WDR Lokalzeit, Dortmunds Forscher (tv)
- 02/2013 Ruhr Nachrichten, Dortmund D1 Süd, Dortmunds junge Forscher,
28th February 2013 (newspaper)
- 2012 2012 Analytix inside, Newsletter ISAS e.V. No. 1/2012 (journal)